MODELING OF THERMAL PERFORMANCE OF LIQUID FLOW WITH NANOSIZED PARTICLES OF PHASE CHANGE MATERIAL IN MICROCHANNELS

BY

AWAD BIN SAUD ALQUAITY

A Thesis Presented to the
DEANSHIP OF GRADUATE STUDIES

KING FAHD UNIVERSITY OF PETROLEUM & MINERALS

DHAHRAN, SAUDI ARABIA

In Partial Fulfillment of the
Requirements for the Degree of

MASTER OF SCIENCE

In

MECHANICAL ENGINEERING

MAY 2011

KING FAHD UNIVERSITY OF PETROLEUM & MINERALS

DHAHRAN 31261, SAUDI ARABIA

DEANSHIP OF GRADUATE STUDIES

This thesis, written by Awad Bin Saud Alquaity under the direction of his thesis advisor and approved by his thesis committee, has been presented to and accepted by the Dean of Graduate Studies, in partial fulfillment of the requirements for the degree of **MASTER OF SCIENCE in MECHANICAL ENGINEERING**.

Thesis Committee

S.A.

Dr. Salem A. Al-Dini (Advisor)

Dr. Bekir S. Yilbas (Member)

Dr. Ahmet Z. Sahin (Member)

Dr. Amro M. Al- Qutub
Department Chairman

Dr. Salam A. Zummo
Dean of Graduate Studies

28/5/11

Date

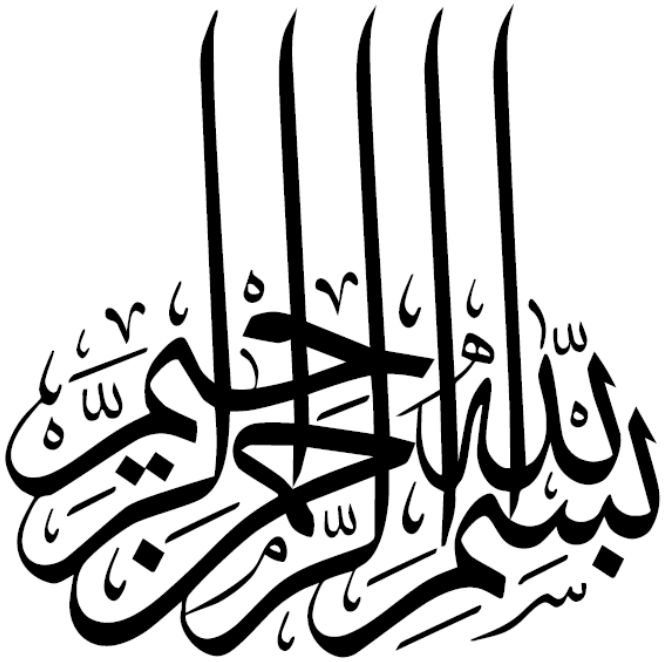

Dedicated to

My parents and sister for their duas and constant support and encouragement throughout my life

ACKNOWLEDGEMENT

All praise belongs to Almighty Allah (s.w.t.) for bestowing me with health, knowledge and patience to carry out this work and complete my M.S. successfully at King Fahd University of Petroleum and Minerals, Dhahran. I am happy to have had a chance to glorify His name in the sincerest way through this small accomplishment and ask Him to accept my efforts.

Acknowledgement is due to King Fahd University of Petroleum and Minerals for providing me financial support and good academic environment during the course of my M.S. Special thanks is also due to the Center of Excellence for Scientific Research Collaboration with M.I.T.

My deep gratitude and appreciation goes to my thesis advisor Dr.Salem Al-Dini for his constant help, guidance and motivation during the course of my study. His priceless suggestions made this work interesting and challenging for me. I also wish to express my deep appreciation to Dr.Yilbas for his help, guidance, and constant encouragement during my M.S. I am greatly indebted to Dr.Yilbas for the valuable time he spent throughout my thesis work and also for always being supportive and helping me during difficult times. Sincere thanks to Dr.Sahin for his interest, cooperation and constructive criticism.

I would also like to acknowledge all the Mechanical Engineering faculty members with whom I took courses during my M.S. especially Dr.Shuja and Dr.Zubair who helped me a lot, guided me and encouraged me during my coursework and related research.

Special thanks to Mr.Omeir Momin for his constant help and valuable inputs to my work. I am grateful to Mr.Usama Siddiqui for introducing me to Mendeley software at a critical time during the writing of my M.S. Thesis. Thanks are also due to all the graduate students and faculty with whom I interacted during my Masters namely Abdul Subhan, Ahmed Etar, Eng.Ammar, Aqeel, Azhar, Eng. Bilal Qureshi, Faisal, Eng.Hasan Baig, Iqbal, Masood, Eng.Murtuza, Najam, Omeir Momin, Pervez, Riyaz, Dr.Saad Bin Mansoor, Siddharth, Eng.Sarfaraz, Usama, Zabi and Zameer.

TABLE OF CONTENTS

ACKNOWLEDGEMENT ..... **iv**

LIST OF TABLES ..... **x**

LIST OF FIGURES ..... **xi**

THESIS ABSTRACT (ENGLISH) ..... **xxi**

THESIS ABSTRACT (ARABIC) ..... **xxii**

CHAPTER 1 ..... **1**

INTRODUCTION **1**

1.1 Research Background 1

1.2 Scope of the Work 5

1.3 Objectives 8

1.4 Thesis Outline 9

CHAPTER 2 ..... **11**

LITERATURE REVIEW **11**

2.1 P.C.M. Slurry Flow in Conventional Channels and Minichannels 11

2.2 P.C.M. Slurry Flow in Microchannels 20

2.3 Summary of Literature Review 24

CHAPTER 3 25

MODEL STUDY 25

3.1 Models and Formulation 25

3.1.1 Discrete Phase Model 26

3.1.2 Homogeneous Model 30

3.1.3 Bulk Fluid Thermo-physical Properties 32

3.2 Problem Statement and Boundary Conditions 37

3.2.1 Boundary Conditions 39

CHAPTER 4 45

NUMERICAL STUDY 45

4.1 Grid Independence 46

4.2 Validation 48

CHAPTER 5 54

RESULTS AND DISCUSSION 54

5.1 Identification of a Unified Model 54

5.2 Effectiveness Ratio, Performance Index and Merit Number 69

5.2.1 Effectiveness Ratio 69

5.2.2 Performance Index 80

5.2.3 Merit Number 91

5.3 Volumetric Entropy Generation Rate due to Heat Transfer and Fluid Friction 100

5.3.1 Volumetric Entropy Generation Rate due to Heat Transfer 100

5.3.2 Volumetric Entropy Generation Rate due to Fluid Friction 118

5.4 Normalized Length of Phase Change and Total Phase Change Length 126

5.4.1 Normalized Length of Phase Change 126

5.4.2 Normalized Total Phase Change Length 138

CHAPTER 6 150

CONCLUSION AND FUTURE WORK 150

6.1 Identification of a Unified Model 150

6.2 Effectiveness Ratio, Performance Index and Merit Number 151

6.3 Volumetric Entropy Generation Rate due to Heat Transfer and Fluid Friction 152

6.4 Normalized Length of Phase Change and Total Phase Change Length 153

6.5 Future Work 154

Nomenclature 157

References 160

Vita 165

LIST OF TABLES

Table 3.1 Comparison between 2D and 3D simulations..... 41

Table 3.2 Thermo-physical properties of P.C.M. particles..... 43

Table 3.3 Comparison between constant properties and temperature dependent properties

..... 44

LIST OF FIGURES

Figure 1.1 Typical microchannel array [3] 2

Figure 3.1 Thermal conductivity ratio of nanosized P.C.M. particles 35

Figure 3.2 Schematic diagram of the microchannel used in the FLUENT^{TM} simulations (H = 50 μm). 38

Figure 3.3 Geometry and flow direction in the 2D microchannel used in the FLUENT^{TM} simulations. 38

Figure 4.1 Grid independence test for Nusselt number along the axial distance of the microchannel. 47

Figure 4.2 Wall temperatures obtained using D.P.M. and homogeneous model with experimental data for Stefan number of 2 [20]. 49

Figure 4.3 Wall temperatures obtained using D.P.M. and homogeneous model with experimental data for Stefan number of 3 [20]. 50

Figure 4.4 Comparison of Nusselt number obtained using homogeneous model with experimental data [33]. 51

Figure 4.5 Dimensionless entropy generation rate along the tube radius, obtained using simulation with analytical values. 53

Figure 5.1 Temperature contour of carrier fluid along the microchannel length for 0% volume concentration of particles. 56

Figure 5.2 Temperature contour of carrier fluid along the microchannel length for 10% volume concentration of particles using D.P.M..... 56

Figure 5.3 Temperature contour of bulk fluid along the microchannel length for 10% volume concentration of particles using homogeneous model. 57

Figure 5.4 Mass weighted average fluid temperature along the microchannel length, where VF 0, VF 5, and VF 10 represents 0%, 5% and 10% volume concentration of the particles, respectively..... 59

Figure 5.5 Nusselt number variation in case of D.P.M., where VF 0, VF 5 and VF 10 represents 0%, 5% and 10% volume concentration of particles, respectively..... 63

Figure 5.6 Nusselt number variation in case of homogeneous model, where VF 0, VF 5 and VF 10 represents 0%, 5% and 10% volume concentration of particles, respectively.64

Figure 5.7 Average Nusselt number variation with volume concentration of particles. .. 66

Figure 5.8 Pressure distribution along the microchannel length, where VF 0, VF 5 and VF 10 represents 0%, 5% and 10% volume concentration of particles, respectively..... 68

Figure 5.9 Variation of effectiveness ratio with heat flux for mass flow rate of 10^{-5} kg/s, where VF 3, VF 5, VF 7 and VF 10 represents 3%, 5%, 7% and 10% volume concentration of the particles, respectively..... 74

Figure 5.10 Variation of effectiveness ratio with heat flux for mass flow rate of 2×10^{-5} kg/s, where VF 3, VF 5, VF 7 and VF 10 represents 3%, 5%, 7% and 10% volume concentration of the particles, respectively..... 75

Figure 5.11 Variation of effectiveness ratio with heat flux for mass flow rate of 3 x 10^{-5} kg/s, where VF 3, VF 5, VF 7 and VF 10 represents 3%, 5%, 7% and 10% volume concentration of the particles, respectively..... 76

Figure 5.12 Variation of effectiveness ratio with heat flux for mass flow rate of 4 x 10^{-5} kg/s, where VF 3, VF 5, VF 7 and VF 10 represents 3%, 5%, 7% and 10% volume concentration of the particles, respectively..... 77

Figure 5.13 Variation of effectiveness ratio with ratio of heat flux to mass flow rate of P.C.M. slurry, where VF 3, VF 5, VF 7 and VF 10 represents 3%, 5%, 7% and 10% volume concentration of the particles, respectively..... 78

Figure 5.14 Variation of effectiveness ratio with bulk fluid Reynolds number for heat flux of 20000 W/m^2, where VF 3, VF 5, VF 7 and VF 10 represents 3%, 5%, 7% and 10% volume concentration of the particles, respectively..... 79

Figure 5.15 Variation of performance index with heat flux for mass flow rate of 10^{-5} kg/s, where VF 3, VF 5, VF 7 and VF 10 represents 3%, 5%, 7% and 10% volume concentration of the particles, respectively..... 85

Figure 5.16 Variation of performance index with heat flux for mass flow rate of 2 x 10^{-5} kg/s, where VF 3, VF 5, VF 7 and VF 10 represents 3%, 5%, 7% and 10% volume concentration of the particles, respectively..... 86

Figure 5.17 Variation of performance index with heat flux for mass flow rate of 3 x 10^{-5} kg/s, where VF 3, VF 5, VF 7 and VF 10 represents 3%, 5%, 7% and 10% volume concentration of the particles, respectively..... 87

Figure 5.18 Variation of performance index with heat flux for mass flow rate of 4 x 10^{-5} kg/s, where VF 3, VF 5, VF 7 and VF 10 represents 3%, 5%, 7% and 10% volume concentration of the particles, respectively..... 88

Figure 5.19 Variation of performance index with ratio of heat flux to mass flow rate of P.C.M. slurry, where VF 3, VF 5, VF 7 and VF 10 represents 3%, 5%, 7% and 10% volume concentration of the particles, respectively..... 89

Figure 5.20 Variation of performance index with Reynolds number for heat flux of 20000 W/m^2, where VF 3, VF 5, VF 7 and VF 10 represents 3%, 5%, 7% and 10% volume concentration of the particles, respectively..... 90

Figure 5.21 Variation of Merit number with heat flux for mass flow rate of 10^{-5} kg/s, where VF 3, VF 5, VF 7 and VF 10 represents 3%, 5%, 7% and 10% volume concentration of the particles, respectively..... 94

Figure 5.22 Variation of Merit number with heat flux for mass flow rate of 2 x 10^{-5} kg/s, where VF 3, VF 5, VF 7 and VF 10 represents 3%, 5%, 7% and 10% volume concentration of the particles, respectively..... 95

Figure 5.23 Variation of Merit number with heat flux for mass flow rate of 3 x 10^{-5} kg/s, where VF 3, VF 5, VF 7 and VF 10 represents 3%, 5%, 7% and 10% volume concentration of the particles, respectively..... 96

Figure 5.24 Variation of Merit number with heat flux for mass flow rate of 4 x 10^{-5} kg/s, where VF 3, VF 5, VF 7 and VF 10 represents 3%, 5%, 7% and 10% volume concentration of the particles, respectively..... 97

Figure 5.25 Variation of Merit number with ratio of heat flux to mass flow rate of P.C.M. slurry, where VF 3, VF 5, VF 7 and VF 10 represents 3%, 5%, 7% and 10% volume concentration of the particles, respectively..... 98

Figure 5.26 Variation of Merit number with Reynolds number for heat flux of 20000 W/m^2, where VF 3, VF 5, VF 7 and VF 10 represents 3%, 5%, 7% and 10% volume concentration of the particles, respectively..... 99

Figure 5.27 Volumetric entropy generation rate due to heat transfer for mass flow rate of 10^{-5} kg/s ; where VF0,VF 3, VF 5, VF 7 and VF 10 represent 0%, 3%, 5%, 7% and 10% volume concentration of the particles, respectively..... 106

Figure 5.28 Volumetric entropy generation rate due to heat transfer for mass flow rate of 2 x 10^{-5} kg/s ; where VF0,VF 3, VF 5, VF 7 and VF 10 represent 0%, 3%, 5%, 7% and 10% volume concentration of the particles, respectively 107

Figure 5.29 Volumetric entropy generation rate due to heat transfer for mass flow rate of 3 x 10^{-5} kg/s ; where VF0,VF 3, VF 5, VF 7 and VF 10 represent 0%, 3%, 5%, 7% and 10% volume concentration of the particles, respectively. 108

Figure 5.30 Volumetric entropy generation rate due to heat transfer for mass flow rate of 4 x 10^{-5} kg/s ; where VF0,VF 3, VF 5, VF 7 and VF 10 represent 0%, 3%, 5%, 7% and 10% volume concentration of the particles, respectively. 109

Figure 5.31 Temperature gradient along microchannel length for heat flux of 8000 W/m^2 and mass flow rate of 10^{-5} kg/s ; where VF0,VF 3, VF 5, VF 7 and VF 10 represent 0%, 3%, 5%, 7% and 10% volume concentration of the particles, respectively..... 110

Figure 5.32 Temperature gradient along microchannel length for heat flux of 20000 W/m^2 and mass flow rate of 10^{-5} kg/s ; where VF0,VF 3, VF 5, VF 7 and VF 10 represent 0%, 3%, 5%, 7% and 10% volume concentration of the particles, respectively. 111

Figure 5.33 Temperature gradient along microchannel length for heat flux of 8000 W/m^2 and mass flow rate of 4 x 10^{-5} kg/s ; where VF0,VF 3, VF 5, VF 7 and VF 10 represent 0%, 3%, 5%, 7% and 10% volume concentration of the particles, respectively. 112

Figure 5.34 Temperature gradient along microchannel length for heat flux of 20000 W/m^2 and mass flow rate of 4 x 10^{-5} kg/s ; where VF0,VF 3, VF 5, VF 7 and VF 10 represent 0%, 3%, 5%, 7% and 10% volume concentration of the particles, respectively. 113

Figure 5.35 Temperature gradient along microchannel height at axial distance of 0.0345 m from inlet, for heat flux of 8000 W/m^2 and mass flow rate of 10^{-5} kg/s ; where VF0,VF 3, VF 5, VF 7 and VF 10 represent 0%, 3%, 5%, 7% and 10% volume concentration of the particles, respectively..... 114

Figure 5.36 Temperature gradient along microchannel height at axial distance of 0.0345 m from inlet,for heat flux of 20000 W/m^2 and mass flow rate of 10^{-5} kg/s ; where VF0,VF 3, VF 5, VF 7 and VF 10 represent 0%, 3%, 5%, 7% and 10% volume concentration of the particles, respectively..... 115

Figure 5.37 Temperature gradient along microchannel height at axial distance of 0.0345 m from inlet,for heat flux of 8000 W/m^2 and mass flow rate of 4 x 10^{-5} kg/s ;

where VF0,VF 3, VF 5, VF 7 and VF 10 represent 0%, 3%, 5%, 7% and 10% volume concentration of the particles, respectively..... 116

Figure 5.38 Temperature gradient along microchannel height at axial distance of 0.0345 m from inlet,for heat flux of 20000 W/m^2 and mass flow rate of 4×10^{-5} kg/s ; where VF0,VF 3, VF 5, VF 7 and VF 10 represent 0%, 3%, 5%, 7% and 10% volume concentration of the particles, respectively..... 117

Figure 5.39 Volumetric entropy generation rate due to fluid friction for mass flow rate of 10^{-5} kg/s ; where VF0,VF 3, VF 5, VF 7 and VF 10 represent 0%, 3%, 5%, 7% and 10% volume concentration of the particles, respectively..... 120

Figure 5.40 Volumetric entropy generation rate due to fluid friction for mass flow rate of 2×10^{-5} kg/s ; where VF0,VF 3, VF 5, VF 7 and VF 10 represent 0%, 3%, 5%, 7% and 10% volume concentration of the particles, respectively. 121

Figure 5.41 Volumetric entropy generation rate due to fluid friction for mass flow rate of 3×10^{-5} kg/s ; where VF0,VF 3, VF 5, VF 7 and VF 10 represent 0%, 3%, 5%, 7% and 10% volume concentration of the particles, respectively. 122

Figure 5.42 Volumetric entropy generation rate due to fluid friction for mass flow rate of 4×10^{-5} kg/s ; where VF0,VF 3, VF 5, VF 7 and VF 10 represent 0%, 3%, 5%, 7% and 10% volume concentration of the particles, respectively. 123

Figure 5.43 Pressure drop along microchannel length for heat flux of 8000 W/m^2 and mass flow rate of 10^{-5} kg/s ; where VF0,VF 3, VF 5, VF 7 and VF 10 represent 0%, 3%, 5%, 7% and 10% volume concentration of the particles, respectively..... 124

Figure 5.44 Pressure drop along microchannel length for heat flux of 20000 W/m^2 and mass flow rate of 10^{-5} kg/s ; where VF0,VF 3, VF 5, VF 7 and VF 10 represent 0%, 3%, 5%, 7% and 10% volume concentration of the particles, respectively. 125

Figure 5.45 Normalized length of phase change for mass flow rate of 10^{-5} kg/s, where VF 3, VF 5, VF 7 and VF 10 represents 3%, 5%, 7% and 10% volume concentration of the particles, respectively. 130

Figure 5.46 Normalized length of phase change for mass flow rate of 1.5 x 10^{-5} kg/s, where VF 3, VF 5, VF 7 and VF 10 represents 3%, 5%, 7% and 10% volume concentration of the particles, respectively. 131

Figure 5.47 Normalized length of phase change for mass flow rate of 2 x 10^{-5} kg/s, where VF 3, VF 5, VF 7 and VF 10 represents 3%, 5%, 7% and 10% volume concentration of the particles, respectively. 132

Figure 5.48 Normalized length of phase change for heat flux of 10000 W/m^2, where VF 3, VF 5, VF 7 and VF 10 represents 3%, 5%, 7% and 10% volume concentration of the particles, respectively. 133

Figure 5.49 Normalized length of phase change for heat flux of 12000 W/m^2, where VF 3, VF 5, VF 7 and VF 10 represents 3%, 5%, 7% and 10% volume concentration of the particles, respectively. 134

Figure 5.50 Normalized length of phase change for heat flux of 15000 W/m^2, where VF 3, VF 5, VF 7 and VF 10 represents 3%, 5%, 7% and 10% volume concentration of the particles, respectively. 135

Figure 5.51 Normalized length of phase change for heat flux of 18000 W/m^2, where VF 3, VF 5, VF 7 and VF 10 represents 3%, 5%, 7% and 10% volume concentration of the particles, respectively. 136

Figure 5.52 Normalized length of phase change for heat flux of 20000 W/m^2, where VF 3, VF 5, VF 7 and VF 10 represents 3%, 5%, 7% and 10% volume concentration of the particles, respectively. 137

Figure 5.53 Normalized total phase change length for mass flow rate of 10^{-5} kg/s, where VF 3, VF 5, VF 7 and VF 10 represents 3%, 5%, 7% and 10% volume concentration of the particles, respectively. 140

Figure 5.54 Normalized total phase change length for mass flow rate of 1.5 x 10^{-5} kg/s, where VF 3, VF 5, VF 7 and VF 10 represents 3%, 5%, 7% and 10% volume concentration of the particles, respectively. 141

Figure 5.55 Normalized total phase change length for mass flow rate of 2 x 10^{-5} kg/s, where VF 3, VF 5, VF 7 and VF 10 represents 3%, 5%, 7% and 10% volume concentration of the particles, respectively. 142

Figure 5.56 Normalized total phase change length for heat flux of 10000 W/m^2, where VF 3, VF 5, VF 7 and VF 10 represents 3%, 5%, 7% and 10% volume concentration of the particles, respectively. 143

Figure 5.57 Normalized total phase change length for heat flux of 12000 W/m^2, where VF 3, VF 5, VF 7 and VF 10 represents 3%, 5%, 7% and 10% volume concentration of the particles, respectively. 144

Figure 5.58 Normalized total phase change length for heat flux of 15000 W/m^2, where VF 3, VF 5, VF 7 and VF 10 represents 3%, 5%, 7% and 10% volume concentration of the particles, respectively. 145

Figure 5.59 Normalized total phase change length for heat flux of 18000 W/m^2, where VF 3, VF 5, VF 7 and VF 10 represents 3%, 5%, 7% and 10% volume concentration of the particles, respectively. 146

Figure 5.60 Normalized total phase change length for heat flux of 20000 W/m^2, where VF 3, VF 5, VF 7 and VF 10 represents 3%, 5%, 7% and 10% volume concentration of the particles, respectively. 147

Figure 5.61 Variation of L_t/D_h with operating conditions. 149

THESIS ABSTRACT (ENGLISH)

NAME: AWAD BIN SAUD ALQUAITY

TITLE: MODELING OF THERMAL PERFORMANCE OF LIQUID FLOW WITH NANOSIZED PARTICLES OF PHASE CHANGE MATERIAL IN MICROCHANNELS

MAJOR: MECHANICAL ENGINEERING

DATE: MAY 2011

In the present study, a numerical model is identified and used for investigating laminar flow in a microchannel incorporating suspension of nanosized P.C.M. particles. The effect of different parameters such as mass flow rate, heat flux applied to P.C.M. slurry and particle volume concentrations on the thermal performance is investigated. Effectiveness Ratio, Performance Index and Merit Number are used for the investigation of the thermal performance of P.C.M. slurry. Further a detailed investigation is performed to examine the effects of operating conditions and particle volume concentration on the volumetric entropy generation rate due to heat transfer and fluid friction. Lastly, a detailed study is performed to calculate the length of the microchannel required for obtaining maximum enhancement in heat storage capacity for different operating conditions and particle volume concentrations. The results show a significant improvement in heat storage capacity of slurry due to the addition of P.C.M. particles.

MASTER OF SCIENCE DEGREE

KING FAHD UNIVERSITY OF PETROLEUM & MINERALS

Dhahran, Saudi Arabia

THESIS ABSTRACT (ARABIC)

الاسم: عوض بن سعود القعيطي .

العنوان: تصميم الاداء الحراري للسائل المتدفق المحمل بجزيئات متناهيه الصغر"نانو" في الانابيب الدقيقه"مايكرو".

التخصص: الهندسة الميكانيكية .

التاريخ: مايو 2011 .

في هذه الدراسه, التصميم العددي قد حدد واستخدم لدراسه تدفق "لامينر " محملا بجزيئات متناهيه الصغر في انابيب دقيقه. تأثير عوامل مختلفه مثل: معدل التدفق, كميه الحراره المعرض لها الجزيئات التناهيه الصغر,و حجم الجزيئات المتناهيه الصغر. نسبه الكفائه و مؤشر الاداء,و رقم "ميرت" حيث استخدموالدراسه الاداء الحراري للجزيئات المتناهيه الصغر. نتيجه لذلك, دراسه مفصله قد عملت لدراسه وفهم تأثير عوامل التشغيل و تركيز حجم الجزيئات المتناهيه الصغر على توليد الانتروبي نتيجه للالانتقال الحراري واحتكاك السائل الناقل للحراراه. اخيرا, دراسه تفصيليه قد عملت لمعرفه اقصى طول للالانابيب الدقيقه عند تغير عوامل التشغيل و حجم الجزيئات المتناهيه الصغر.

درجة الماجستير في العلوم

جامعة الملك فهد للبترول و المعادن

الظهران المملكة العربية السعودية

CHAPTER 1

INTRODUCTION

1.1 Research Background

Microchannels are defined as flow channels which have the characteristic dimension in the range of 10 to 200 micrometers [1]. Figure 1.1 shows a typical microchannel fabricated using deep reactive ion etch fabrication technology. In early 1980's, the concept of using microchannels for cooling of electronic devices was introduced by Tuckerman and Pease [2]. In comparison to conventional cooling techniques, microchannel heat sinks provide one of the most effective ways for cooling electronic devices due to their intrinsic attributes of large heat transfer coefficient, high heat transfer surface area per unit volume, and small quantity of heat transferring fluid required. The requirement of reduced electronic device size coupled with increased reliability in device operation provides a huge impetus to microchannel research. The advancements in microfabrication technology further fuel the growth of microchannels. Microchannels have attracted attention in major applications including microelectronics, microscale sensors and actuators, fuel cell systems, biomedical applications and advanced heat sinks.

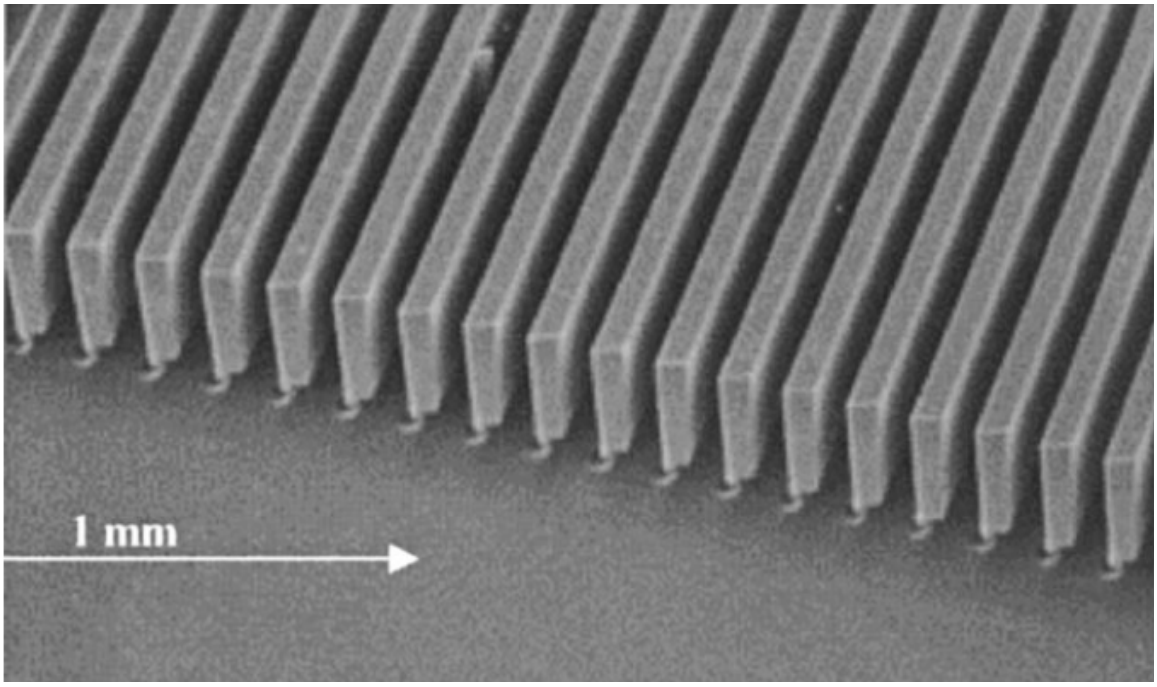

Figure 1.1 Typical microchannel array [3]

The flow of liquids in microchannels is in the continuum regime as the channel dimensions are much larger than the molecular mean free path of liquids [3]. However, the flow of gases through microchannels may or may not be continuum medium based on the gas Knudsen number. Navier-Stokes equations are appropriate for describing fluid flow in microchannels as long as the microchannel depth is greater than 1.7 μm [4]. Numerous experimental studies presented in the literature for liquid flow in microchannels [4-7] support the above observation.

The significant increase in heat transfer coefficient obtained using microchannels can be understood by having a close look at the equation for heat transfer coefficient, which is calculated as:

$$h = \frac{Nu\ k}{D_h} \tag{1.1.1}$$

The Nusselt number for fully developed laminar flow is constant and its value depends on the thermal conditions applied at the boundaries. Equation (1.1.1) shows that the heat transfer coefficient in internal laminar flows scales inversely with the hydraulic diameter of the flow passage. As a result, decreasing the size of the flow passage leads to high heat transfer coefficient and improved heat transfer rates. Therefore, microchannels with hydraulic diameters in the range of 10 to 200 micrometers have very high heat transfer coefficients, which make them attractive for various high heat flux applications as indicated above.

However there are some problems associated with microchannel flow. The small cross-sectional area of the microchannels leads to a large pressure drop and non-uniform

temperature distribution in the microchannel walls. In applications like cooling of electronic devices, the non-uniformity in the temperature distribution can cause significant difference in thermal expansion and damage the electronic device [8]. In order to reduce the non-uniformity in temperature distribution, the mass flow rate of the heat transferring fluid has to be increased; however this further increases the pressure drop across the microchannel. In addition to the problem of non-uniform temperature distribution, the cooling requirements of electronic devices have increased significantly in the past few years. The cooling capacity of microelectronics has a direct influence on its switching speed. A cooling capacity of the order of 10^5 W/cm^3 is required to reach the switching speeds needed for next generation computing devices. This requirement cannot be met by current liquid cooling systems including microchannel heat sinks [9]. One promising technique to meet the electronic cooling demands for next generation devices is the use of suspension of Phase Change Material (P.C.M.) particles in the carrier fluid. The use of P.C.M. particles reduces temperature rise within the microchannel, thereby, reducing the problem of non-uniform temperature distribution along the channel length.

P.C.M. particles have a high latent heat of fusion and absorb large amount of heat while undergoing phase change from solid to liquid states. When thermal energy is required, the P.C.M. particles solidify while releasing a large amount of heat. Therefore, they are used for storing thermal energy and have received considerable attention in recent years for possible applications in cooling of electronic devices. One of the most important properties while selecting a P.C.M. particle is a high latent heat of fusion. The P.C.M.

particle should be selected such that the operating temperature of heating or cooling matches closely with the melting temperature of P.C.M. It is also desirable that the P.C.M. has high thermal conductivity, cycling stability and undergoes a low volume change during phase change. P.C.M. particles in all cases should be non-flammable, non-toxic and non-explosive. Low cost and abundant availability of the P.C.M. is also a very important criterion in their selection [10]. Some examples of P.C.M. particles include salt hydrates and paraffins [11]. In 1975, Mehalick and Tweedie [12] introduced the concept of using encapsulated P.C.M. particles suspended in heat transferring fluid. Since 1975 considerable amount of research work has been conducted on P.C.M. slurry flow because of the fact that it combines the high heat storage capacity of P.C.M. particles with the high heat transfer rates of the slurry [12].

1.2 Scope of the Work

In the past two decades, many researchers have used microencapsulated P.C.M. particles to improve the thermal properties of the carrier fluid. However, use of microencapsulated P.C.M. particles leads to problems such as sedimentation and erosion, which has hindered their use in practical applications [13]. Moreover they crush each other during pumping which results in deterioration of their performance with repeated cycling [14]. Therefore nanosized P.C.M. particles have been used in the present study.

Significant efforts have focused on improving the thermal performance of P.C.M. slurries in regular channels in the past decade. However, few studies have focused on the thermal

performance of P.C.M. slurries in microchannels. Previous numerical studies have used different modeling approaches to solve the flow and heat transfer problem of P.C.M. slurry flow in microchanels. However, none of these numerical studies mention the rationale behind the selection of their particular modeling methodology. Therefore, a model that provides insight into how various parameters affect heat transfer performance of P.C.M. slurry flows in microchannels is needed, that will also guide future experiments. This work aims at identifying a unified model that can provide design guidelines for P.C.M. slurry flows in microchannels based on P.C.M. particle volume concentrations, slurry mass flow rates and wall heat fluxes. For this purpose, two different models, namely, Discrete Phase Model [15] and homogeneous model have been compared in this study.

None of the previous studies have presented the volumetric entropy generation rate due to the addition of P.C.M. particles into the carrier fluid. Therefore, in this study, the effect of different parameters including mass flow rate, heat flux, and particle volume concentrations, on the volumetric entropy generation rate due to heat transfer and fluid friction is investigated thoroughly. Additionally, Merit number is defined to incorporate the thermodynamic irreversibility in the flow system. Effectiveness ratio and Performance Index along with Merit number have been used to determine the optimum operating conditions in order to obtain the maximum benefit in terms of enhancement in heat storage by the addition of P.C.M. particles.

The phase change of the P.C.M. particles in the fluid significantly enhances its heat storage capacity and consequently increases its ability to absorb high heat fluxes. In order to obtain maximum enhancement by introduction of P.C.M. particles, it is necessary to determine the length of the microchannel required for the phase change of P.C.M. particles to be complete for different operating conditions. Maximum enhancement of heat storage capacity of the bulk fluid can be obtained when the ratio of latent heat to the heat input is maximum. The sensible heating of the bulk fluid near the inlet of the microchannel cannot be avoided, but the sensible heating of the bulk fluid after the phase change can be avoided by selecting the operating conditions such that the phase change of particles is completed as close to the exit of the microchannel as possible. If the operating conditions like mass flow rate and heat flux to be dissipated is known beforehand, then the optimum microchannel length can be calculated such that the phase change is complete near its exit. On the other hand, if the microchannel length is fixed, then optimum operating conditions can be calculated to obtain maximum enhancement in heat storage capacity. Therefore, a parametric study is carried out to understand the effects of various parameters namely mass flow rate, heat flux, and particle volume concentrations, on the normalized length of phase change and normalized total phase change length. The normalized length of phase change is defined as the ratio of the length of the microchannel in which phase change of P.C.M. particles takes place to the total length of the microchannel. Total phase change length is defined as the axial distance from the inlet of the microchannel to the axial location at which the phase change of

P.C.M. particles is complete. Therefore, the normalized total phase change length is defined as the ratio of total phase change length to the total length of the microchannel.

1.3 Objectives

The objectives of this thesis work are summarized below:

1. To identify a unified model that can provide design guidelines for P.C.M. slurry flows in microchannels based on P.C.M. particle volume concentrations, slurry mass flow rates and wall heat fluxes.
2. To determine the operating conditions required to obtain the maximum benefit in terms of enhancement in heat storage capacity by the addition of P.C.M. particles. This objective is achieved by evaluating the Effectiveness ratio, Performance Index and Merit number for different operating conditions.
3. To investigate the effect of different parameters including mass flow rate, heat flux, and particle volume concentrations on the volumetric entropy generation rate due to heat transfer and fluid friction.
4. To determine the normalized length of phase change and normalized total phase change length.

1.4 Thesis Outline

This thesis contains six chapters.

Chapter 1 introduces the subject of liquid flow in microchannels. It also discusses the problems related to the use of microchannels in important practical applications like cooling of electronic devices. The first chapter then discusses the possible solutions and defines the objectives of this thesis work under scope of work and objectives sections respectively.

Chapter 2 reviews the literature related to P.C.M. slurry flows in conventional channels, minichannels and microchannels. Summary of literature review presents a gist of the previous work done in the area of P.C.M. slurry flow and highlights the contributions of the present work to existing knowledge in the field of P.C.M. slurry flow in microchannels.

In Chapter 3, the different approaches used for modeling laminar flow of P.C.M. slurry flow are presented with the relevant mathematical formulation. The problem statement and the boundary conditions used in this thesis are also presented in this chapter.

In Chapter 4 the numerical method used for solving the flow and heat transfer problem of P.C.M. slurry in microchannels is discussed. The results of grid independence test and validation of the C.F.D code used in this thesis are presented.

Chapter 5 is divided into four sections; with each section discussing the results obtained corresponding to the objectives discussed in Chapter 1.

In Chapter 6, the conclusions of this study are presented. The directions in which this study can be extended in future are also discussed.

CHAPTER 2

LITERATURE REVIEW

The literature presented in this chapter is divided into two sections. The first section presents the research work done for P.C.M. slurry flows in conventional channels and minichannels. Kandlikar and Grande [3] defined flow passages with hydraulic diameter more than 3 mm as conventional channels. Flow passages with hydraulic diameter in the range of 200 μm to 3 mm are called minichannels [3]. In the second section, the research work accomplished for P.C.M. slurry flows in microchannels is presented. The last section of this chapter presents summary of literature review.

2.1 P.C.M. Slurry Flow in Conventional Channels and Minichannels

In the past two decades, significant efforts have focused on improving the thermal performance of P.C.M. slurries in conventional channels.

Colvin et al. [16] investigated the use of micro-encapsulated P.C.M. slurries in spacecrafts, avionics and electronics systems. Their results showed that micro-encapsulated P.C.M. slurries significantly enhanced the thermal capacitance of the slurry.

Charunyakorn et al. [17] numerically studied forced convection heat transfer in microencapsulated P.C.M. slurry flow in circular ducts. They used a homogeneous fluid model for their study and modeled phase change using heat source term in the energy equation. They found the particle concentration, bulk Stefan number, the duct/particle radius ratio; the particle-fluid conductivity ratio, and a modified Peclet number as the governing parameters. They concluded that, heat fluxes about 2-4 times higher than single phase flow may be achieved by a slurry system.

Roy and Sengupta [18] conducted an experimental study to evaluate the properties of micro-encapsulated P.C.M. particles. Two different P.C.M. and microcapsules with two different wall thickness were used in the study. Their results showed that microcapsules with thinner walls were unable to withstand thermal cycling. On the other hand, thick walled microcapsules were thermally and structurally stable for a minimum of 100 cycles beyond the melting point. They concluded that microencapsulated P.C.M. particles can be used in practical applications.

Choi et al. [19] studied experimentally the increase in convective heat transfer coefficient and thermal capacity of the heat transfer fluid by using P.C.M. particles in turbulent flow. Uniform heat flux was applied on a long heating section of 10.16 mm diameter to study the effect of phase change of P.C.M. particles. They came up with a new technique to generate very fine P.C.M. particles of about 0.1 mm diameter using emulsifier. They proposed a new three-region melting model and provided an explanation of the physical mechanism of the convective heat transfer enhancement due to the P.C.M. particles.

Goel et al. [20] conducted an experimental study using n-eicosane microcapsules in water for laminar, hydrodynamically fully-developed flow in a circular tube with a constant heat flux boundary condition. Their results showed that the wall temperature could be reduced up to 50% by using a P.C.M. suspension instead of a single phase fluid for the same dimensionless parameters. Though their results agreed qualitatively with that of predictions by Charunyakorn et al. [17], however, there was a quantitative difference greater than 45% between them. They also observed that the degree of homogeneity of the suspension had no observable effect on the wall temperatures.

Zhang and Faghri [21]conducted a numerical study of laminar flow of P.C.M. slurry in a circular tube subjected to a uniform heat flux. The phase change of P.C.M. particles was modeled using a temperature transforming model. The influence of microcapsule shell, phase change temperature range and initial subcooling was considered in their model. The difference between their numerical results and experimental results presented by Goel et al. [20] was found to be 34%. They concluded that further experimental work is necessary to determine the melting range used in the modeling of phase change of P.C.M. particles.

Roy and Avanic [22] experimentally studied the laminar flow in a circular tube subjected to constant heat flux using P.C.M. emulsion (n-octadecane in water). In their study, they used bulk Stefan numbers up to 3.0 and volume concentration of P.C.M. particles up to 30% by volume. Their results showed that the heat transfer characteristics for P.C.M. emulsions were similar to those of microencapsulated P.C.M. suspensions, hence

confirming that the microcapsule walls do not affect the heat transfer process significantly. They concluded that the type of suspension, i.e. either microencapsulated or emulsion, should be selected based on practical considerations and not on heat transfer criterion.

Alisetti and Roy [23] used a homogeneous model to investigate convection heat transfer of P.C.M. slurries in circular ducts with constant wall temperature boundary condition. They used an effective specific heat method to model phase change of particles in the slurry. They also showed that the effect of using different specific heat profiles for modeling the phase change of P.C.M. particles on the final solution is less than 4%. Their results showed that the dominant parameters are the degree of subcooling and the bulk Stefan number and the influence of the specific heat ratio is quite small in the range of parameters studied.

Yamagishi et al. [24] studied the heat transfer enhancement using micro-encapsulated P.C.M. slurry in a circular tube. A uniform heat flux was applied to the circular tube of diameter 10.1 mm for both laminar and turbulent flows. They used n-octadecane slurries with particle volume concentrations up to 30%. The local heat transfer coefficient was found to increase in turbulent flow with increasing volume concentration of P.C.M. particles, degree of turbulence and heating rate in the circular tube. As the particle volume fraction was increased, the flow regime changed from turbulent to laminar.

Roy and Avanic [25] also used a homogeneous model in their numerical study. They used effective specific heat approach to model the phase change of P.C.M. particles. A constant heat flux was applied to the circular tube and the flow at the inlet to the tube was hydro dynamically fully developed. Their numerical study showed that the Stefan number is the only parameter that has a significant impact on the heat transfer for typical P.C.M. suspensions and operating conditions. A correlation to predict the wall temperature rise as a function of the distance along the length of the tube was also developed.

Hu and Zhang [26] numerically studied convective heat transfer enhancement with microencapsulated P.C.M. slurry in a circular tube subjected to a constant heat flux. They used a homogeneous model for solving the fluid flow and heat transfer of the P.C.M. slurry in the tube. The melting of P.C.M. particle was modeled using the effective specific heat method. They compared four different specific heat functions for modeling the phase change of P.C.M. particles within the melting range and reported that the knowledge of exact nature of phase change process is more important in the thermal entry region. They concluded that the Stefan number and volume concentration of P.C.M. particles are the most important parameters influencing the heat transfer enhancement of P.C.M. slurries. Increase in bulk Reynolds number was also found to increase heat transfer significantly for a given fluid. The degree of enhancement in heat transfer is greater in thermally fully developed region as compared to thermal entry region.

Zhang et al. [27] conducted a theoretical investigation of heat transfer enhancement using microencapsulated P.C.M. slurries in tubes subjected to constant wall temperature

boundary condition. They used an effective specific heat method to model the phase change of P.C.M. particles. They defined a new Nusselt number to accurately describe the effect of convective heat transfer enhancement. They reported that the improved Nusselt number is capable of describing the heat transfer enhancement for both internal and external flows. They concluded that Stefan number and volume concentration of P.C.M. particles are the most important parameters influencing the enhancement of heat transfer in P.C.M. slurries.

Chen et al. [28] conducted an experimental study on laminar flow of phase change emulsion. The average diameter of microsized particles in the phase change emulsion of 30 wt% was 50.97 μm. Their main focus in this study was on the investigation of rheological behavior, flow stability and friction factor characteristics of the phase change emulsion. From the analysis of the rheological behavior, they concluded that the phase change emulsion can be considered a Newtonian fluid. The viscosity of the phase change emulsion was found to be 5.57 times that of water and was lower than the value reported in literature. Their results also showed that the mass flow rate of phase change emulsion required for transporting the same amount of heat decreases significantly as compared to water.

Alvarado et al. [29] investigated the thermal performance of microencapsulated P.C.M. slurry in a copper tube subjected to a constant heat flux. The flow within the tube was in the turbulent regime. They concluded that the mass fraction of the slurry and the phase change process of the P.C.M. particles influence the heat transfer process. Their results

reveal a significant enhancement in heat capacity even at low mass flow rates when microencapsulated P.C.M. slurry is used. The slurry was found to exhibit Newtonian behavior at mass fractions below 17.7%. However, the heat transfer coefficient of the microencapsulated P.C.M. slurry was found to be lower than water. Use of enhanced surfaces to improve heat transfer was proposed.

Wang et al. [30] studied the performance of micro-encapsulated slurries in a horizontal circular tube by varying the mass fractions of slurries from 5% to 27.6%. They investigated the influence of P.C.M. volume concentrations, flow structure and heating rates on the heat transfer performance. Their pressure drop measurements showed a clear transition when flow regime changed from laminar to turbulent. A new correlation for heat transfer coefficients for laminar flow slurries in a horizontal circular tube was developed. The new correlation was found to be capable of predicting heat transfer data within an error of 15%. The results from the study were expected to be useful in designing thermal storage systems and compact heat exchangers using micro-encapsulated P.C.M. slurries.

Rao et al. [31] studied convective heat transfer characteristics in rectangular copper minichannels using microencapsulated n-octadecane P.C.M. particles in water. They used channels with a hydraulic diameter of 2.71 mm. Micro-encapsulated P.C.M. particles with average size of 4.97 μm were used and their volume concentration was varied between 0 to 20%. All the experiments were performed in the laminar flow regime by varying the mass flow rates and heat flux applied. Their study showed that 5%

suspension always gave a better cooling performance than water within the range of mass flow rates from 0.05 to 0.35 kg/min. The suspensions with higher mass concentrations were found to be effective only at low flow rates. They proposed the use of high concentration of micro-encapsulated P.C.M. particles at low flow rates to obtain better cooling performance.

Wang et al. [32] conducted an experimental study using microencapsulated bromohexadecane P.C.M. particles with mass concentrations ranging from 0 to 27.6%. They used a circular tube of 4 mm internal diameter in their experiments. Two new Nusselt number correlations were proposed for predicting the heat transfer behaviors of microencapsulated P.C.M. slurry in a circular tube. The newly developed correlations for laminar and turbulent flow regime predict heat transfer data within an error of 10%.

Chen et al. [33] studied heat transfer in microencapsulated P.C.M. suspension for laminar flow through a circular tube under constant heat flux. They used bromohexadecane as the P.C.M. particle with an average size of 8.2 μm. The wall temperature was measured using temperature sensors and the mixed mean fluid temperature was obtained by calculation. The mixed mean fluid temperature was obtained by dividing the tube length into three sections namely solid region, phase change region and liquid region. Homogeneous model was used for calculating the thermo-physical properties of the P.C.M. slurry. Their results showed that about 30% decrease in dimensionless internal wall temperature can be obtained as compared to pure water. Phase change of 15.8 wt% of micro-encapsulted P.C.M. suspension was found to increase the effective specific heat

by 28.1% when compared with pure water. They also developed a new expression for Stefan number.

Ravi [11] numerically studied forced convection heat transfer behavior of P.C.M. slurry in tubes with internal longitudinal fins. Two boundary conditions namely uniform axial and peripheral temperature and uniform axial heat flux with constant peripheral temperature were used in his study. The flow at the inlet of the tube was assumed to be hydro dynamically fully developed. The phase change of P.C.M. particles was modeled using effective specific heat method. He observed that the Nusselt number results were strongly dependent on the Stefan number in case of smooth circular tube containing P.C.M. slurry. For tube with internal longitudinal fins, the Nusselt number was found to depend on Stefan number, fin height and thermal conductivity of fins.

Zeng et al. [34] studied both experimentally and numerically the heat transfer characteristics of microencapsulated P.C.M. slurry in a circular tube under constant heat flux. Their results showed that Ste number and the melting range were the most important parameters influencing the Nusselt number fluctuation profile and the dimensionless wall temperature in the phase change heat transfer region. The dimensionless wall temperature and the Nusselt number profile were also influenced by bulk Reynolds number and P.C.M. volume concentration.

2.2 P.C.M. Slurry Flow in Microchannels

Compared to conventional channels, few studies have focused on the thermal performance of P.C.M. slurry flow in microchannels.

Xing et al. [35] were the first authors to investigate the heat transfer performance of P.C.M. slurry flow in microchannels. They evaluated the performance of liquid flow with microsized or nanosized encapsulated P.C.M. particles in circular microchannels. A two phase, non thermal equilibrium model was used to solve the fluid flow and heat transfer in the microchannel while considering the effects of particle-particle interaction and the particle depletion boundary near the wall. In the simulations, the particle viscosity was taken as 0.01 $Pa \cdot s$ as a first degree of approximation. A tube of 122 μm diameter with a length of 12.2 cm was used in the simulations. Spherical P.C.M. particles of n-octadecane with a diameter of 6.3 μm were used in carrier fluid water. The results presented in this study correspond to 25% volume concentration of P.C.M. particles in the carrier fluid. The local heat transfer coefficient of the P.C.M. slurry along the length of the tube was lower than water at all locations except during phase change. The local heat transfer coefficient of the P.C.M. slurry exceeded the local heat transfer coefficient of water during the phase change of P.C.M. particles. The authors defined effectiveness factor and performance index to investigate the heat transfer performance under different Reynolds number and wall heat fluxes. Maximum heat transfer enhancement with P.C.M.

particles was achieved at low Reynolds number when optimum wall heat flux was applied.

Sabbah et al. [36] performed a three-dimensional numerical study on the performance of microchannel heat sinks using micro-encapsulated P.C.M.s. They considered the thermal resistance of the heat sink walls while taking temperature dependent physical properties for the P.C.M. slurry. The effects of micro-convection around solid particles, particle-wall interactions and particle-particle interactions were taken into account by using effective thermal conductivity. The P.C.M. volume concentrations were varied between 0 to 25% using microencapsulated P.C.M. particles of 10 μm diameter. They emphasized the need to use temperature dependent slurry properties especially for pressure drop estimation as the dynamic viscosity of water is a very sensitive function of temperature. They concluded that lower and uniform temperature can be obtained in electronic devices when micro-encapsulated P.C.M. slurries are used as compared to water. Moreover, a lower mass flow rate was required to obtain low temperatures in electronic devices when micro-encapsulated P.C.M. slurries were employed as the heat transfer fluid.

Kondle et al. [37] numerically studied heat transfer characteristics of P.C.M.s in laminar flow for circular and rectangular microchannels. The bulk fluid consisting of carrier fluid and particles was modeled using homogeneous model while a specific heat model was used to model the phase change of particles. In their study, they used 15% volume concentration of n-Eicosane P.C.M. particle in carrier fluid water. The effect of particle-particle interaction effects were neglected in their study. A fully developed velocity

profile was used at the inlet. The heat transfer characteristics of P.C.M. slurry flow for various aspect ratios of microchannels were also compared in the study. They used microchannels with aspect ratios of 1:2, 1:4 and 1:8. The authors concluded that the Nusselt number was higher for the constant axial heat flux with constant peripheral temperature boundary condition compared to that corresponding to the constant heat flux with variable peripheral temperature.

Thermal performance of nano-encapsulated P.C.M. slurry in microchannels was numerically studied by Kuravi et al. [38]. They used nano-encapsulated P.C.M. particles of n-octadecane in carrier fluid poly-alpha-olefin (PAO). The effect of shell material was neglected due to its negligible thickness for nanosized particles. They studied the influence of particle concentration, inlet temperature, melting range of the P.C.M. and heat flux on the heat transfer performance. They also used a homogeneous model and modeled the phase change of particles using effective specific heat method. Due to the small microchannel dimensions used, the flow within the microchannel was not developed. A sine profile was used for varying specific heat in the melting range. Their results show that increase in volume concentration of P.C.M. particles improves the heat transfer performance of the slurry. Their findings reveal that inlet temperature has a significant effect on the thermal performance of the slurry. Their results were expected to depend on channel dimensions.

Kuravi et al. [39] investigated the heat transfer performance of water-based microencapsulated P.C.M. slurry in manifold microchannels both experimentally and

numerically. For the experimental study, they used water as the carrier fluid and 5 μm diameter n-octadecane as the P.C.M. particle. A microchannel of hydraulic diameter of 170 μm was used in their study. Their findings reveal that the slurry performance was poorer compared with pure fluid due to the large size of particles used and lower thermal conductivity of slurry compared with water. They also performed a parametric study with nano-encapsulated P.C.M. slurry flow. In the parametric study, water and poly-alpha-olefin (PAO) were used as the base fluids with n-octadecane as the P.C.M. particle. The particle size was 100nm and the microchannel width was 101 μm. The enhancement in thermal conductivity due to micro-convection was found to be negligible for 100 nm sized particles. Their numerical study showed that using higher-thermal-conductivity P.C.M., narrower channels, smaller particles will aid in obtaining better thermal performance of P.C.M. slurry compared with pure fluid.

Alquaity et al. [40] numerically investigated microchannel flow with water in the presence of micro-sized lauric acid P.C.M. particles. They used the Discrete Phase Model (D.P.M.) [15] to model the flow and heat transfer in the microchannel. The D.P.M. model treats the carrier fluid as continuous phase by solving the Navier-Stokes equation. The P.C.M. particles are treated as dispersed phase and their flow is solved by tracking the particles through the calculated flow field [15]. An effective specific heat method was used to model the phase change of particles with a constant value of specific heat in the melting range. Their study showed that increase in P.C.M. particle concentration increases the heat storage capability of the carrier fluid.

2.3 Summary of Literature Review

Most of the previous numerical studies conducted using P.C.M. slurry flow in regular channels or microchannels have used homogeneous model. However, the numerical studies completed using modeling frameworks other than homogeneous model have not presented the reasons behind the selection of their particular modeling methodology. Moreover previous studies did not present the effect of volumetric entropy generation in the microchannel due to the addition of P.C.M. particles. The effect of operating conditions like mass flow rate of the slurry and heat flux on the length required for phase change of the P.C.M. particles for different particle volume concentrations was also not investigated in detail. Therefore, in this thesis work, two different modeling approaches are first compared and homogeneous model is identified to be used for further analysis. Using homogeneous model, the effectiveness ratio, performance index and merit number are calculated for different operating conditions and volume concentrations of P.C.M. particles. These three ratios, namely effectiveness ratio, performance index and Merit number guide the designer regarding the conditions to be used in order to obtain maximum benefit in terms of heat storage capacity by the addition of P.C.M. particles. This thesis work is the first study to present the volumetric entropy generation rate due to heat transfer and fluid friction in case of P.C.M. slurry flows. Also the length required for the phase change of P.C.M. particles is presented for different operating conditions.

CHAPTER 3

MODEL STUDY

This chapter consists of two sections. The first section gives detailed information about the different models used for formulating the fluid flow and heat transfer problem of P.C.M. slurry in microchannel. The second section of this chapter defines the problem statement along with the required boundary conditions.

3.1 Models and Formulation

Presently there are two approaches available for the modeling of two phase flows viz. the Euler-Lagrange approach and the Euler-Euler approach. One of the main objectives of this thesis work is to identify a unified model that can provide design guidelines for experiments using P.C.M. slurry flows in microchannels. Therefore, both the aforementioned modeling approaches are compared in this study. The Discrete Phase Model (D.P.M.) [15] in CFD software FLUENT^{TM} follows the Euler-Lagrange approach. The homogeneous model follows the Euler-Euler approach.

3.1.1 Discrete Phase Model

In this model, the carrier fluid is treated as continuum by solving the Navier-Stokes equation, while the dispersed phase (P.C.M. particles in this case) is solved by calculating the particle movement through the calculated flow field. The dispersed phase is allowed to exchange momentum and energy with carrier fluid.

The following assumptions are made in the formulation of the problem:

1. A steady and laminar flow exists within the microchannel.
2. The phase change of particles occurs between the solidus and liquidus temperatures.
3. There is no temperature gradient inside the P.C.M. particle [38].
4. The effect of particle-particle interaction is negligible.
5. Negligible effect of the shell material encapsulating the nanosized P.C.M. particle [39].

The equations governing laminar flow for the carrier fluid are shown below:

Conservation of mass:

$$\nabla \cdot \vec{v} = 0 \tag{3.1.1}$$

Conservation of momentum:

$$\nabla \cdot \left(\rho \vec{v} \vec{v} \right) = -\nabla p + \mu \nabla^2 v + \vec{F} \tag{3.1.2}$$

Conservation of energy:

$$\nabla \cdot \left(\vec{v}\left(\rho E + p \right) \right) = \nabla \cdot k \nabla T + S \tag{3.1.3}$$

where *v* is the carrier fluid velocity, ρ is the carrier fluid density, p is the pressure, μ is the carrier fluid viscosity. *F* in the above equation represents the momentum change of the particles as it passes through a control volume. In the energy equation, *E* represents the energy per unit mass, *k* represents the carrier fluid thermal conductivity, *T* is the temperature of the carrier fluid and *S* represents the change in thermal energy of the particle as it passes through a control volume.

The particles are injected uniformly at the inlet of the microchannel. The trajectory of the particles in the flow domain is obtained by integrating the force balance on the particle. The forces acting on the particle are the drag force and the virtual mass force [15]. The force balance equating the inertia of the particle to the forces acting on the particle, in the x direction is given below:

$$\frac{du_P}{dt} = F_D\left(u_f - u_P \right) + F_x \tag{3.1.4}$$

where F_D is the drag force per unit particle mass , F_x is the virtual mass force per unit mass acting on the particle, u_P is the x-component of particle velocity and u_f is the x-component of carrier fluid velocity. The drag force per unit particle mass is given as:

$$F_D = \frac{18\mu_f}{d_P^2 \rho_P} \frac{C_D \operatorname{Re}_{rel}}{24} \tag{3.1.5}$$

The virtual mass force F_x is defined as:

$$F_x = \frac{1}{2}\frac{\rho_f}{\rho_P}\frac{d\left(u_f - u_P\right)}{dt} \tag{3.1.6}$$

where μ_f is the carrier fluid viscosity, d_p is the particle diameter, ρ_f is the carrier fluid density and ρ_p is the density of P.C.M. particles.

Re_{rel} is the relative Reynolds number which is:

$$\mathrm{Re}_{rel} = \frac{\rho_f d_p \left|u_p - u_f\right|}{\mu_f} \tag{3.1.7}$$

The drag coefficient C_D for smooth spherical particles is

$$C_D = b_1 + \frac{b_2}{\mathrm{Re}_{rel}} + \frac{b_3}{\mathrm{Re}_{rel}^{\ 2}} \tag{3.1.8}$$

where b_1, b_2 and b_3 are constants given by Morsi and Alexander [41].

The momentum transfer from the fluid to the particles is obtained by computing the change in momentum of the particle as it passes through each control volume as given below:

$$\overrightarrow{F} = \sum\left(F_D\left(u_P - u_f\right) + F_x\right)\dot{m}_P \Delta t \tag{3.1.9}$$

where $\dot{m}_P$ is the mass flow rate of the particle. The momentum transfer appears as a sink or source in the momentum equation for the carrier fluid. The heat transfer from the carrier fluid to the particles is obtained by computing the change in thermal energy of

particles as it passes through each control volume. The change in thermal energy of particles as they pass through each control volume is calculated as:

$$S = m_P \int_{T_r}^{T_{in}} c_p dT - m_P \int_{T_r}^{T_{out}} c_p dT \tag{3.1.10}$$

The heat transfer term in the above equation appears as a source or sink term in the energy equation for the carrier fluid (Equation (3.1.3)).In order to account for the phase change of the particles, a specific heat model is used [37]. In the specific heat model, the phase change of particles is modeled by varying the specific heat capacity of the particles between the solidus and the liquidus temperatures. The equations used for calculating the specific heat capacity of the particles are as follows:

For $T_p < T_{solidus}$

$$c_p = c_{p,S} \tag{3.1.11}$$

For $T_{solidus} < T_p < T_{liquidus}$

$$c_p = \frac{c_{p,S} + c_{p,L}}{2} + \frac{L_{fusion}}{T_{liquidus} - T_{solidus}} \tag{3.1.12}$$

For $T_P > T_{liquidus}$

$$c_p = c_{p,L} \tag{3.1.13}$$

where c_p is the specific heat of the particle. $c_{p,S}$ and $c_{p,L}$ are the specific heats of the particle in solid and liquid states. In the above equations L_{fusion} represents the latent heat

of fusion of the particles, $T_{solidus}$ represents the lower melting temperature of P.C.M. particles and $T_{liquidus}$ represents the upper melting temperature of P.C.M. particles.

There are however certain limitations in the use of the Discrete Phase Model. The volume concentration of the discrete phase is limited to 10-12%. The limit on the discrete phase volume fraction is due to the inherent assumption of negligible particle-particle interaction. However, there is no limit on the mass fraction of the discrete phase and as such the mass of the discrete phase can exceed the mass of the carrier fluid. The D.P.M. does not provide any detailed information about the velocity and temperature of the discrete phase. The D.P.M. only shows the particle tracks for the discrete phase. D.P.M. however, gives detailed information about the temperature, velocity and pressure drop of the carrier fluid. The D.P.M. is also computationally expensive.

3.1.2 Homogeneous Model

In the homogeneous model, the P.C.M. particles and the carrier fluid are assumed to have the same temperature and velocity. The governing equations of mass, momentum, and energy are solved for the bulk fluid with the appropriate effective thermo-physical properties. Therefore the accuracy of the models used for calculating the effective thermo-physical properties is very important.

In order to formulate the flow and heat transfer problem using homogeneous model, the following assumptions are made:

1. The flow of the bulk fluid inside the microchannel is steady and laminar.

2. The distribution of particles inside the microchannel is homogeneous [38].
3. The bulk fluid is Newtonian up to particle volume concentrations of 30% [38].
4. The P.C.M. particle melts instantaneously once the melting temperature is reached i.e. there is no temperature gradient within the P.C.M. particle [38].
5. The phase change of particles occurs between the solidus and liquidus temperatures.
6. The effect of the shell material encapsulating the nanosized P.C.M. particle is negligible [39].

The equations governing laminar flow for the bulk fluid are shown below:

Conservation of mass:

$$\nabla \cdot \vec{v} = 0 \tag{3.1.14}$$

Conservation of momentum:

$$\nabla \cdot \left(\rho_b \vec{v}\vec{v} \right) = -\nabla p + \mu_b \nabla^2 v \tag{3.1.15}$$

Conservation of energy:

$$\nabla \cdot \left(\rho_b \vec{v} c_{pb} T \right) = \nabla \cdot \left(k_b \nabla T \right) \tag{3.1.16}$$

where v is the bulk fluid velocity, ρ_b is the bulk fluid density, p is the pressure, and μ_b is the viscosity of the bulk fluid. In the above equation c_{pb} represents the bulk fluid specific heat, k_b is the bulk fluid thermal conductivity and T is the temperature of the bulk fluid.

3.1.3 Bulk Fluid Thermo-physical Properties

The models used for calculating the effective thermo-physical properties of the bulk fluid are given below:

3.1.3.1 Viscosity. The introduction of P.C.M. nanoparticles into the carrier fluid increases its viscosity. Fang et al. [14] measured the slurry viscosity of nano-encapsulated P.C.M. particles of average diameter of 124 nm. They used n-octadecane as the P.C.M., polystyrene as the shell material and water as the carrier fluid. Slurry viscosity for different mass concentrations and slurry temperatures was measured. The experimental data available for slurry viscosity at 303 K is compared with the bulk viscosity calculated using Vand's correlation [42]. The bulk viscosity using Vand's correlation is calculated as [42]:

$$\mu_b = \left(1 - c - 1.16c^2\right)^{-2.5} \mu_f \tag{3.1.17}$$

where μ_f is the viscosity of the carrier fluid and c is the volume concentration of P.C.M. particles.

The above correlation for bulk viscosity is in good agreement with experimental data presented by Fang et al. [14] for nanoparticle volume concentrations below 11%. Therefore Vand's correlation is used for the calculation of bulk viscosity in this study.

3.1.3.2 Thermal conductivity. The thermal conductivity of solid-liquid suspensions was observed to increase in laminar flow because of the effects of microconvection around the solid particles and the particle-to-particle interaction. The degree of the enhancement of thermal conductivity was found to increase with increasing particle diameter [24]. However, for nanosized particles, the enhancement in thermal conductivity is found to be negligible.

A lot of experimental studies have been done in the past decade to measure the thermal conductivity of nanofluids. The nanofluid thermal conductivity data was sparse and inconsistent which prompted an International Nanofluid Property Benchmark Exercise (I.N.P.B.E). In I.N.P.B.E., the thermal conductivity of identical samples of nanofluids was measured by over 30 organizations using several experimental approaches. The nanofluids tested in their exercise consisted of nanosized particles of variety of materials and shapes, and at low and high particle concentrations. The highest volume concentration of nanosized particles used in their study was 26%. The effect of temperature on thermal conductivity was, however, not investigated in their study. Their findings revealed that the effective medium theory developed for dispersed particles by Maxwell [43] and generalized by Nan et al. [44] was in good agreement with their experimental data [45]. Their results did not show any anomalous enhancement of thermal conductivity by the addition of small volume concentrations of nanosized particles. For spherical particles and negligible interfacial resistance, Nan's equation reduced to Maxwell's equation. In order to observe the effect of non-spherical particles

and presence of interfacial resistance, effective thermal conductivity calculated using Nan's equations [44] is compared with the value obtained using Maxwell's model. For the comparison, typical value of 10^{-8} m^2 K/W for interfacial resistance is considered [45]. Nano particles in the shape of rods with an aspect ratio of 8 are used to see the effect of shape of nanosized particles on their thermal conductivity. Figure 3.1 shows the comparison of thermal conductivity ratio obtained using Nan's model and Maxwell's model. From Figure 3.1, it can be observed that the change in shape of the particles from sphere to rods causes reduction in the bulk thermal conductivity. Increase in interfacial thermal resistance also reduces the effective thermal conductivity. However, the difference between the effective thermal conductivities obtained in the three different cases is less than 1% (Figure 3.1). Consequently, in this study, Maxwell's model is used for the calculation of effective thermal conductivity of the bulk fluid. The bulk thermal conductivity using Maxwell's model is calculated as [43]:

$$k_b = k_f \frac{2 + k_p/k_f + 2c\left(k_p/k_f - 1\right)}{2 + k_p/k_f - c\left(k_p/k_f - 1\right)} \tag{3.1.18}$$

Where k_p is the particle thermal conductivity and k_f is the carrier fluid thermal conductivity.

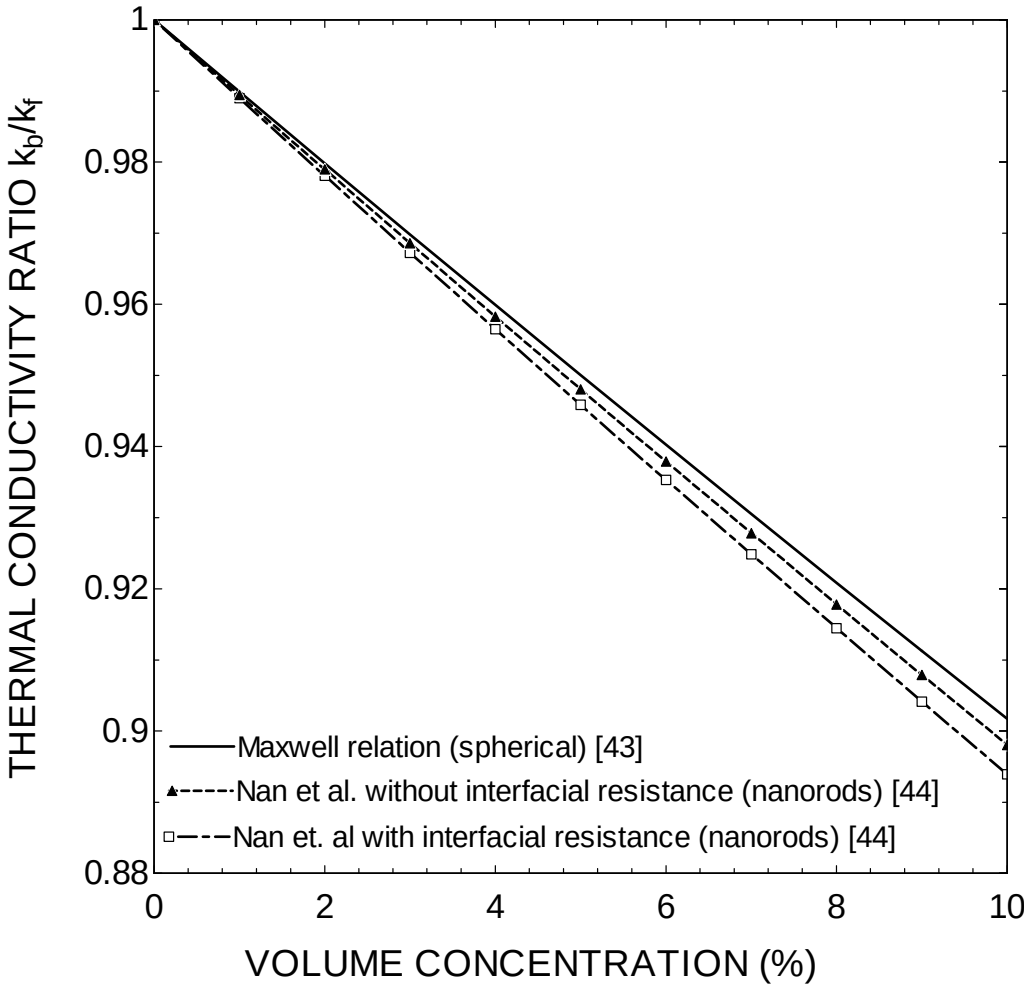

Figure 3.1 Thermal conductivity ratio of nanosized P.C.M. particles

3.1.3.3 Density. The density of the bulk fluid can be calculated using mass balance as [36]:

$$\rho_b = c\rho_p + (1-c)\rho_f \tag{3.1.19}$$

where ρ_p is the density of the particles and ρ_f is the carrier fluid density.

3.1.3.4 Specific heat. An effective specific heat model is used to account for the phase change of the particles in the microchannel by varying the specific heat capacity of the particles across the solidus and the liquidus temperatures. The specific heat of the bulk fluid is calculated using energy balance as [36]:

For $T_p < T_{solidus}$

$$c_{pb} = \frac{c\left(\rho c_{p,S}\right)_p + (1-c)\left(\rho c_p\right)_f}{\rho_b} \tag{3.1.20}$$

For $T_{solidus} < T_p < T_{liquidus}$

$$c_{pb} = \frac{c\left(\rho\left(\frac{c_{p,S}+c_{p,L}}{2} + \frac{L_{fusion}}{T_{liquidus}-T_{solidus}}\right)\right)_p + (1-c)\left(\rho c_p\right)_f}{\rho_b} \tag{3.1.21}$$

For $T_P > T_{liquidus}$

$$c_{pb} = \frac{c\left(\rho c_{p,L}\right)_p + (1-c)\left(\rho c_p\right)_f}{\rho_b} \tag{3.1.22}$$

where $\left(c_p\right)_f$ is the specific heat of the carrier fluid, $\left(c_{p,S}\right)_p$ is the specific heat of the P.C.M. particle in solid state and $\left(c_{p,L}\right)_p$ is the specific heat of the P.C.M. particle in the liquid state.

3.2 Problem Statement and Boundary Conditions

Figure 3.2 shows the schematic diagram of the microchannel used in the present study. The microchannel of constant height (50 μm, H), width (2 mm, A) and length (35 mm, B) is used in the FLUENT™ simulations. The carrier fluid with nanosized particles of 50 nm diameter enters the microchannel at a temperature just below the melting temperature of the particles. A constant heat flux is applied at the bottom wall, which heats up the carrier fluid and nanosized P.C.M. particles. After traversing a certain length of the microchannel, the particles undergo phase change. The phase change of the particles plays an important role in decreasing the bulk temperature rise of the suspension as compared to the case with no phase change and thereby increases the thermal storage capacity of the suspension.

From Figure 3.2 it can be easily observed that the microchannel width is much larger than its height. This shows that the problem can be reduced to 2D and is similar to the flow and heat transfer problem of P.C.M. slurry between parallel plates (Figure 3.3). Figure 3.3 shows the schematic diagram of the 2D microchannel of constant height (50 μm, H) and length (35000 μm, L) used in this model study.

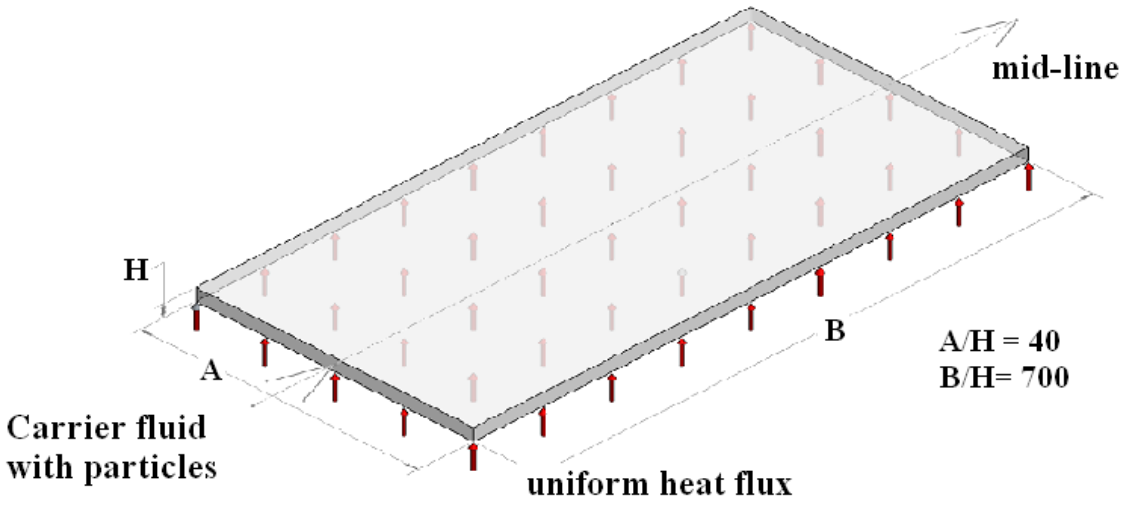

Figure 3.2 Schematic diagram of the microchannel used in the FLUENT™ simulations (H = 50 μm).

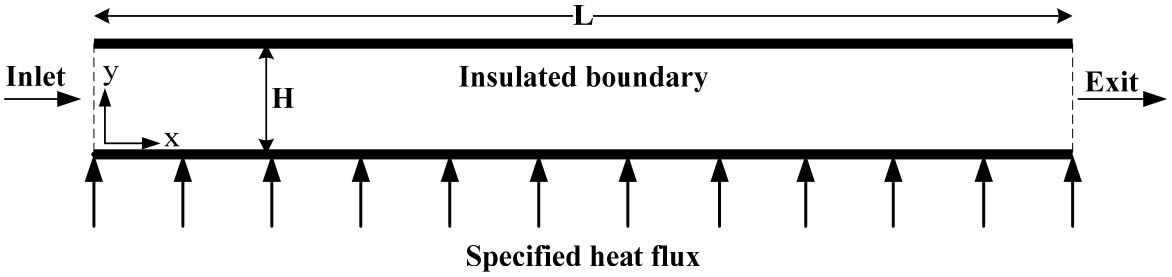

Figure 3.3 Geometry and flow direction in the 2D microchannel used in the FLUENT™ simulations.

Table 3.1 compares the results of 2D simulation with 3D simulation for flow in a microchannel of width 2 mm for D.P.M. and homogeneous models. The results show that there is a negligible difference between values of pressure drop and temperature rise of the fluid for the cases of using 2D and 3D. The maximum percentage difference between 2D and 3D simulation for both the models is well below 2%. Therefore 2D simulations are used for further analysis.

3.2.1 Boundary Conditions

A uniform velocity profile is defined at the inlet of the microchannel. The temperature of the bulk fluid is specified as 315 K at the inlet, which is lower than the melting temperature of the P.C.M. particles.

$$T(0, y) = 315\ K \tag{3.1.23}$$

A constant heat flux is specified at the bottom wall of the microchannel.

$$q'' = -k \left. \frac{\partial T}{\partial y} \right|_{y=0} \tag{3.1.24}$$

Insulated boundary condition is applied at the top wall of the microchannel.

$$\left. \frac{\partial T}{\partial y} \right|_{y=H} = 0 \tag{3.1.25}$$

Pressure outlet boundary condition is used at the outlet of the microchannel. The pressure outlet boundary condition assumes an absolute pressure of 1 atm at the outlet and zero diffusion fluxes in the direction normal to the exit plane for all flow variables (i.e., the velocity and temperature) except pressure.

$$\left.\frac{\partial \phi}{\partial x}\right|_{x=L} = 0 \tag{3.1.26}$$

where ϕ is any flow property except pressure and L is the length of the microchannel.

Table 3.1 Comparison between 2D and 3D simulations

	Discrete Phase Model			Homogeneous Model		
	2D	3D	Percentage difference (%)	2D	3D	Percentage difference (%)
ΔT (K)	4.486	4.483	-0.05	4.75	4.74	-0.12
ΔP (Pa)	472.06	473.27	0.26	633.5	643.6	1.57

In this study, water is used as the carrier fluid and lauric acid as the P.C.M. particle with volume concentrations ranging from 0 to 10%. Table 3.2 contains the thermo-physical properties of the P.C.M. particles which are assumed to be constant during the simulations. The thermo-physical properties of carrier fluid are assumed to be temperature dependent.

Table 3.3 shows the comparison of the temperature rise and pressure drop in case of using constant thermo-physical properties and temperature dependent thermo-physical properties. The temperature rise shows a negligible difference in both cases, but the use of constant thermo-physical properties leads to pressure drop being over-estimated by about 30%. This result motivates performing simulations using temperature dependent properties for the carrier fluid despite the longer computation time.

Table 3.2 Thermo-physical properties of P.C.M. particles

Fluid	Density kg/m^3	Specific Heat kJ/kg K	Latent Heat kJ/kg	Thermal conductivity W/m K
Particle (Solid)	1007	1.76	211	0.147
Particle (Liquid)	862	2.27	-	0.147

Table 3.3 Comparison between constant properties and temperature dependent properties

	Constant properties	Temperature dependant properties	Percentage difference (%)
ΔT (K)	33.69	33.7	0.04
ΔP (Pa)	10621.7	8193.8	29.6

CHAPTER 4

NUMERICAL STUDY

Control volume approach is used to discretize the governing equations using FLUENT^{TM} 12.1.2 code [15]. All variables are computed at each grid point except the velocities, which are determined midway between the grid points. A staggered grid arrangement is used in the present study, which links the pressure through the continuity equation and is known as SIMPLE algorithm [46]. The pressure relationship between continuity and momentum is established by transforming the continuity equation into a Poisson equation for pressure.

The flow of P.C.M. slurry through the microchannel is solved as a two dimensional problem using the double precision solver. The default under-relaxation factors provided in FLUENT^{TM} 12.1.2 are used for pressure, x-momentum, y-momentum and energy equations. The convergence criterion for the scaled residuals is set to 10^{-6} for continuity and 10^{-9} for energy equation. . In addition to the scaled residuals, the temperature at the outlet of the microchannel is monitored using a surface monitor to ensure convergence.

Second order upwind schemes are used for discretization of momentum and energy equations.

4.1 Grid Independence

A numerical mesh generator is used to create the geometry and mesh the domain using hexahedral elements. A fine mesh is created near the walls to capture the large gradients normal to the flow direction. Three different grid resolutions, 35x18000, 40x28000 and 50x35000 are used to obtain a grid-independent solution. Figure 4.1 compares the local Nusselt number obtained using the three grids and shows a good agreement between the local Nusselt number values. The maximum difference in Nusselt number for the three different grids used is 0.14.

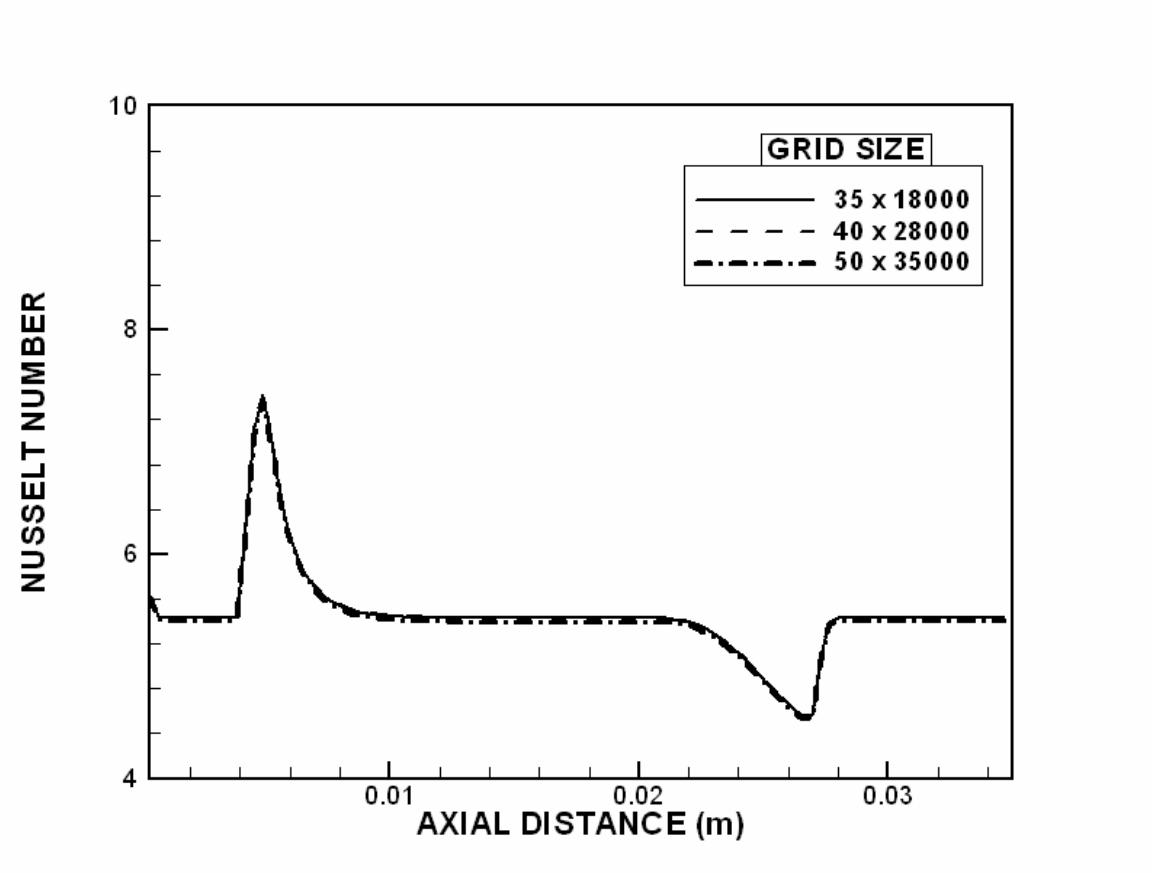

Figure 4.1 Grid independence test for Nusselt number along the axial distance of the microchannel.

4.2 Validation

The D.P.M. and homogeneous models used in this study are validated by comparing with experimental data for P.C.M. slurry flow in a 3.14 mm diameter circular tube [20]. Figures 4.2 and 4.3 show the comparison of wall temperature obtained using D.P.M. and homogeneous models with the experimental data for 10% particle volume concentration and slurry Reynolds number of 200 presented in [20]. Figure 4.2 compares the wall temperature for Stefan number of 2, while Figure 4.3 shows the comparison of the wall temperature for Stefan number of 3. It can be observed that the wall temperatures predicted by both models compare well with the experimental data presented for the two Stefan numbers.

Figure 4.4 compares the Nusselt number predicted using homogeneous model with experimental data presented for 15.8 wt% P.C.M. slurry flow in 4 mm diameter tube [33]. The comparison is done for two Reynolds number and Stefan number combinations i.e. Reynolds numbers of 691 and 1418, and Stefan numbers of 1.09 and 1.38. It can be observed that the Nusselt number predicted by the homogeneous model compares well with the experimental data.

The non-dimensional length used in Figure 4.4 is defined as

$$x^{+} = \frac{2x}{D_h \,\mathrm{Re}\,\mathrm{Pr}} \tag{4.2.1}$$

where D_h is the hydraulic diameter of the microchannel, Re is the Reynolds number of the bulk fluid and Pr is the Prandtl number of the bulk fluid.

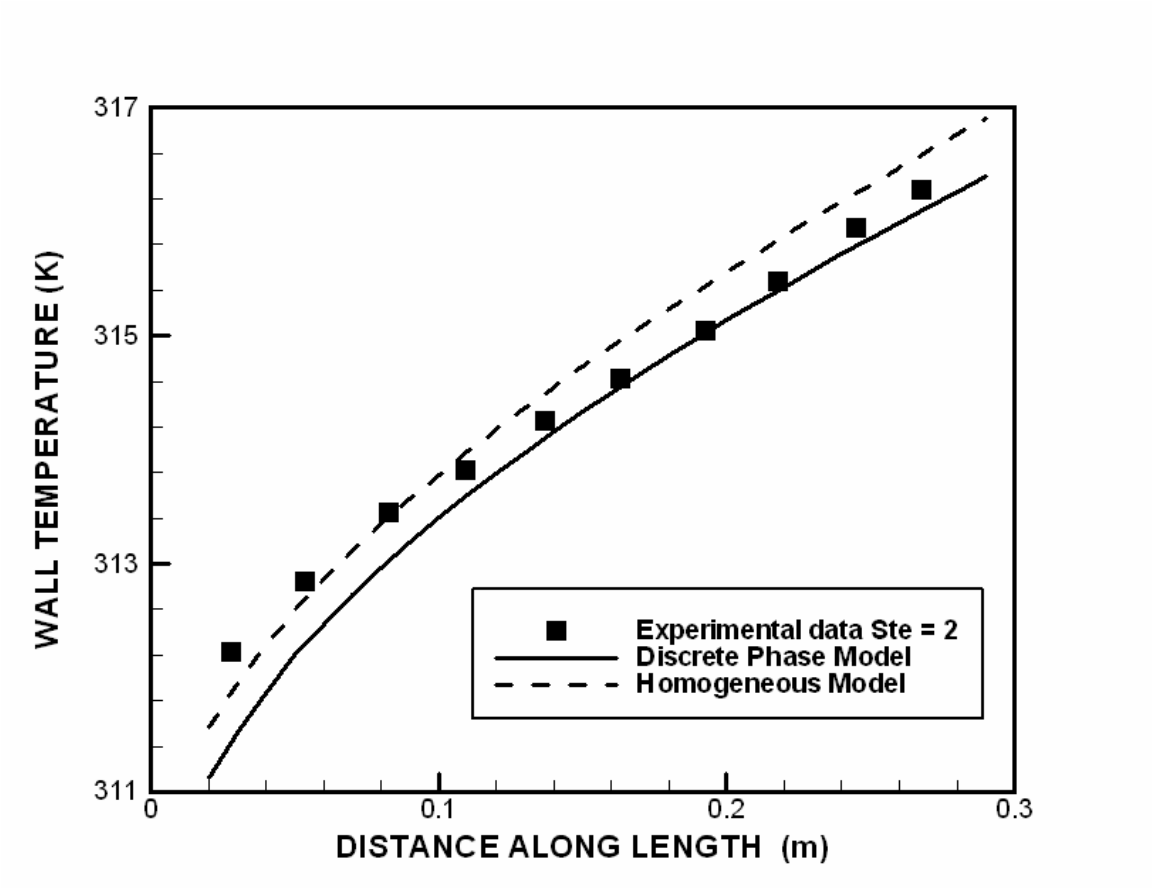

Figure 4.2 Wall temperatures obtained using D.P.M. and homogeneous model with experimental data for Stefan number of 2 [20].

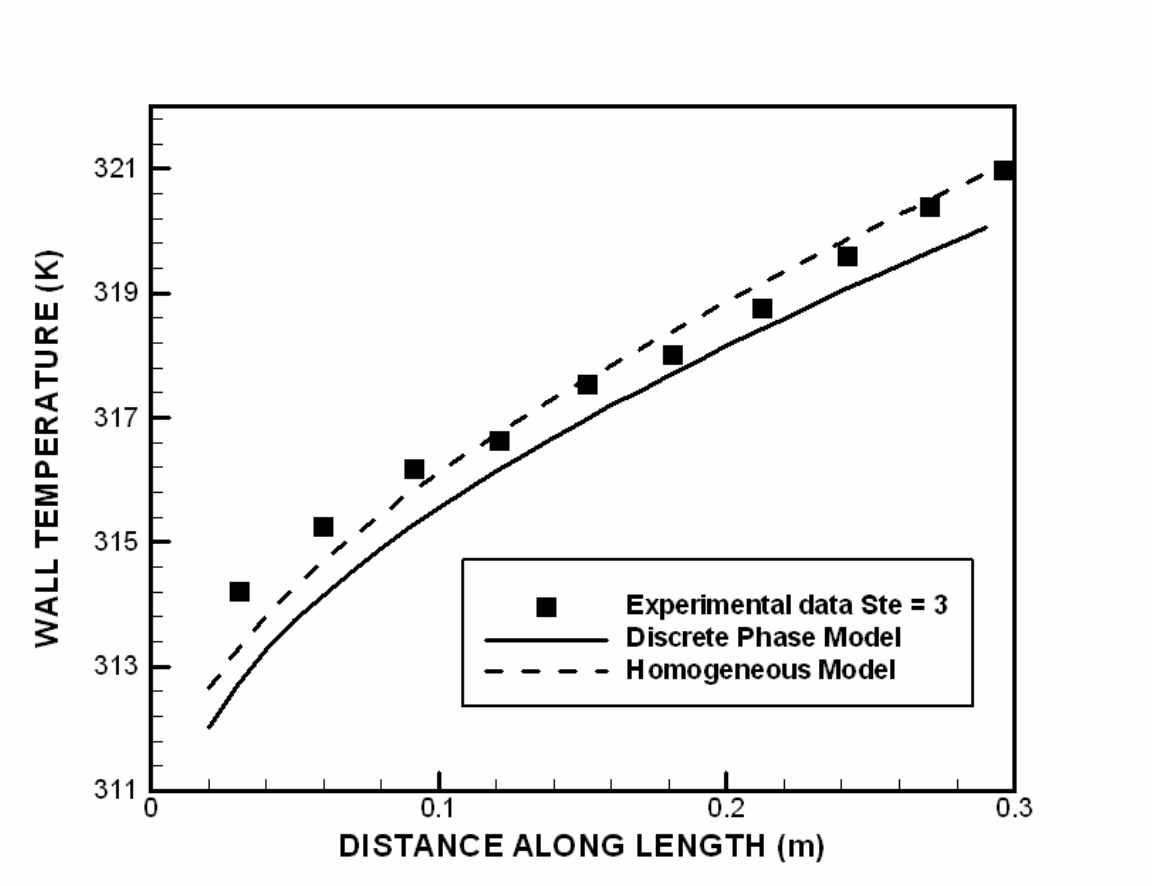

Figure 4.3 Wall temperatures obtained using D.P.M. and homogeneous model with experimental data for Stefan number of 3 [20].

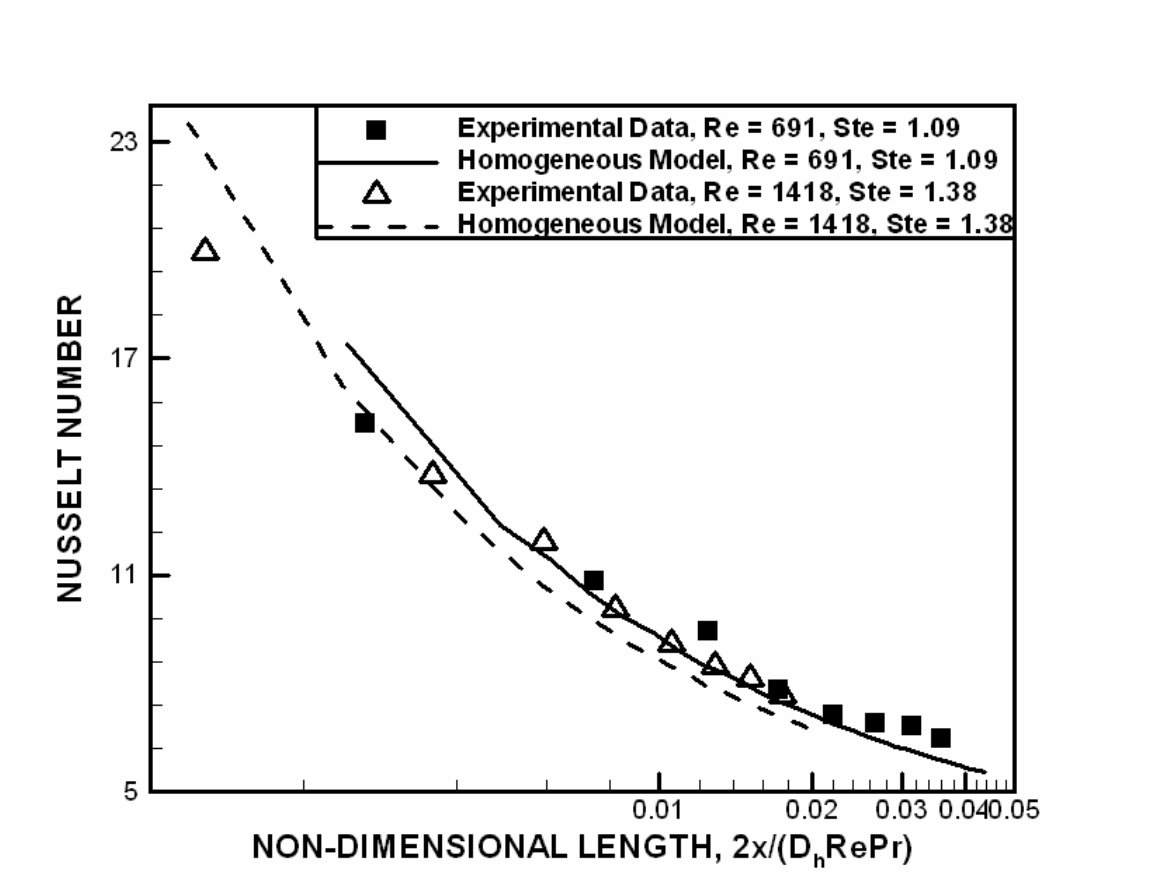

Figure 4.4 Comparison of Nusselt number obtained using homogeneous model with experimental data [33].

After the grid independence test, the grid used for the simulations is validated against analytical Nusselt number and fanning friction factor results for 2D parallel plate subjected to constant heat flux boundary condition at the top and bottom walls [1]. The numerical value of Nusselt number is within 2% of analytical Nusselt number, while the numerical value of friction factor matched exactly with the analytical value.

The entropy generation rate calculated using FLUENT^{TM} is validated by comparing with analytical results for entropy generation rate in a uniformly heated tube. Pure water flow is considered in a tube of radius 50 μm and length 4cm. The dimensionless entropy generation rate for Hagen-Poiseuille flow through a smooth tube of radius r_0 subjected to a uniform heat flux q can be expressed as [47]:

$$S_{gen}''' \frac{kT_{in}^2}{q''^2} = \left(\frac{2kT_{in}}{\rho c_p u r_0 T} \right)^2 + \left(\left(2\frac{r}{r_0} - \left(\frac{r}{r_0} \right)^3 \right) \frac{T_{in}}{T} \right)^2 + \frac{16\mu k T_{in}^2 u^2}{q''^2 T r_0^2} \left(\frac{r}{r_0} \right)^2 \qquad (4.2.2)$$

where T_{in} is the inlet temperature to the tube, q'' is the uniform heat flux applied to the tube and r_0 is the tube radius.

Figure 4.5 shows a comparison between the dimensionless entropy generation rate obtained using FLUENT^{TM}, and the analytical value given by Equation (4.2.2). It can be observed that the dimensionless entropy generation rate values obtained using the simulation match well with the analytical values.

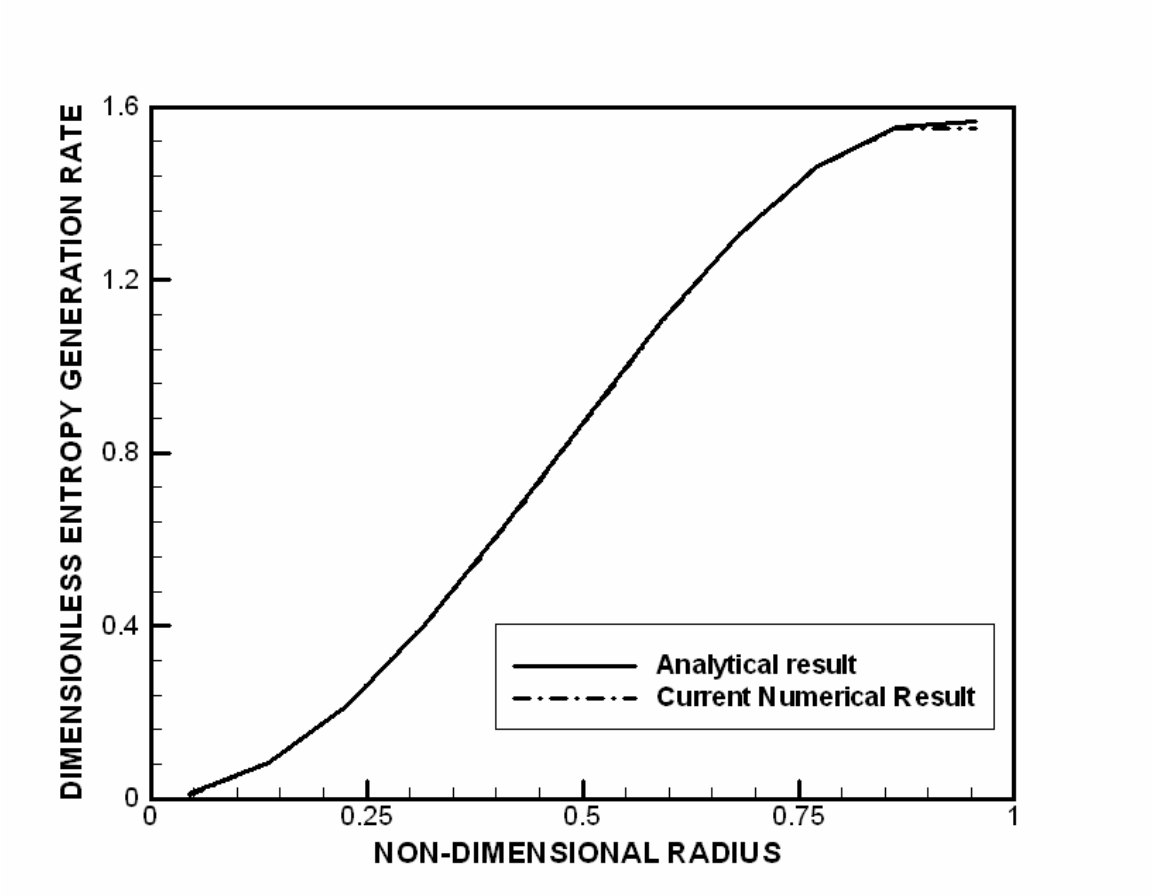

Figure 4.5 Dimensionless entropy generation rate along the tube radius, obtained using simulation with analytical values.

CHAPTER 5

RESULTS AND DISCUSSION

This chapter consists of four sections. In each section, the operating conditions used for the study and the results obtained are presented and discussed. The results presented in each section pertain to the objectives discussed in the first chapter.

5.1 Identification of a Unified Model

The numerical simulation of velocity and temperature fields is carried out for liquid flow with nanosized P.C.M. particles in a microchannel using D.P.M. and homogeneous models. The temperature field, pressure drop and Nusselt number obtained using the two models are presented in this section.

In both the D.P.M. and homogeneous models, an average velocity of 0.1 m/s for both the carrier fluid and the particles is prescribed at the inlet (Re = 9.95). The temperature of the particles and carrier fluid is kept at 315 K at the inlet, which is less than the melting temperature of the particles. A constant heat flux of 7000 W/m^2 is applied at the bottom wall of the microchannel.

Figures 5.1, 5.2 and 5.3 show temperature contours along the microchannel length for the case with no P.C.M. particles, with 10% particle volume concentration using D.P.M. and with 10% particle volume concentration using homogeneous model respectively. Temperature contours obtained using D.P.M. and homogeneous model are similar. Although, the friction in the shear layer contributes to temperature rise along the microchannel length, the temperature increase in the microchannel is primarily a result of external heating. Consequently, the major contributor to the temperature increase is the external heat input to the microchannel. Moreover, increasing the concentration of P.C.M. particles contributes to the temperature decrease in the microchannel towards the microchannel exit, which is attributed to the latent heat of fusion associated with the phase change of the P.C.M. particles. This effect is more pronounced at higher concentrations of P.C.M. particles.

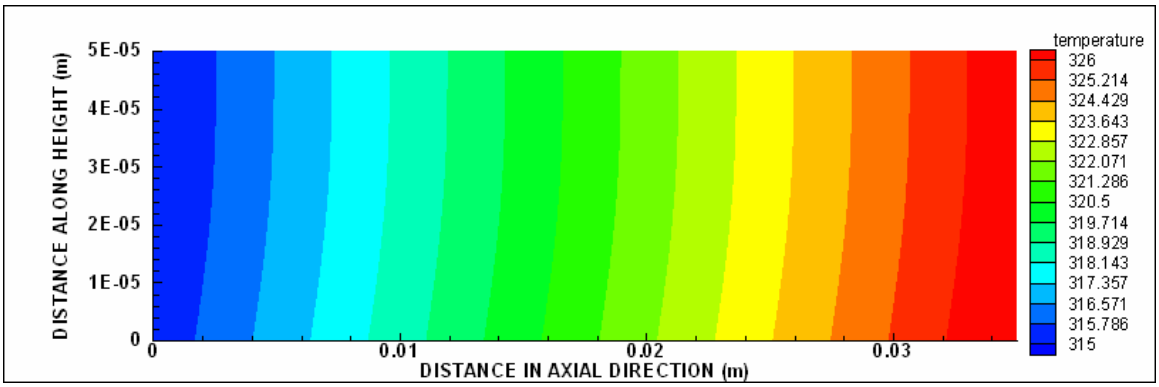

Figure 5.1 Temperature contour of carrier fluid along the microchannel length for 0% volume concentration of particles.

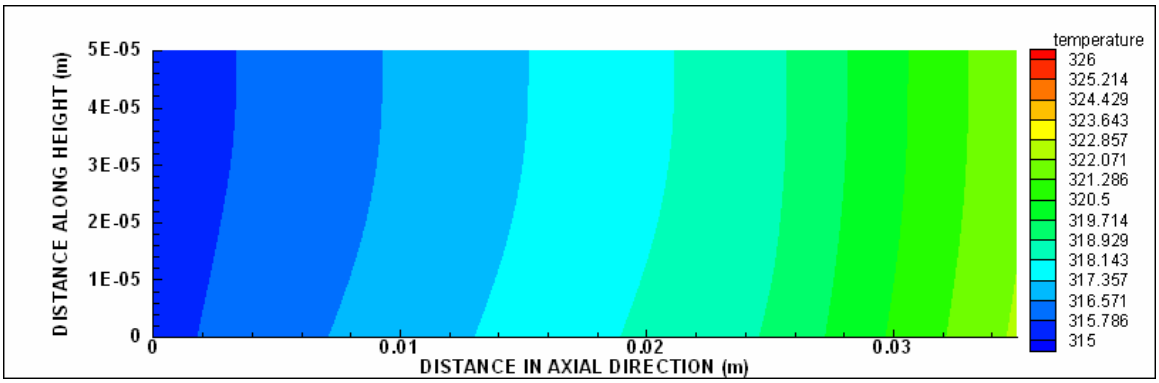

Figure 5.2 Temperature contour of carrier fluid along the microchannel length for 10% volume concentration of particles using D.P.M.

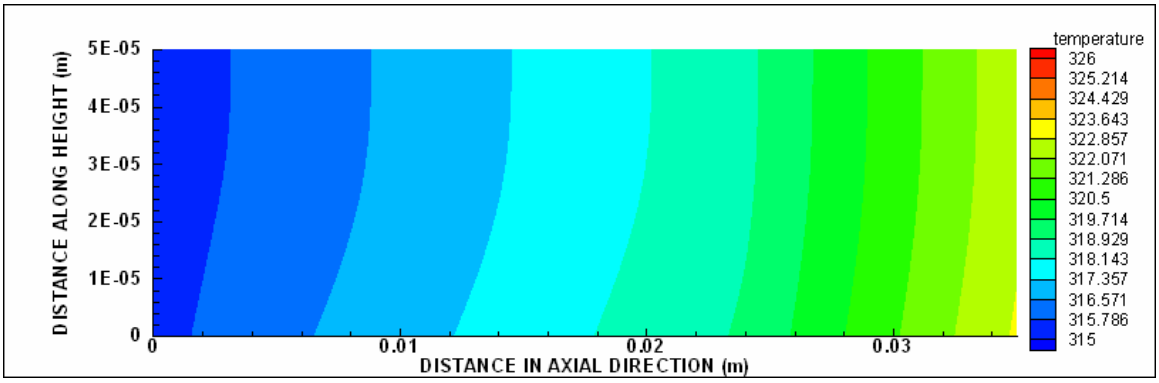

Figure 5.3 Temperature contour of bulk fluid along the microchannel length for 10% volume concentration of particles using homogeneous model.

The mass weighted average temperature of a fluid at a particular axial location is defined as

$$T_b = \frac{\sum_{i=1}^{n} T_i \rho_i \left| \vec{v}_i \bullet \vec{A}_i \right|}{\sum_{i=1}^{n} \rho_i \left| \vec{v}_i \bullet \vec{A}_i \right|} \tag{5.1.1}$$

Where A is the cross-sectional area of the microchannel.

Figure 5.4 shows the variation of the mass weighted average temperature along the length of the microchannel. It should be noted that the D.P.M. shows the mass averaged temperature of the carrier fluid, while the homogeneous model shows the mass averaged temperature of the fluid with bulk properties. The phase change of particles is indicated by the change in slope of the mass weighted average temperature. Figure 5.4 shows a constant slope for mass averaged temperature in the absence of particles. In the presence of particles, both the D.P.M. and homogeneous model show a significant change in the slope of the mass weighted average temperature in the melting range. The presence of 10% volume concentration of particles in the carrier fluid reduces its temperature by 40.9% and by 34.6% when D.P.M. and homogeneous models are used respectively. The D.P.M. assumes that the entire microchannel is filled with the carrier fluid, and particles are injected into the microchannel. This assumption leads to a higher carrier fluid mass flow rate being used in the D.P.M. Consequently, a lower value of mass averaged temperature is obtained when D.P.M. is used as compared to homogeneous model. The results for both models indicate that significant improvements in thermal storage capacity of the carrier fluid are possible by increasing P.C.M. particle concentration.

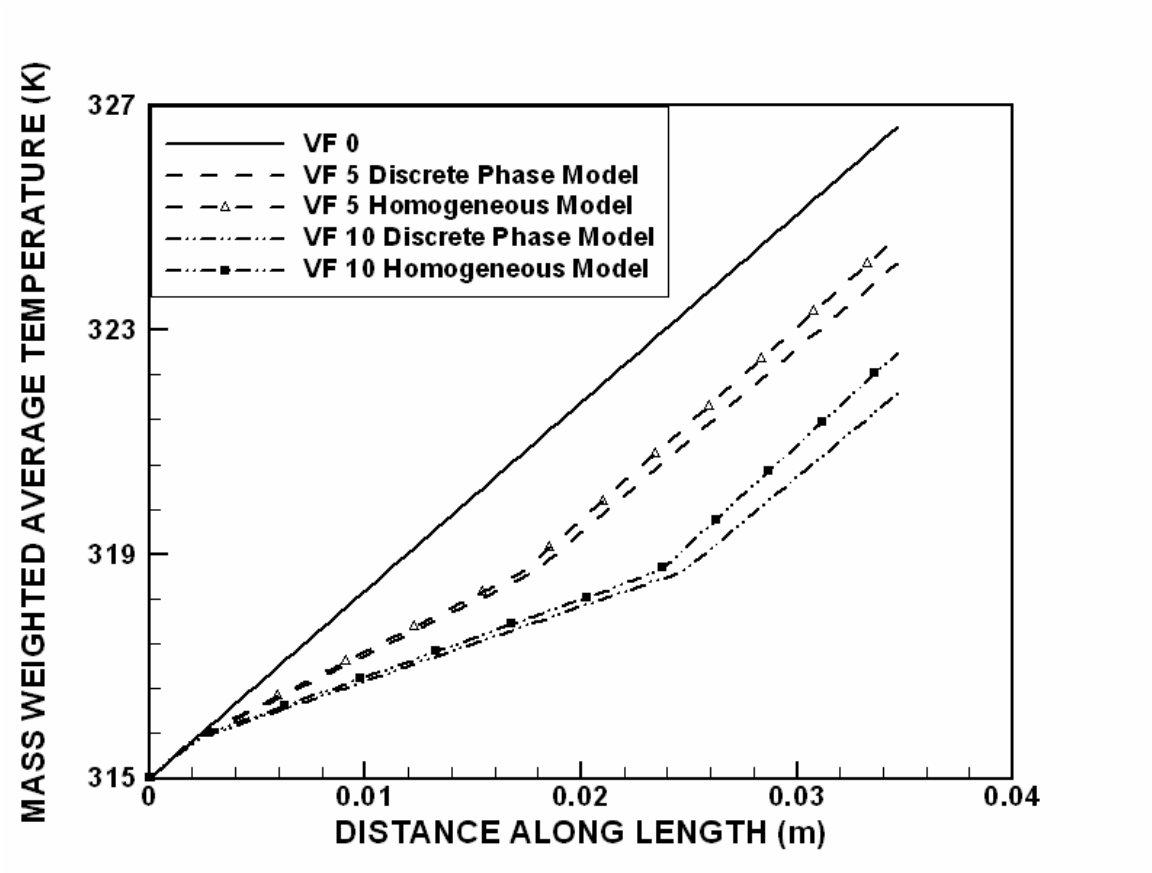

Figure 5.4 Mass weighted average fluid temperature along the microchannel length, where VF 0, VF 5, and VF 10 represents 0%, 5% and 10% volume concentration of the particles, respectively.

The heat transfer coefficient is calculated as

$$h = \frac{q''}{T_w - T_b} \tag{5.1.2}$$

where q'' is the heat flux and T_w is the wall temperature.

The Nusselt Number can be calculated as

$$Nu = \frac{hD_h}{k} \tag{5.1.3}$$

In case of D.P.M., the carrier fluid thermal conductivity is used for calculating Nusselt number, while in case of homogeneous model; the bulk fluid thermal conductivity is used.

The non-dimensional length is defined as

$$x^+ = \frac{2x}{D_h \,\mathrm{Re}\,\mathrm{Pr}} \tag{5.1.4}$$

where Re is the Reynolds number and Pr is the Prandtl number of the carrier fluid and the bulk fluid in case of D.P.M. and homogeneous models respectively.

Figures 5.5 and 5.6 show the Nusselt number variation for different volume concentrations of particles in case of D.P.M. and homogeneous models respectively. It should be noted that the Nusselt number decreases and reaches a fully developed value for carrier fluid without particles (The case is labeled as VF0 in the figures). In presence of particles, the Nusselt number decreases initially, and then, at the beginning of the phase change process, it increases and reaches its maximum value. The Nusselt number,

then, decreases rapidly and reaches its fully developed value. Subsequently, the Nusselt number, starts decreasing again towards the end of the phase change process, and reaches a minimum value before increasing and converging with the fully developed single fluid value. A similar Nusselt number profile was obtained by Kondle [3] for P.C.M. slurry flow through microchannels. With increase in the volume concentration of particles, the distance between beginning and end of phase change process in the microchannel increases. The Nusselt number in both the D.P.M. and homogeneous model exhibits a similar trend; therefore, Figure 5.5 is used to explain the observed trend in Nusselt number.

Since the microchannel is heated at its bottom wall, the carrier fluid temperature at any axial location is maximum near the bottom wall and minimum at the top of the microchannel. The value of Nusselt number initially decreases as the flow is becoming thermally fully developed. However, after a certain microchannel length is exceeded, the value of Nusselt number suddenly starts increasing. This axial distance corresponds to the point at which the temperature near the bottom wall enters the melting range of particles; thereby, starting the phase change process in the region close to the bottom. Due to the phase change process near the bottom wall, the wall temperature increases slowly, but the mass averaged fluid temperature keeps increasing, and this causes a decrease in the difference between the wall temperature and the mass averaged fluid temperature. The decrease in the denominator of Nusselt number causes an increase in its value. The Nusselt number continues to increase and reaches a maximum value and, then, starts

decreasing along the microchannel length. Just after reaching the peak, the mass averaged temperature of the carrier fluid exceeds the solidus temperature of P.C.M. particles, and, therefore, the rate of increase of mass averaged temperature decreases. As a result, the difference between wall and mass averaged temperature increases. Therefore, the Nusselt number continues to decrease until it reaches the fully developed value. From this axial location onwards to the point where Nusselt number starts decreasing again, the fluid along the entire microchannel height undergoes phase change and the difference between the wall temperature and the mass averaged fluid temperature is almost constant, which in turn makes Nusselt number value almost constant. After a certain distance from the inlet, the fluid near the bottom wall exceeds the liquidus temperature, thereby, completing the phase change process. Subsequently, the wall temperature starts increasing rapidly whereas most of the fluid is still within the melting range. This causes an increase in the difference between the wall and mass averaged fluid temperature and Nusselt number continues to decrease beyond this axial location. Immediately after Nusselt number reaches its minimum value, the mass averaged fluid temperature exceeds the liquidus temperature, and, consequently, it starts increasing again until a constant difference between wall temperature and mass averaged fluid temperature is maintained. Therefore, the Nusselt number keeps increasing till it converges with the fully developed value.

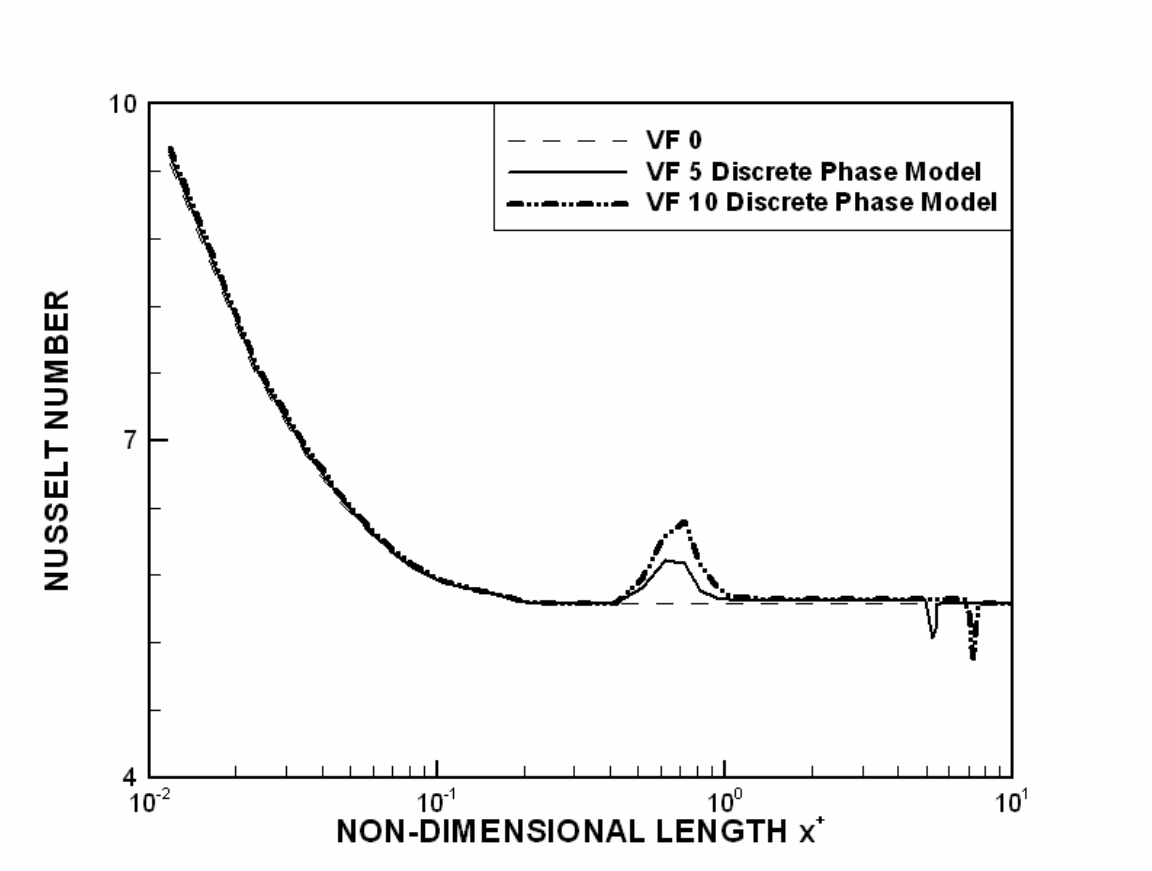

Figure 5.5 Nusselt number variation in case of D.P.M., where VF 0, VF 5 and VF 10 represents 0%, 5% and 10% volume concentration of particles, respectively.

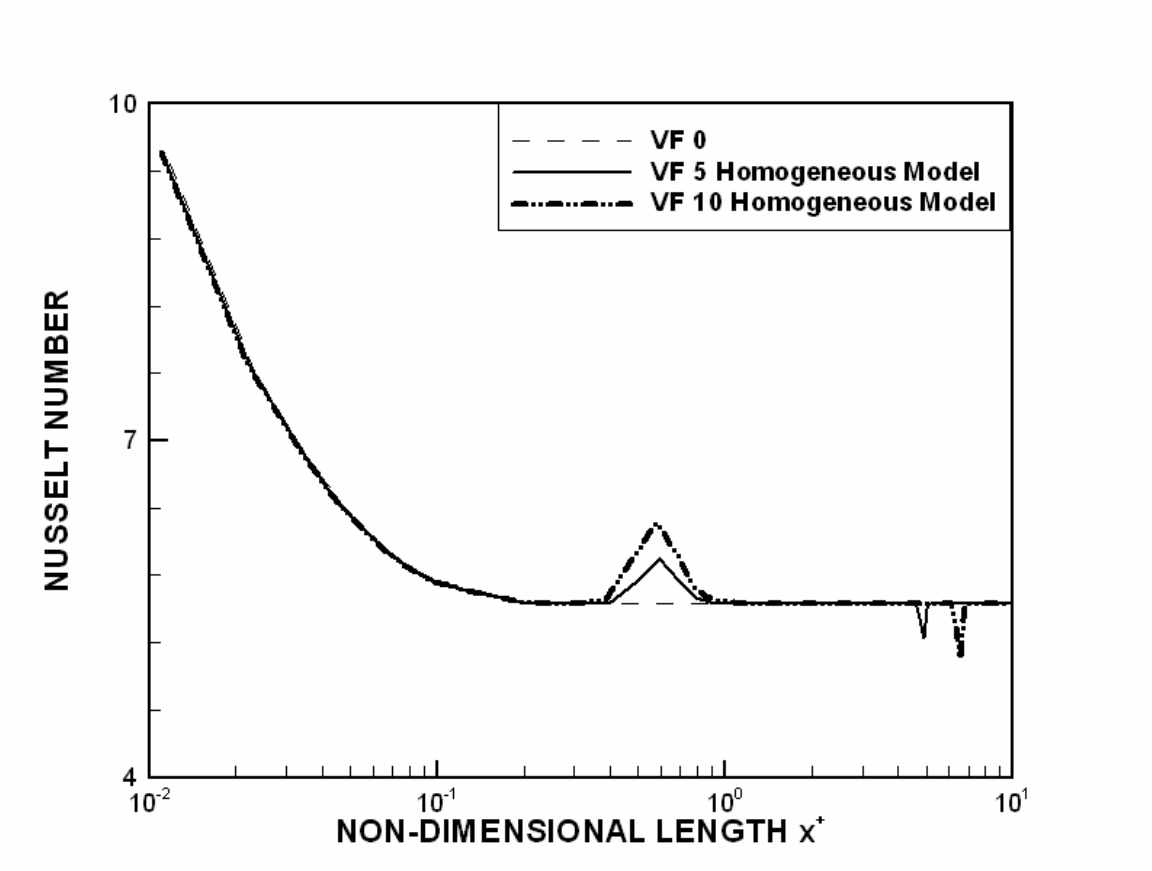

Figure 5.6 Nusselt number variation in case of homogeneous model, where VF 0, VF 5 and VF 10 represents 0%, 5% and 10% volume concentration of particles, respectively.

The average Nusselt number is found to increase with increasing volume concentration of particles as shown in Figure 5.7. However, a maximum increase of 0.6% is obtained in case of carrier fluid with 10% volume concentration of particles. Therefore, it can be concluded that the influence of particles on the increase of Nusselt number is negligible.

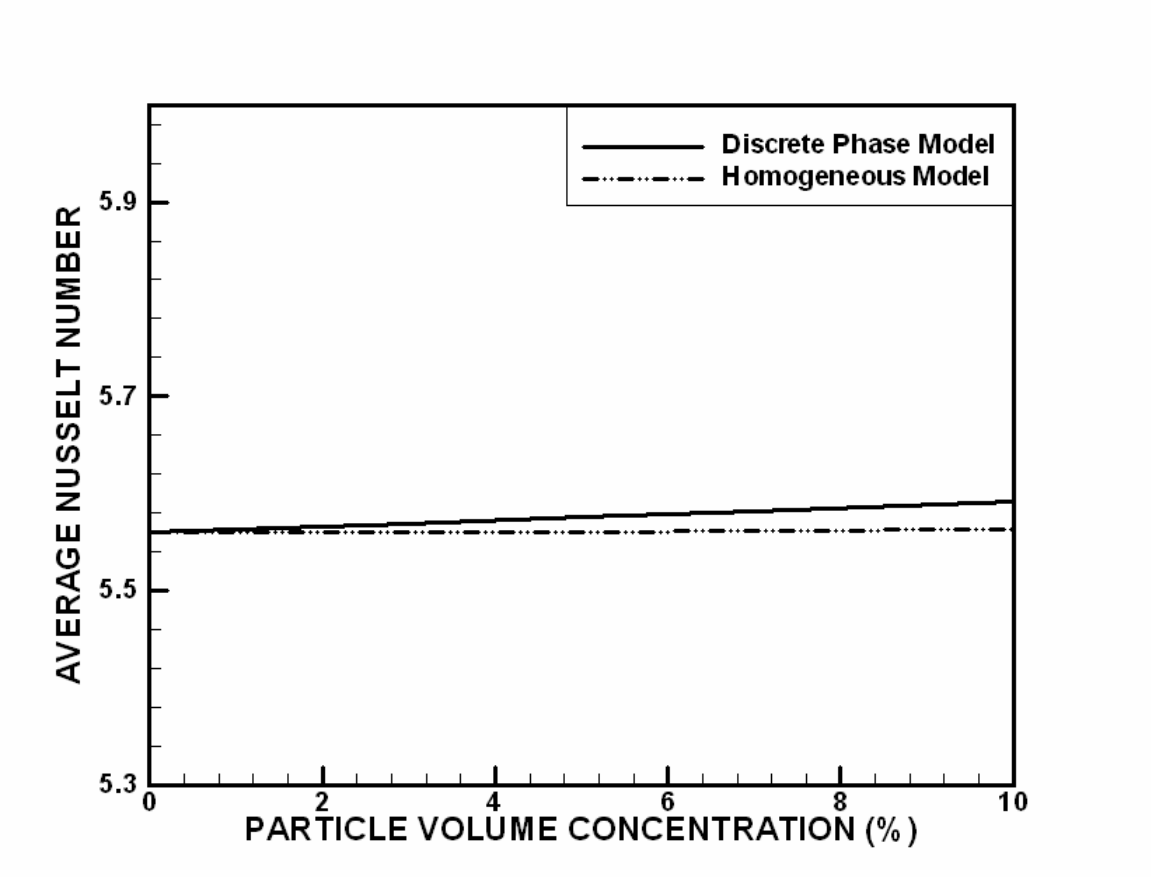

Figure 5.7 Average Nusselt number variation with volume concentration of particles.

Figure 5.8 shows the pressure drop along the microchannel length for different volume concentrations of P.C.M. particles. Figure 5.8 reveals that the D.P.M. does not show any increase in pressure drop due to the addition of nanoparticles, while homogeneous model shows an increase in pressure drop with increase in the volume concentration of nanoparticles in the carrier fluid. The prediction of D.P.M. indicates that pressure drop due to addition of even 10% volume concentration of nanoparticles is negligible. However, homogeneous model prediction reveals an increase of 34.4% in the pressure drop due to the presence of 10% volume concentration of nanoparticles. The increase in volume concentration of nanoparticles is found to increase the viscosity of the bulk fluid. Since the flow in the microchannel is laminar, therefore, increase in viscosity of the bulk fluid results in an increase in pressure drop as predicted by the homogeneous model.

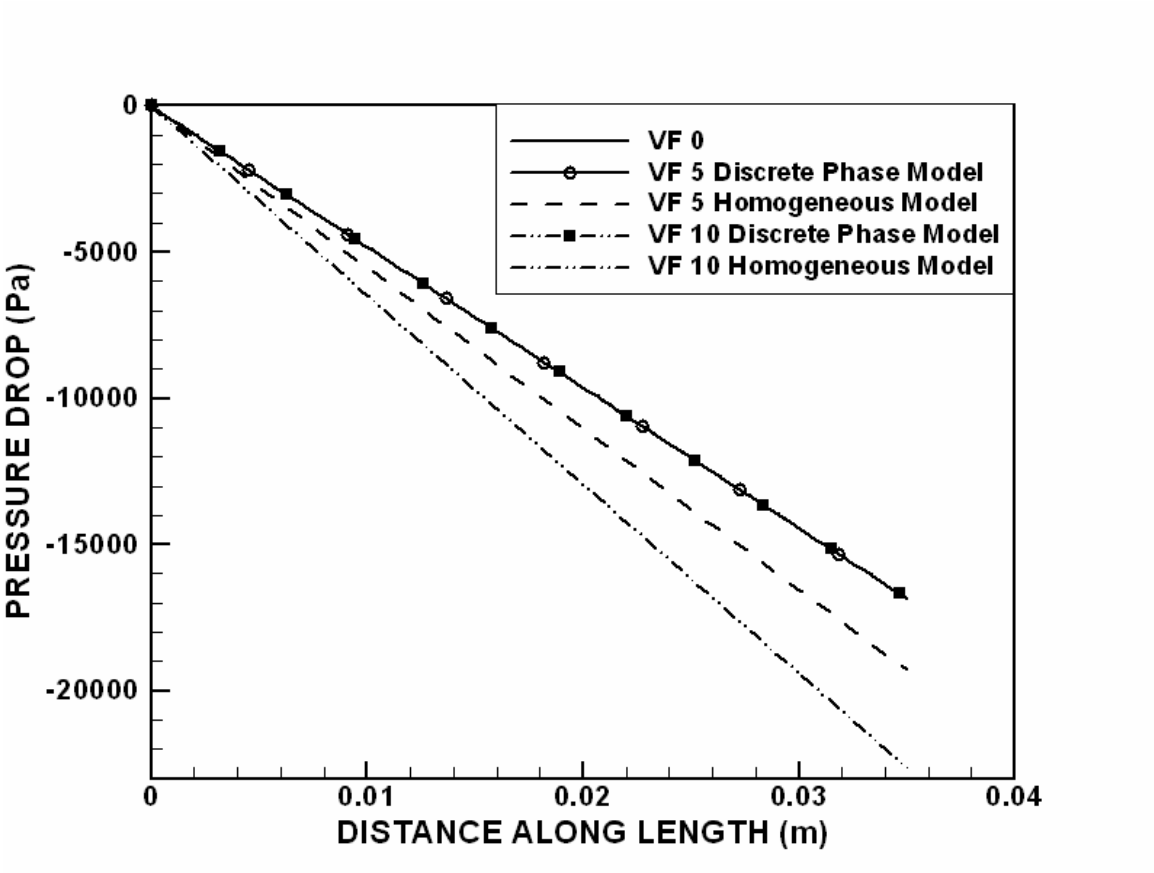

Figure 5.8 Pressure distribution along the microchannel length, where VF 0, VF 5 and VF 10 represents 0%, 5% and 10% volume concentration of particles, respectively.

5.2 Effectiveness Ratio, Performance Index and Merit Number

Parametric analysis is carried out to investigate the effect of particle volume concentration, mass flow rate and heat flux on the thermal performance of bulk fluid inside the microchannel. The effectiveness ratio [35], performance index [35], and Merit number are used for comparison purpose.

In this study, the mass flow rate of the bulk fluid at the inlet is varied between 10^{-5} kg/s to 4 x 10^{-5} kg/s. The heat flux at the bottom wall of the microchannel is varied between 8000 W/m^2 to 20000 W/m^2. The temperature of the particles and carrier fluid is 315 K at the inlet, which is less than the melting temperature of the P.C.M. particles.

5.2.1 Effectiveness Ratio

The effectiveness ratio is defined as the ratio of heat transfer rate of bulk fluid to the heat transfer rate of carrier fluid for the same temperature rise from inlet to exit of the microchannel. The effectiveness ratio is defined as [35] :

$$\varepsilon_{effectiveness} = \frac{\dot{Q}_b}{\dot{Q}_f} \tag{5.2.1}$$

where

$$\dot{Q}_b = q'' \times Length \times Width \tag{5.2.2}$$

$$\dot{Q}_f = \dot{m} c_{p,f} \Delta T_f \tag{5.2.3}$$

where $\dot{m}$ is the mass flow rate, $c_{p,f}$ is the specific heat of the carrier fluid and ΔT_f is the temperature rise of the carrier fluid.

For the same carrier fluid and bulk fluid mass flow rates, the effectiveness ratio simply reduces to a ratio of their average specific heats. Figures 5.9 to 5.12 show the variation of effectiveness ratio with heat flux for different particle volume concentrations and mass flow rates. Figure 5.9 shows that for all particle volume concentrations, the maximum effectiveness ratio is obtained for the lowest heat flux of 8000 W/m^2. In Figure 5.10, the effectiveness ratio for 3%, 5%, and 7% volume concentrations is highest for heat flux of 8000 W/m^2, while for 10% volume concentration, the effectiveness ratio is maximum for heat flux of 9162 W/m^2. In Figure 5.11, the effectiveness ratio for 3% volume concentration is highest for heat flux of 8000 W/m^2, while for 5%, 7% and 10% volume concentrations, the effectiveness ratio is maximum for heat flux of 9295 W/m^2, 11000 W/m^2 and 13600 W/m^2 respectively. Figure 5.12 shows that the effectiveness ratio for 3%, 5%, 7% and 10% volume concentrations is highest for the heat flux of 10000 W/m^2, 12000 W/m^2, 14000 W/m^2 and 17500 W/m^2 respectively. Figures 5.9 to 5.12 show that increasing the mass flow rate and volume concentration of the bulk fluid increases the value of the heat flux, at which the maximum effectiveness ratio is obtained. Figures 5.9 to 5.12 show that for a given mass flow rate, the maximum value of effectiveness ratio is obtained for the case of 10% volume concentration of particles.

The variation of effectiveness ratio has also been presented in a single figure (Figure 5.13) by plotting effectiveness ratio against heat flux to mass flow rate ratio for different volume concentrations of P.C.M. particles. Initially, the effectiveness ratio increases with increasing heat flux to mass flow rate ratio of P.C.M. slurry and keeps increasing until it reaches a peak value. Further increase in heat flux to mass flow rate ratio decreases the effectiveness ratio. The heat flux to mass flow rate ratio required to reach the peak effectiveness ratio value increases with increasing volume concentration of particles. Moreover, for higher volume concentration of P.C.M. particles, the peak value of effectiveness ratio is higher. The above trends in the effectiveness ratio can be explained as follows:

For a given mass flow rate, the effectiveness ratio is the highest when the ratio of latent heat to sensible heat of the bulk fluid in the microchannel is the largest. The maximum value of latent heat to sensible heat ratio occurs when the particles reach the liquidus temperature (upper melting temperature) at the exit of the microchannel. This ensures that sensible heating occurs only near the inlet of the microchannel, and, therefore, the latent heat ratio is the maximum. For low heat flux to mass flow rate ratio values, the phase change of P.C.M. particles is not complete due to the low value of heat flux applied. Therefore, at low heat flux to mass flow rate ratio, increase in heat flux is reflected in an increase in the value of effectiveness ratio. The effectiveness ratio keeps increasing with increase in heat flux to mass flow rate ratio up to the point that enough heat flux is applied to complete the melting of P.C.M. particles in the microchannel. Due

to a unique value of the optimum heat flux to mass flow rate ratio, increase in mass flow rate leads to increase in the heat flux required to obtain maximum enhancement in heat storage capacity. The heat flux to mass flow rate ratio required for complete phase change of P.C.M. particles is larger for higher volume concentration of particles in the carrier fluid. Further increase in heat flux to mass flow rate ratio leads to an increase in the sensible heating of P.C.M. particles after the completion of their phase change, and as a result the effectiveness ratio starts to reduce. Consequently, the effectiveness ratio increases initially, reaches a peak value and, then, decreases for all volume concentration of P.C.M. particles.

Figure 5.14 shows the variation of effectiveness ratio with Reynolds number of the bulk fluid for heat flux 20000 W/m^2. Increasing the volume concentration of particles and Reynolds number results in increasing the effectiveness ratio. This is attributed to the increasing mass flow rate with increasing Reynolds number. In this case, for the fixed heat flux, temperature rise in the P.C.M. slurry reduces with increasing mass flow rate while enhancing the effectiveness ratio. Moreover, increasing volume concentration of P.C.M. particles enhances the effectiveness ratio, which is more pronounced with increasing Reynolds number.

The maximum effectiveness ratio of 2.75 is obtained for P.C.M. particle volume concentration of 10%. The corresponding value of effectiveness ratio indicates that for the same temperature rise, the bulk fluid at the given operating condition can absorb 2.75 times the heat flux, which is absorbed by carrier fluid. From the above discussion, it can

be concluded that for a given volume concentration of particles, there exists a heat flux to mass flow rate ratio at which the effectiveness ratio is maximum. A similar observation was presented in [35].

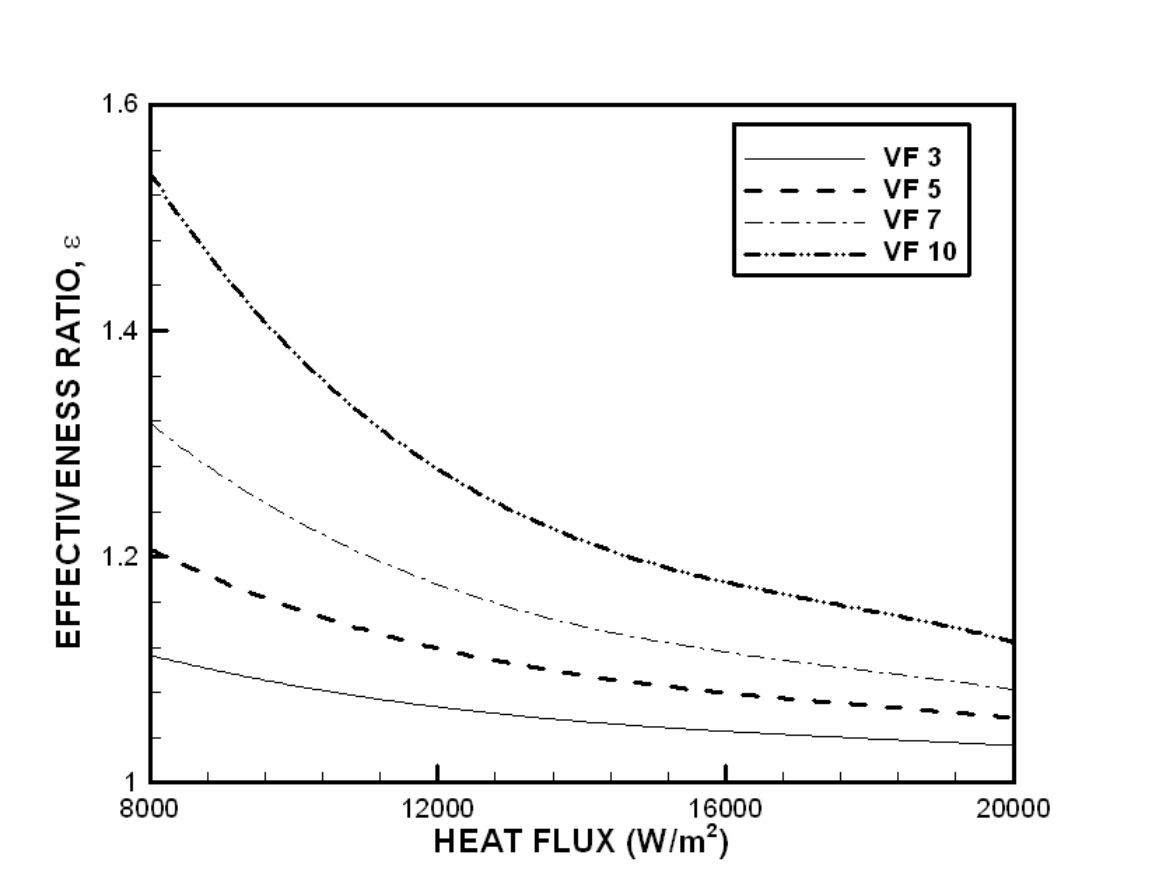

Figure 5.9 Variation of effectiveness ratio with heat flux for mass flow rate of 10^{-5} kg/s, where VF 3, VF 5, VF 7 and VF 10 represents 3%, 5%, 7% and 10% volume concentration of the particles, respectively.

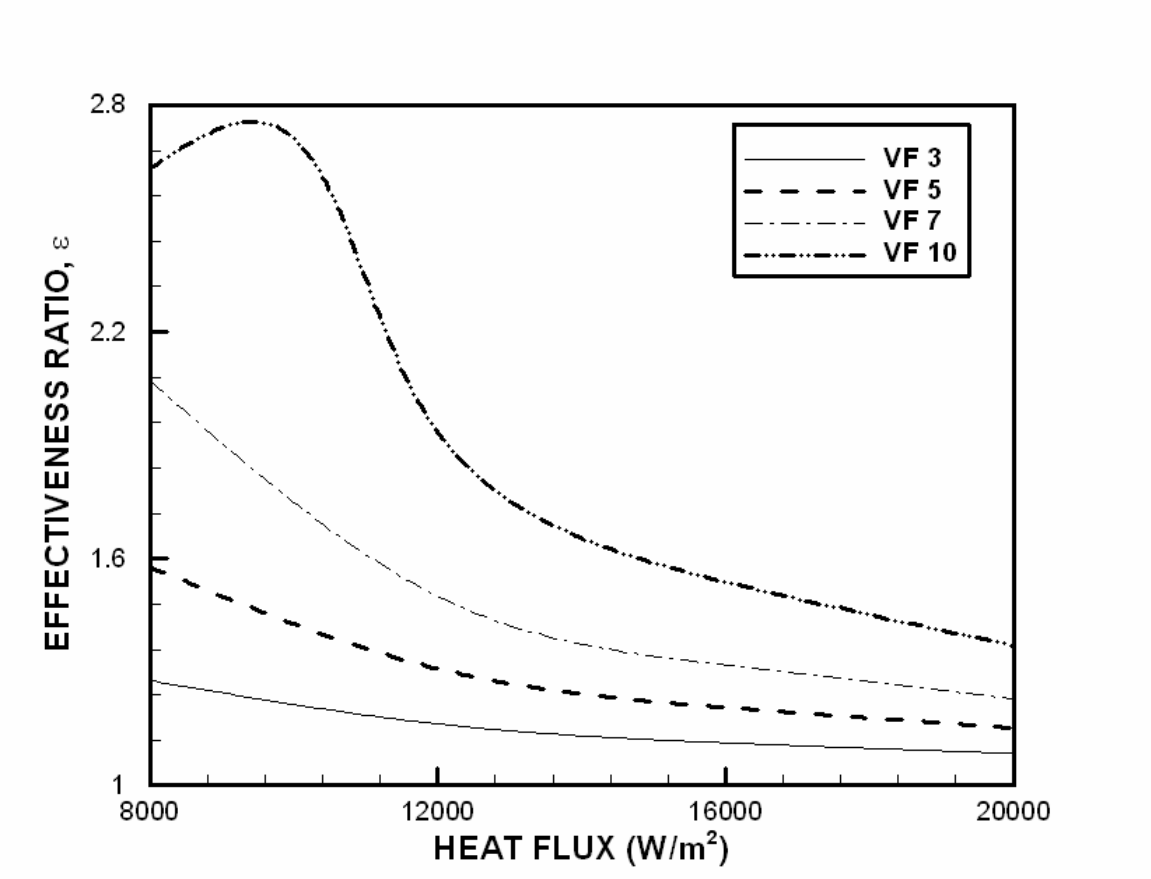

Figure 5.10 Variation of effectiveness ratio with heat flux for mass flow rate of 2×10^{-5} kg/s, where VF 3, VF 5, VF 7 and VF 10 represents 3%, 5%, 7% and 10% volume concentration of the particles, respectively.

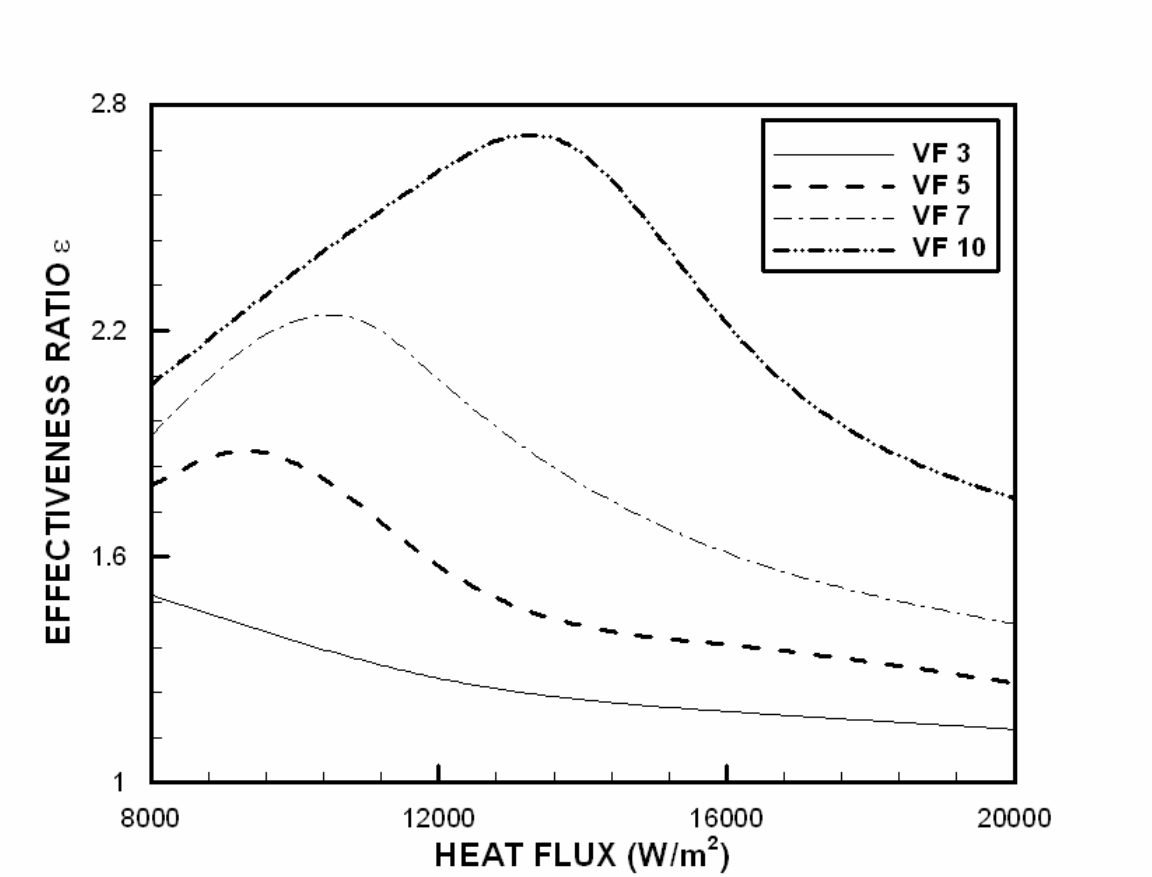

Figure 5.11 Variation of effectiveness ratio with heat flux for mass flow rate of 3×10^{-5} kg/s, where VF 3, VF 5, VF 7 and VF 10 represents 3%, 5%, 7% and 10% volume concentration of the particles, respectively.

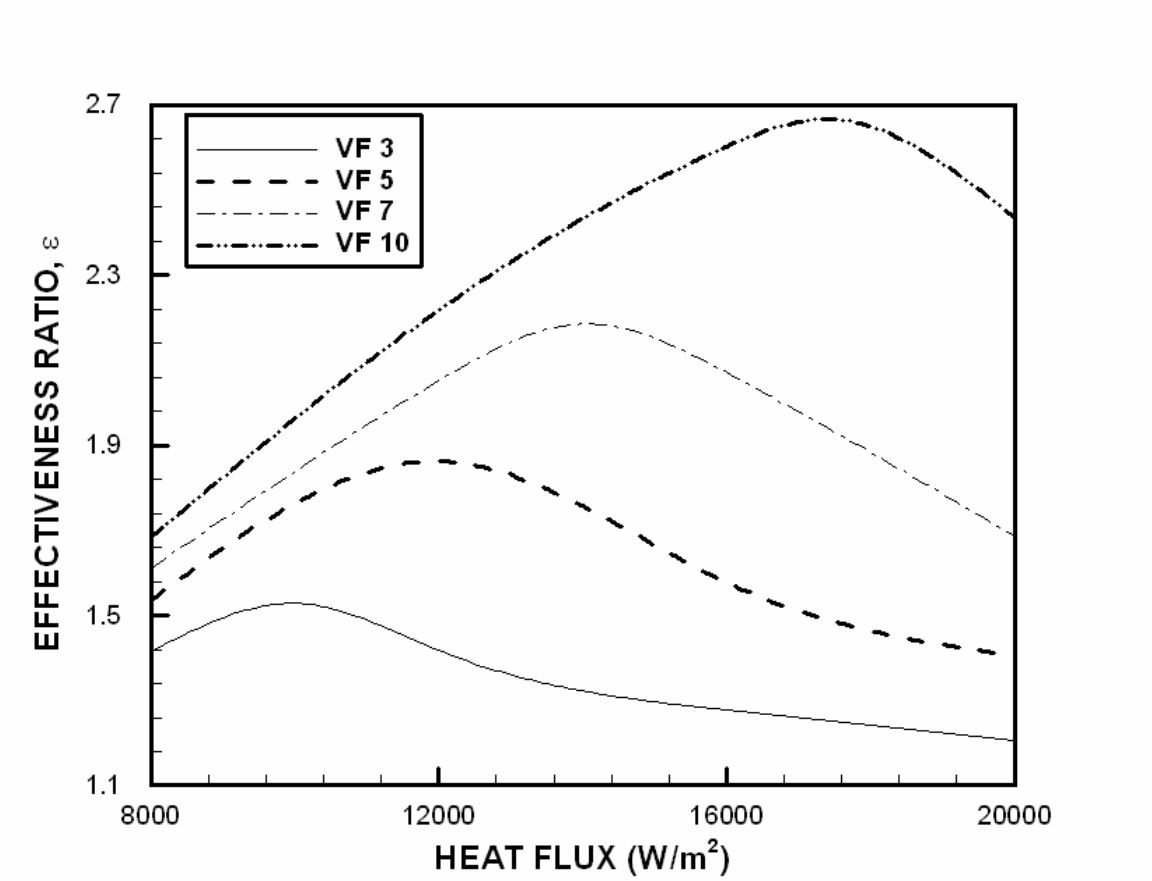

Figure 5.12 Variation of effectiveness ratio with heat flux for mass flow rate of 4×10^{-5} kg/s, where VF 3, VF 5, VF 7 and VF 10 represents 3%, 5%, 7% and 10% volume concentration of the particles, respectively.

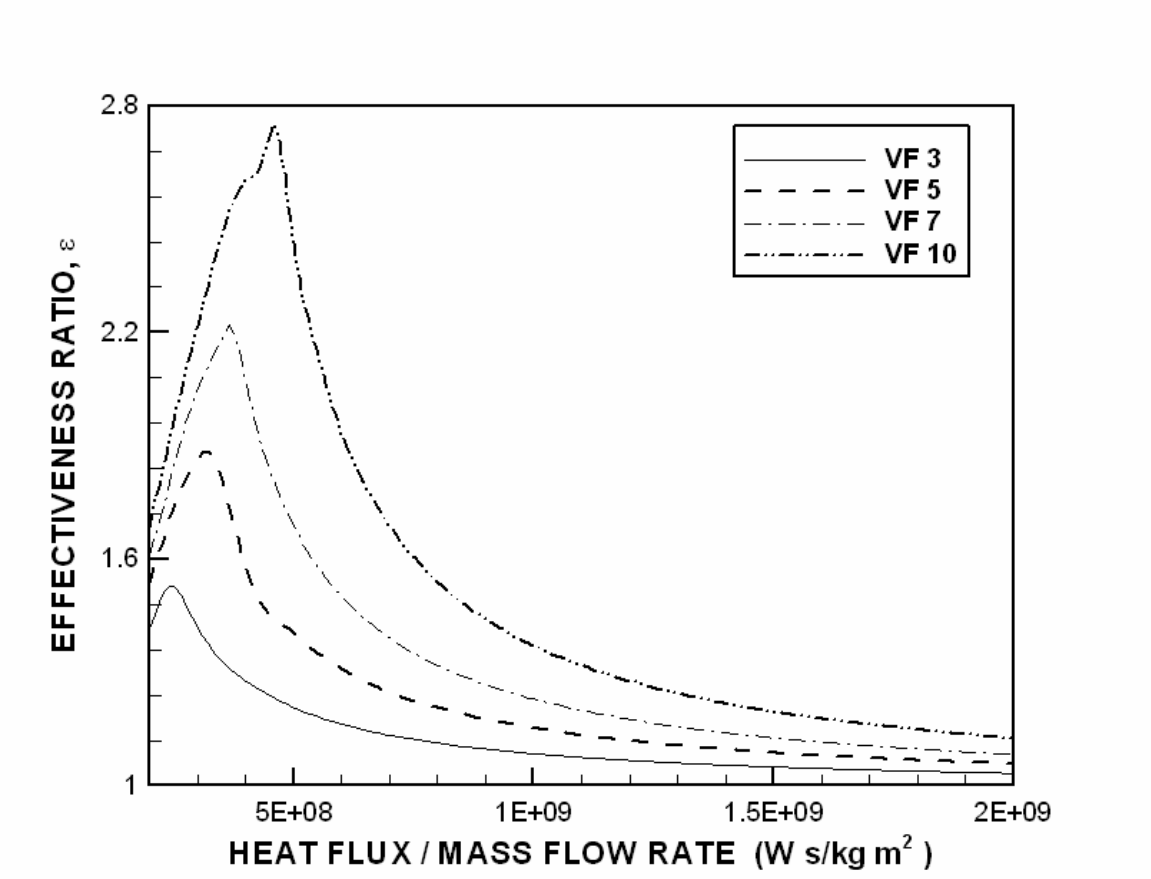

Figure 5.13 Variation of effectiveness ratio with ratio of heat flux to mass flow rate of P.C.M. slurry, where VF 3, VF 5, VF 7 and VF 10 represents 3%, 5%, 7% and 10% volume concentration of the particles, respectively.

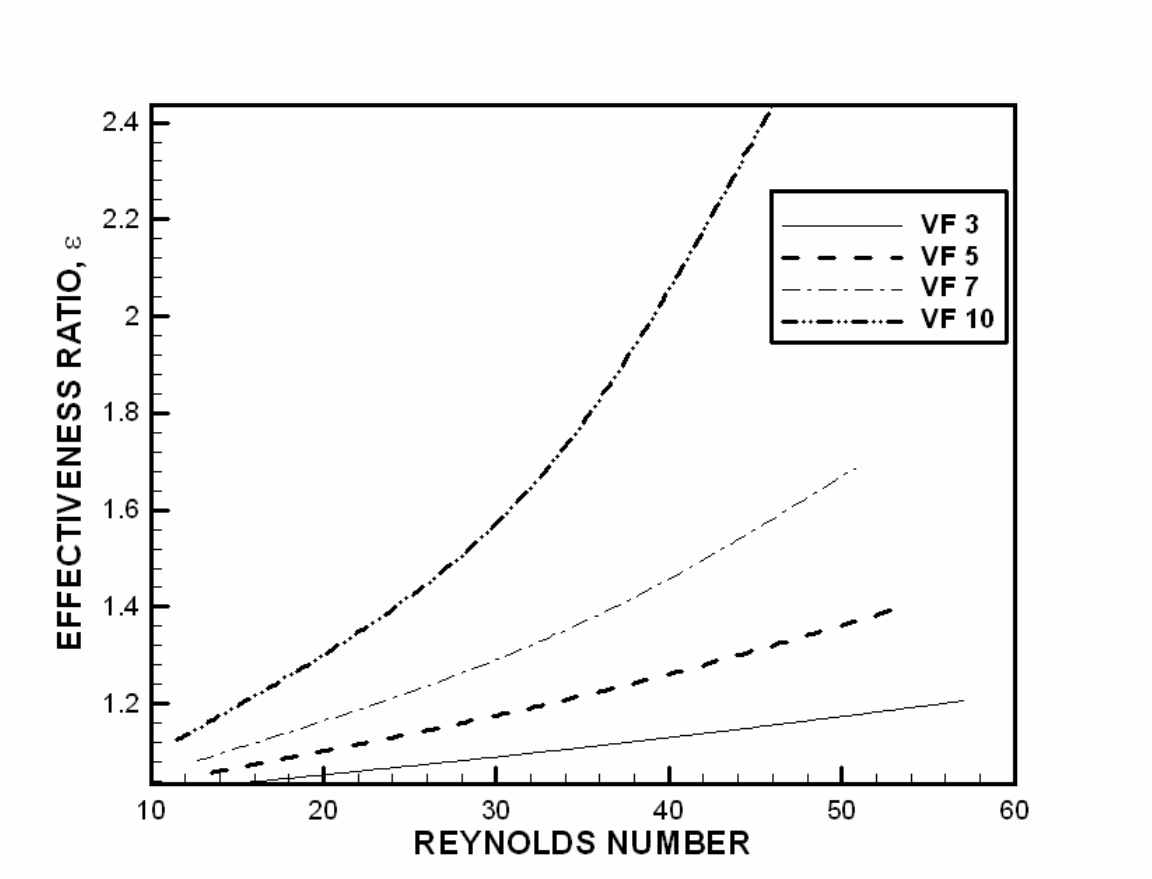

Figure 5.14 Variation of effectiveness ratio with bulk fluid Reynolds number for heat flux of 20000 W/m^2, where VF 3, VF 5, VF 7 and VF 10 represents 3%, 5%, 7% and 10% volume concentration of the particles, respectively.

5.2.2 Performance Index

The performance index is defined as the ratio of heat transfer rate to fluid pumping power of bulk fluid to the heat transfer rate to fluid pumping power of carrier fluid. The performance index is defined as [35] :

$$Performance\ Index = \frac{\left(\dot{Q}/P\right)_b}{\left(\dot{Q}/P\right)_f} \tag{5.2.4}$$

where the pumping power of the bulk fluid and carrier fluid are defined, respectively as

$$P_b = \Delta p_b v_b A \tag{5.2.5}$$

$$P_f = \Delta p_f v_f A \tag{5.2.6}$$

$$\Delta p_f = \frac{32 L \rho_f v_f^2}{\mathrm{Re}_f D_h} \tag{5.2.7}$$

Figures 5.15 to 5.18 show the variation of performance index with heat flux for different particle volume concentrations and mass flow rates. Figure 5.15 shows that for all particle volume concentrations, the maximum value of performance index is obtained for the lowest heat flux of 8000 W/m^2. In Figure 5.16, the performance index for 3%, 5%, and 7% volume concentrations is highest for heat flux of 8000 W/m^2, while for 10% volume concentration, the performance index is maximum for heat flux of 9162 W/m^2. In Figure 5.17, the performance index for 3% volume concentration is highest for heat flux of 8000 W/m^2, while for 5%, 7% and 10% volume concentrations, the performance index is maximum for heat flux of 9295 W/m^2, 11000 W/m^2 and 13600 W/m^2 respectively.

Figure 5.18 shows that the performance index for 3%, 5%, 7% and 10% volume concentrations is highest for the heat flux of 10000 W/m^2, 12000 W/m^2, 14000 W/m^2 and 17500 W/m^2 respectively.

In addition to the above figures, variation of performance index with heat flux to mass flow rate ratio has been plotted in Figure 5.19. The performance index initially increases with increasing heat flux to mass flow rate ratio, reaches a peak value and then decreases. The performance index for each particle volume concentration follows the same trend as effectiveness ratio with the same value of the optimum heat flux to mass flow rate ratio. However, at high heat flux to mass flow rate ratio, the performance index of the bulk fluid with higher volume concentration of particles is lower than the performance index for lower volume concentrations. Figure 5.15 shows that the performance index of the bulk fluid containing 5%, 7% and 10% volume concentrations falls below that of the bulk fluid with 3% volume concentration for the heat flux more than 10000 W/m^2. Similarly, a decrease in performance index of bulk fluid with increase in particle volume concentration within a certain range of heat fluxes is observed in Figures 5.17 and 5.18. This trend is associated with increase in temperature of the bulk fluid, which causes sharp decrease in viscosity. A larger temperature rise inside the microchannel results in lower pressure drop compared to the case in which a lower temperature rise of bulk fluid inside the microchannel is encountered. The use of bulk fluid with high particle concentrations suppresses the temperature rise as well as increases the viscosity of the bulk fluid due to the presence of high particle concentrations. The reduction in temperature rise is due to

the phase change of the particles inside the microchannel, which increases the effectiveness ratio with increasing particle volume concentration, however, this also results in an increase in the pressure drop of the bulk fluid. When the heat flux to mass flow rate ratio is high, the increase in effectiveness ratio due to increase in volume concentration of particles is not significant due to increase in the sensible heating of the bulk fluid inside the microchannel. Therefore, when the increase in effectiveness ratio is unable to offset the increase in pressure drop of the bulk fluid, the performance index decreases. This results in bulk fluid with high particle volume concentrations having a lower performance index as observed in Figure 5.19.

A performance index below unity indicates that the heat transfer rate per fluid pumping power for the bulk fluid is lower than the carrier fluid and, therefore, the bulk fluid should not be used under those operating conditions. For 3% volume concentration of particles in the slurry, the performance index of the bulk fluid for all heat flux to mass flow rate ratios is below unity (Figure 5.19), indicating that the use of bulk fluid entails a lower heat transfer rate to fluid pumping power ratio, as compared to water. Moreover, Figure 5.19 reveals that the performance index of the bulk fluid containing 5%, 7% and 10% volume concentrations exceeds unity only within a narrow range of heat flux to mass flow rate ratio. Additionally for a mass flow rate of 10^{-5} kg/s, the performance index of the bulk fluid for all particle volume concentrations is below one (Figure 5.15)

Figure 5.20 shows the variation of performance index with Reynolds number for heat flux of 20000 W/m^2. From Figure 5.20, it can be observed that at low Reynolds numbers,

the performance index of P.C.M. slurry with 10% volume concentration of particles is the lowest while the performance index of slurry with 3% volume concentration of particles is the highest. However at higher Reynolds numbers, the performance index of P.C.M. slurry with 10% volume concentration of particles becomes highest while performance index for 3% volume concentration of particles becomes lowest. Since the heat flux applied to P.C.M. slurry is 20000 W/m^2, at low Reynolds numbers the sensible heat of the P.C.M. slurry dominates over the latent heat and, consequently, the difference between the effectiveness ratios of 3% volume concentration of particles and 10% volume concentrations becomes small. Moreover, the bulk viscosity for P.C.M. slurry with 10% volume concentration of particles is higher than the P.C.M. slurries containing lower volume concentrations of P.C.M. particles, and, consequently, the pressure drop is also high. Since the increase in effectiveness ratio is not able to compensate the increase in pressure drop, the performance index for slurry with 10% volume concentration of particles is the lowest at low Reynolds numbers. However, at high Reynolds numbers, the increase in effectiveness ratio due to increase in volume concentration of P.C.M. particles is easily able to offset the increase in pressure drop due to high P.C.M. volume concentrations. Therefore, the performance index for 10% volume concentration of particles is the highest. Consequently, at low Reynolds number and high heat flux 20000 W/m^2, increase in volume concentration of P.C.M. slurry reduces the performance index; however, at high Reynolds numbers, the performance index increases with increasing volume concentration of P.C.M. particles.

The maximum performance index of 1.37 is obtained for particle volume concentration of 10%. The performance index follows a similar trend as effectiveness ratio for a given particle volume concentration. From the above discussion, it can be concluded that for a given volume concentration of particles, there exists a heat flux to mass flow rate ratio at which the performance index is the maximum. A similar observation was also made in [35].

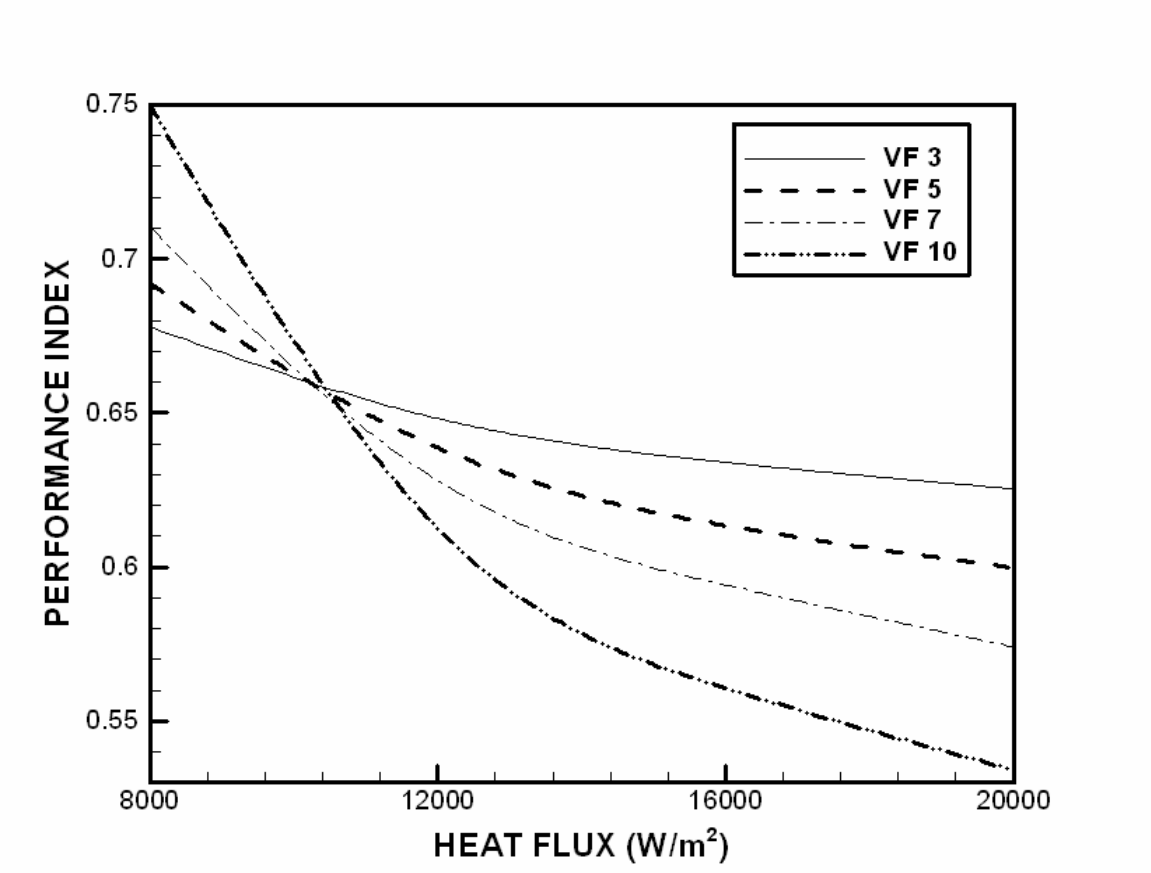

Figure 5.15 Variation of performance index with heat flux for mass flow rate of 10^{-5} kg/s, where VF 3, VF 5, VF 7 and VF 10 represents 3%, 5%, 7% and 10% volume concentration of the particles, respectively.

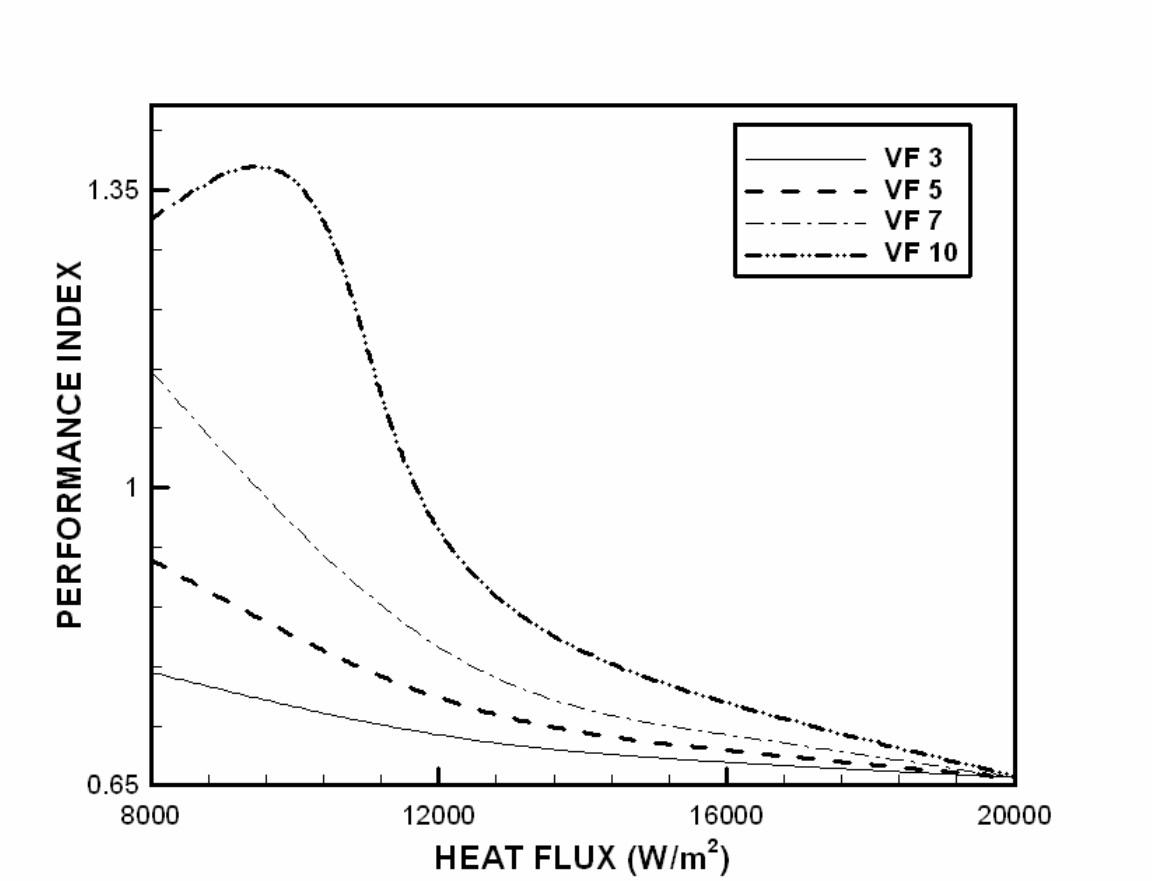

Figure 5.16 Variation of performance index with heat flux for mass flow rate of 2×10^{-5} kg/s, where VF 3, VF 5, VF 7 and VF 10 represents 3%, 5%, 7% and 10% volume concentration of the particles, respectively.

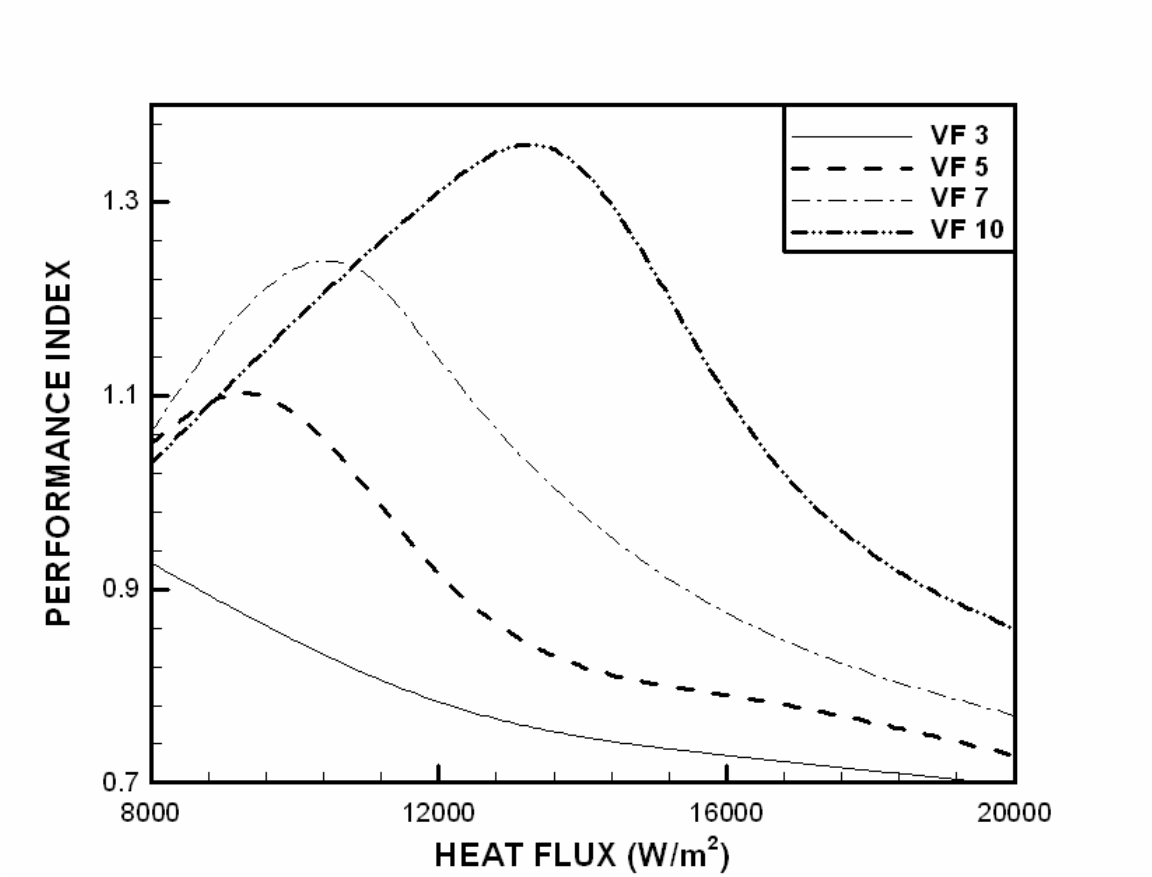

Figure 5.17 Variation of performance index with heat flux for mass flow rate of 3×10^{-5} kg/s, where VF 3, VF 5, VF 7 and VF 10 represents 3%, 5%, 7% and 10% volume concentration of the particles, respectively.

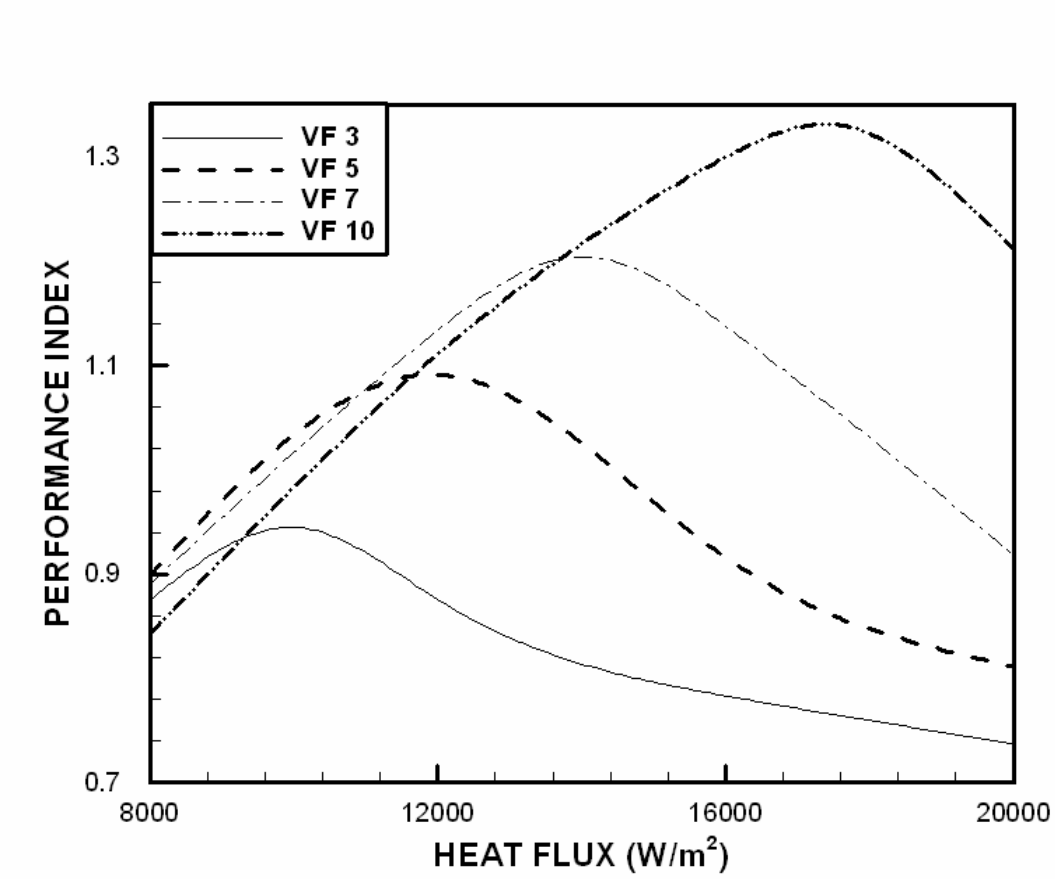

Figure 5.18 Variation of performance index with heat flux for mass flow rate of 4×10^{-5} kg/s, where VF 3, VF 5, VF 7 and VF 10 represents 3%, 5%, 7% and 10% volume concentration of the particles, respectively.

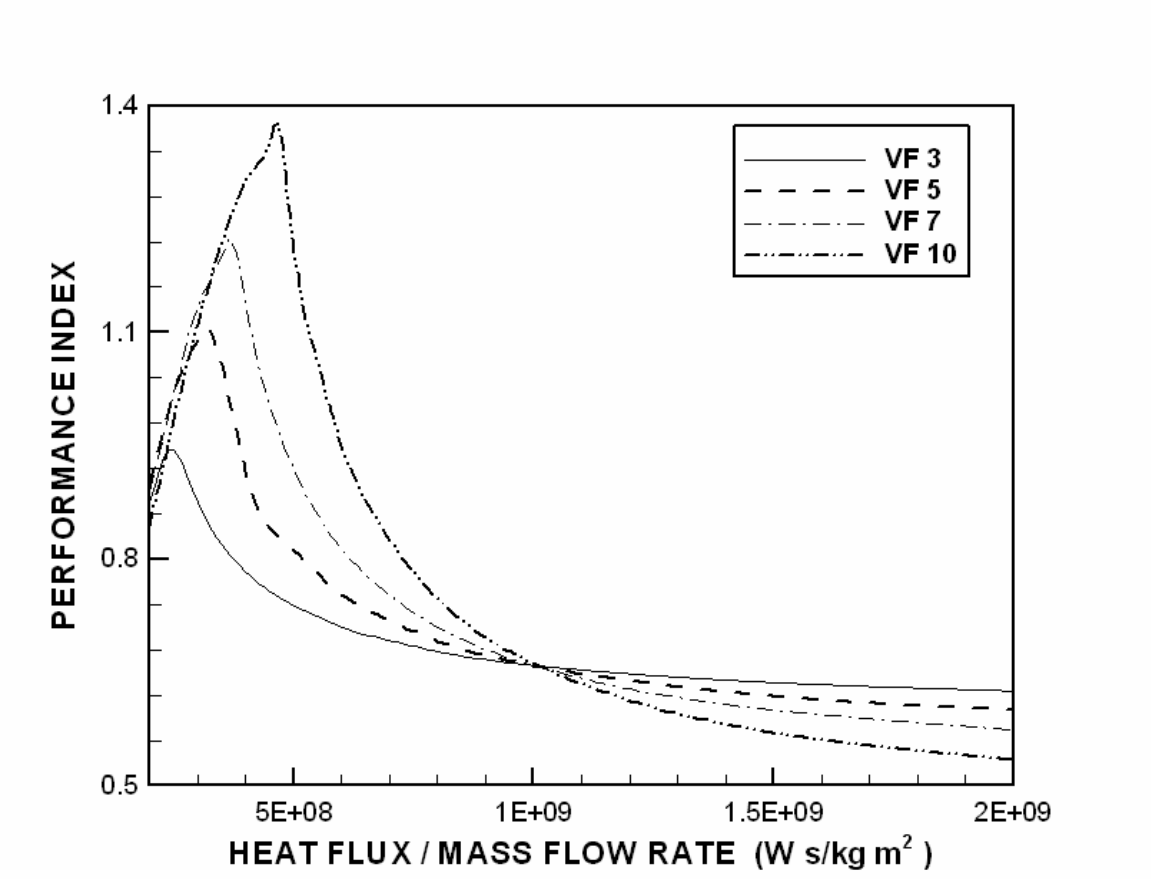

Figure 5.19 Variation of performance index with ratio of heat flux to mass flow rate of P.C.M. slurry, where VF 3, VF 5, VF 7 and VF 10 represents 3%, 5%, 7% and 10% volume concentration of the particles, respectively.

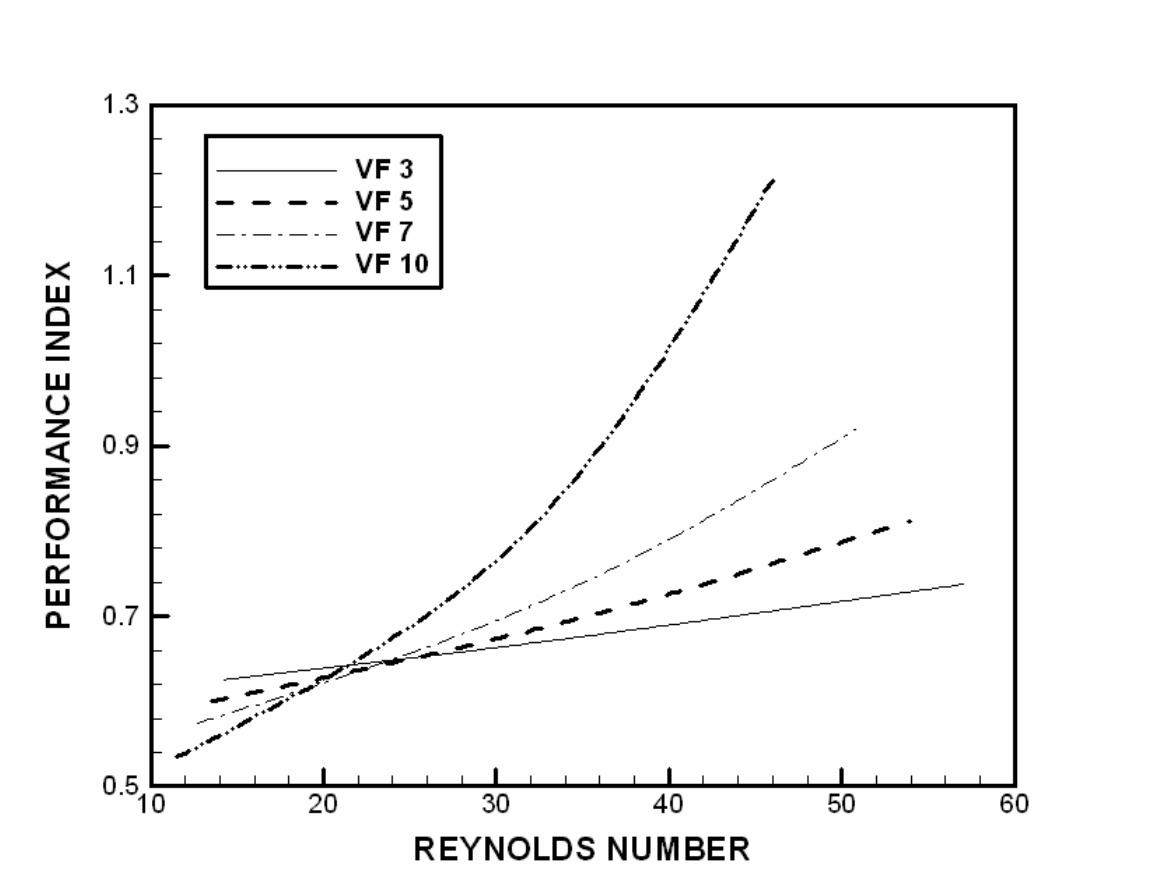

Figure 5.20 Variation of performance index with Reynolds number for heat flux of 20000 W/m^2, where VF 3, VF 5, VF 7 and VF 10 represents 3%, 5%, 7% and 10% volume concentration of the particles, respectively.

5.2.3 Merit Number

The thermal conductivity of the bulk fluid decreases due to the addition of P.C.M. particles into the carrier fluid, in addition to the increase in pressure drop. The decrease in thermal conductivity and increase in pressure drop contribute to an increase in the volumetric entropy generation rate inside the microchannel. However, increase in volume concentration of particles increases the heat flux than can be absorbed by the bulk fluid for a given temperature rise. Therefore, Merit number is introduced to calculate the ratio of the gain versus input and losses due to the addition of particles. The Merit number takes into account the entropy generation rate due to fluid friction and heat transfer caused by the addition of P.C.M. particles. It is defined as the ratio of the gain in heat transfer due to the use of P.C.M. particles to the sum of heat transferred at the bottom wall of the microchannel and the irreversibility. The Merit number is defined as:

$$Merit\ number = \frac{\dot{Q}_{gain}}{\dot{Q}_b + \dot{I}} \tag{5.2.8}$$

Where

$$\dot{Q}_{gain} = \dot{Q}_b - \dot{Q}_f \tag{5.2.9}$$

$$\dot{I} = S'''_{gen,avg} \times volume \times T_r \tag{5.2.10}$$

$$S'''_{gen} = \frac{k_b}{T^2}\left[\left(\frac{\partial T}{\partial x}\right)^2 + \left(\frac{\partial T}{\partial y}\right)^2\right] + \frac{\mu_b}{T}\left(\frac{\partial u}{\partial y}\right)^2 \tag{5.2.11}$$

where $\dot{Q}_b$ is the heat transfer rate to the slurry, $\dot{Q}_f$ is the rate of heat transferred to the carrier fluid, $S'''_{gen,avg}$ is the volume averaged volumetric entropy generation rate and T_r is the reference temperature taken as 298 K.

Figures 5.21 to 5.24 show the variation of Merit number with heat flux for different particle volume concentrations and mass flow rates. In Figure 5.25, Merit number is plotted against heat flux to mass flow rate ratio for different particle volume concentrations. The Merit number follows the same trend as effectiveness ratio with the same value of optimum heat flux for a given mass flow rate and particle volume concentration. The Merit number of the bulk fluid with 10% volume concentration of particles is also the highest for all heat flux and mass flow rates considered in the simulations. This shows that the increase in irreversibility due to the addition of P.C.M. particles is being offset by the gain in heat transfer for all heat flux to mass flow rate ratios considered.

Figure 5.26 shows the variation of Merit number with Reynolds number for heat flux 20000 W/m^2. It can be observed that Merit number increases linearly with increasing Reynolds number; however the slope of Merit number variation depends on the volume concentration of P.C.M. particles; in which case, it is higher for higher volume concentration of P.C.M. particles. Moreover increase in heat storage capacity due to increase in Reynolds number is higher than the increase in irreversibility. At high heat flux, the enhancement in heat storage capacity is highest when Reynolds number is high.

This is attributed to the latent heat effect which dominates over the sensible heat at high Reynolds number for high heat fluxes. Increase in the volume concentration of P.C.M. particles further increases the heat storage capacity of the slurry and Merit number. Therefore, at high heat flux, increasing Reynolds number and volume concentration of P.C.M. particles increases Merit number.

The highest Merit number of 0.64 is obtained for particle volume concentration of 10%. From the above analyses, it can be concluded that for a given volume concentration of particles, there exists a heat flux to mass flow rate ratio at which the Merit number is maximum.

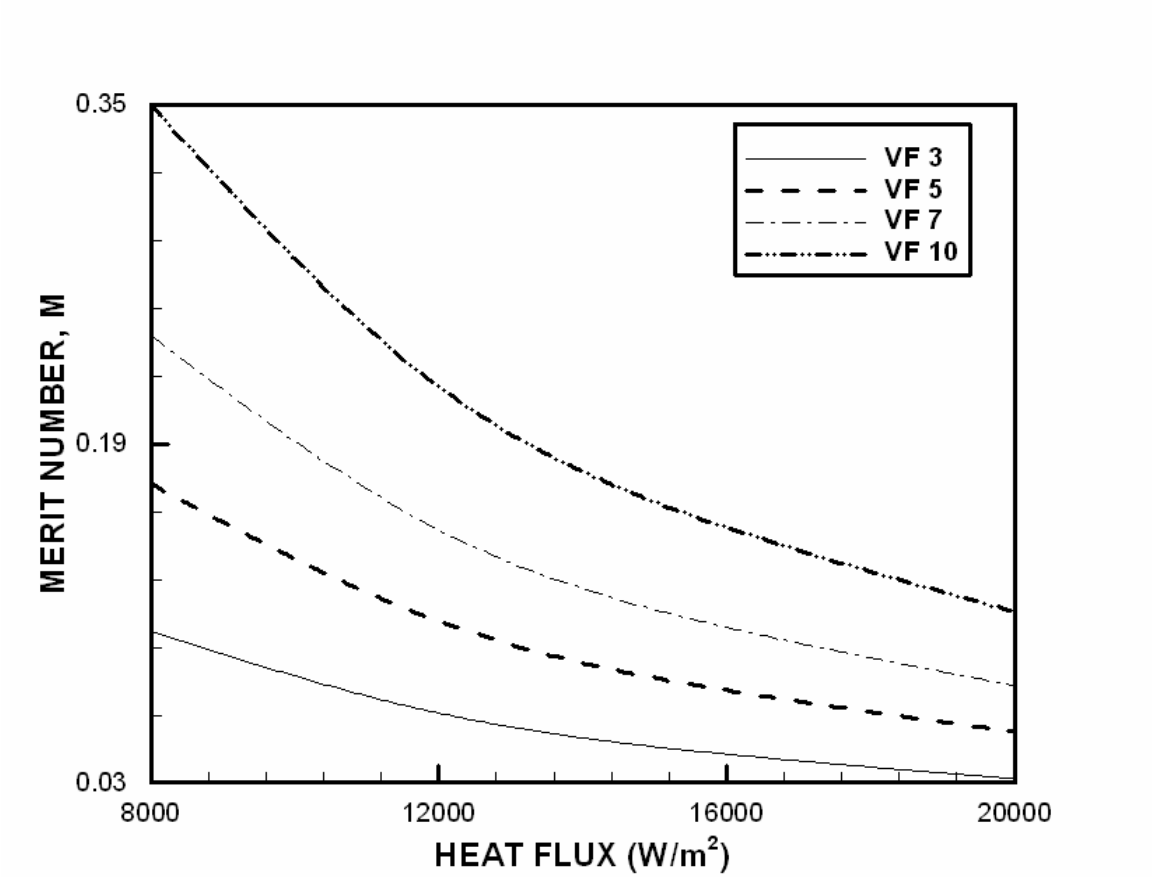

Figure 5.21 Variation of Merit number with heat flux for mass flow rate of 10^{-5} kg/s, where VF 3, VF 5, VF 7 and VF 10 represents 3%, 5%, 7% and 10% volume concentration of the particles, respectively.

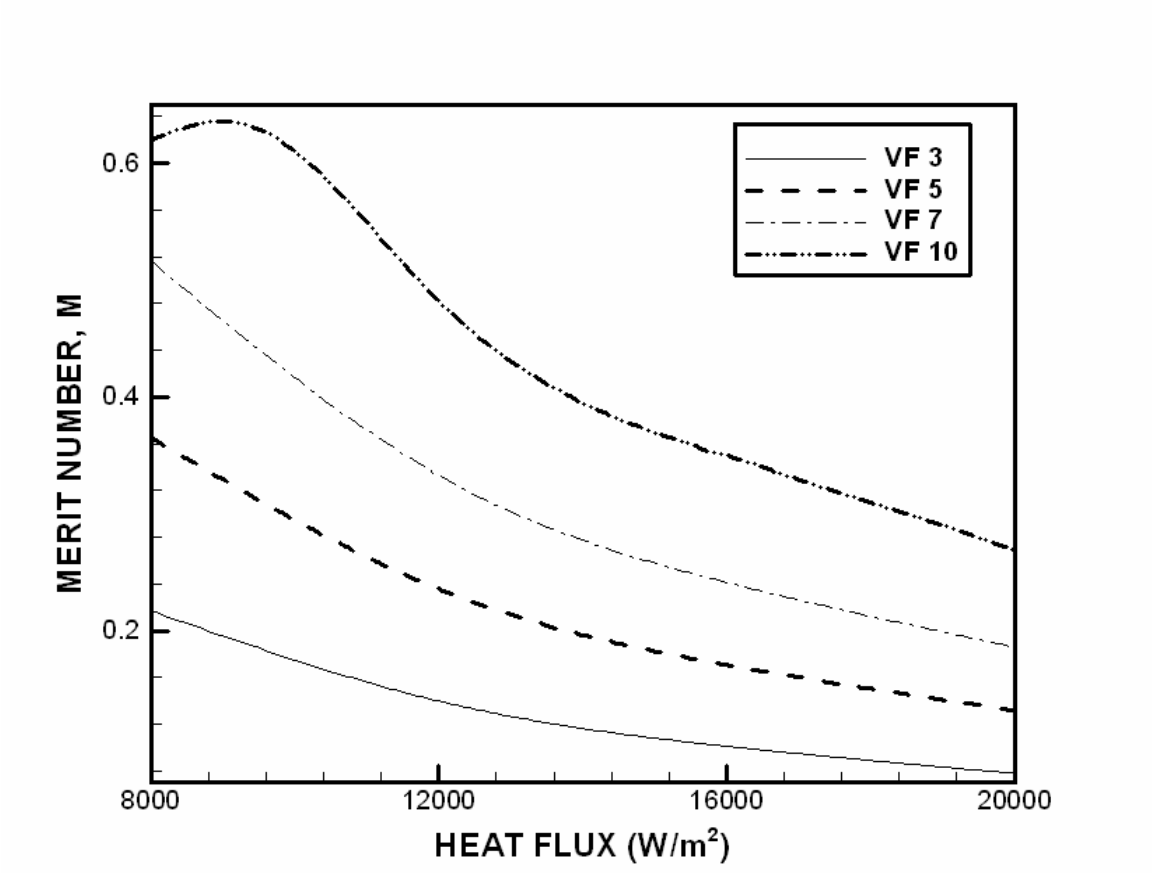

Figure 5.22 Variation of Merit number with heat flux for mass flow rate of 2 x 10^{-5} kg/s, where VF 3, VF 5, VF 7 and VF 10 represents 3%, 5%, 7% and 10% volume concentration of the particles, respectively.

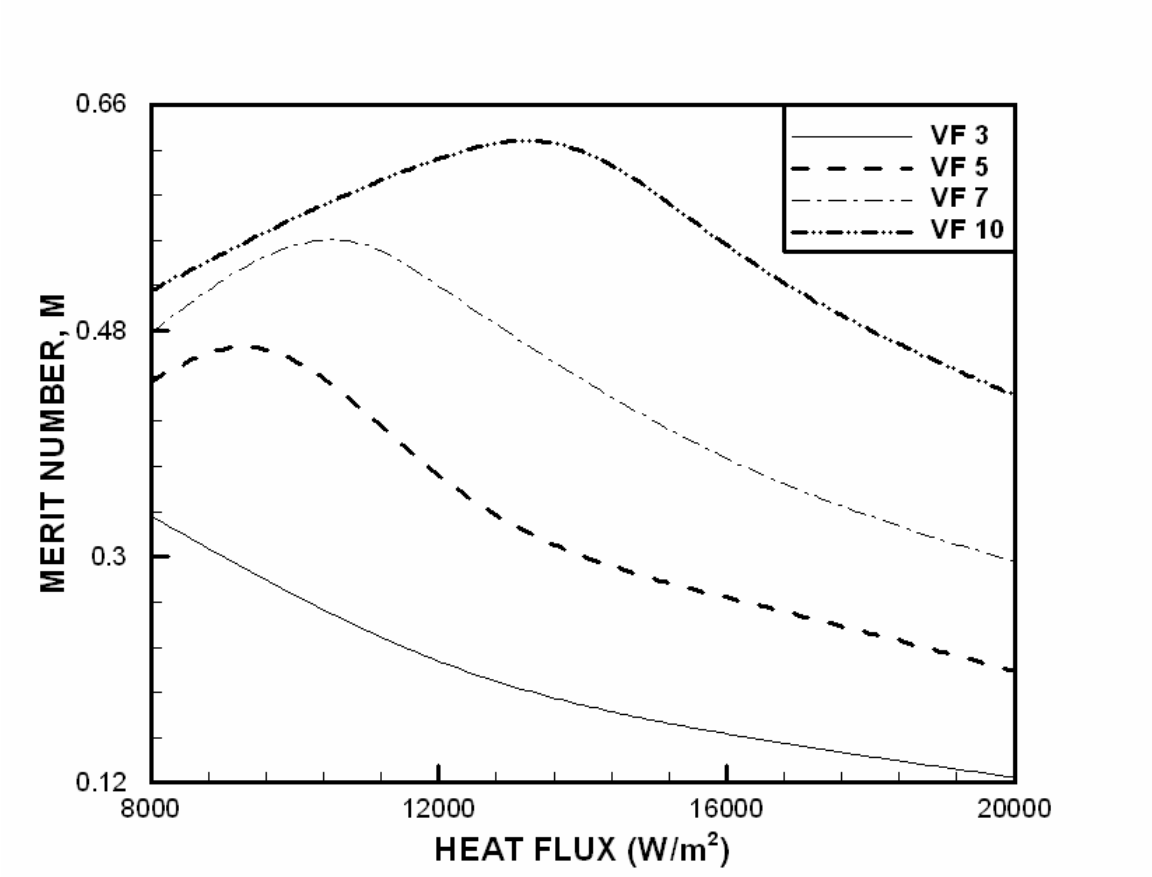

Figure 5.23 Variation of Merit number with heat flux for mass flow rate of 3 x 10^{-5} kg/s, where VF 3, VF 5, VF 7 and VF 10 represents 3%, 5%, 7% and 10% volume concentration of the particles, respectively.

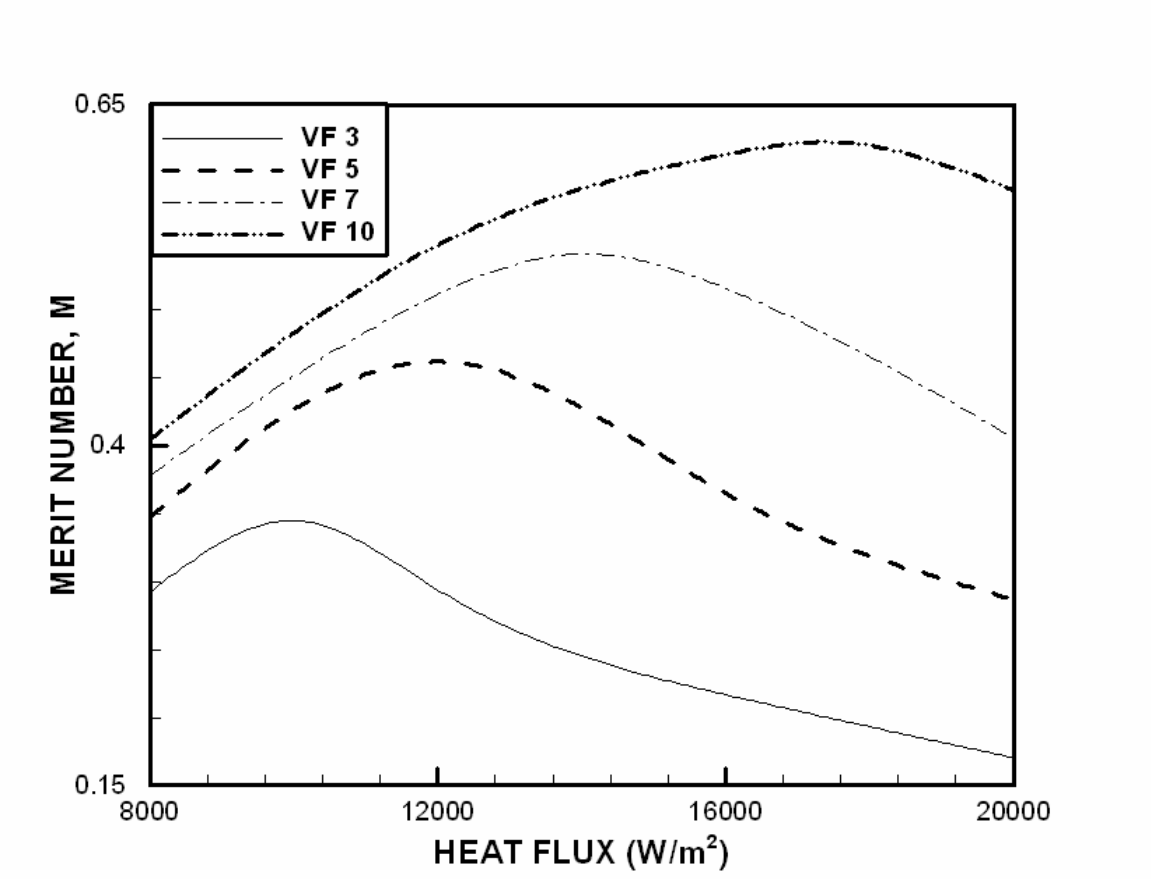

Figure 5.24 Variation of Merit number with heat flux for mass flow rate of 4 x 10^{-5} kg/s, where VF 3, VF 5, VF 7 and VF 10 represents 3%, 5%, 7% and 10% volume concentration of the particles, respectively.

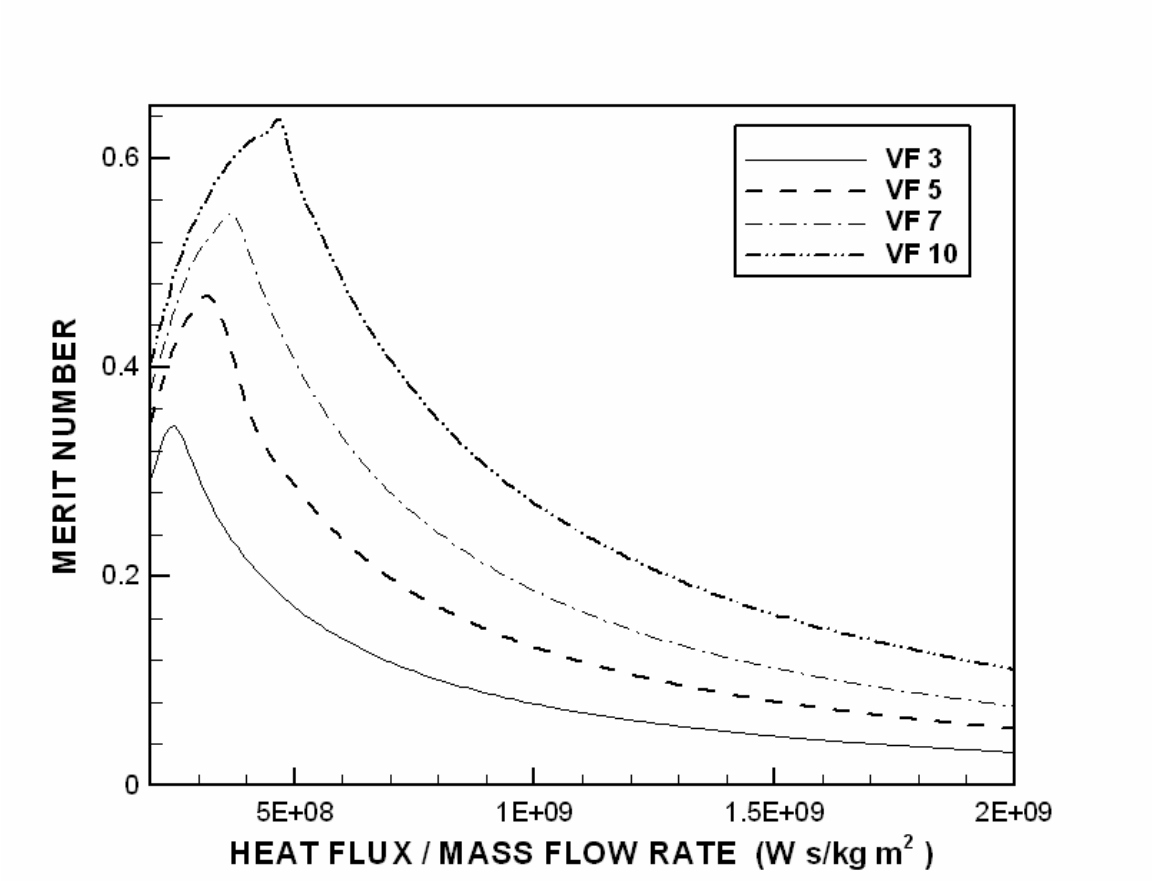

Figure 5.25 Variation of Merit number with ratio of heat flux to mass flow rate of P.C.M. slurry, where VF 3, VF 5, VF 7 and VF 10 represents 3%, 5%, 7% and 10% volume concentration of the particles, respectively.

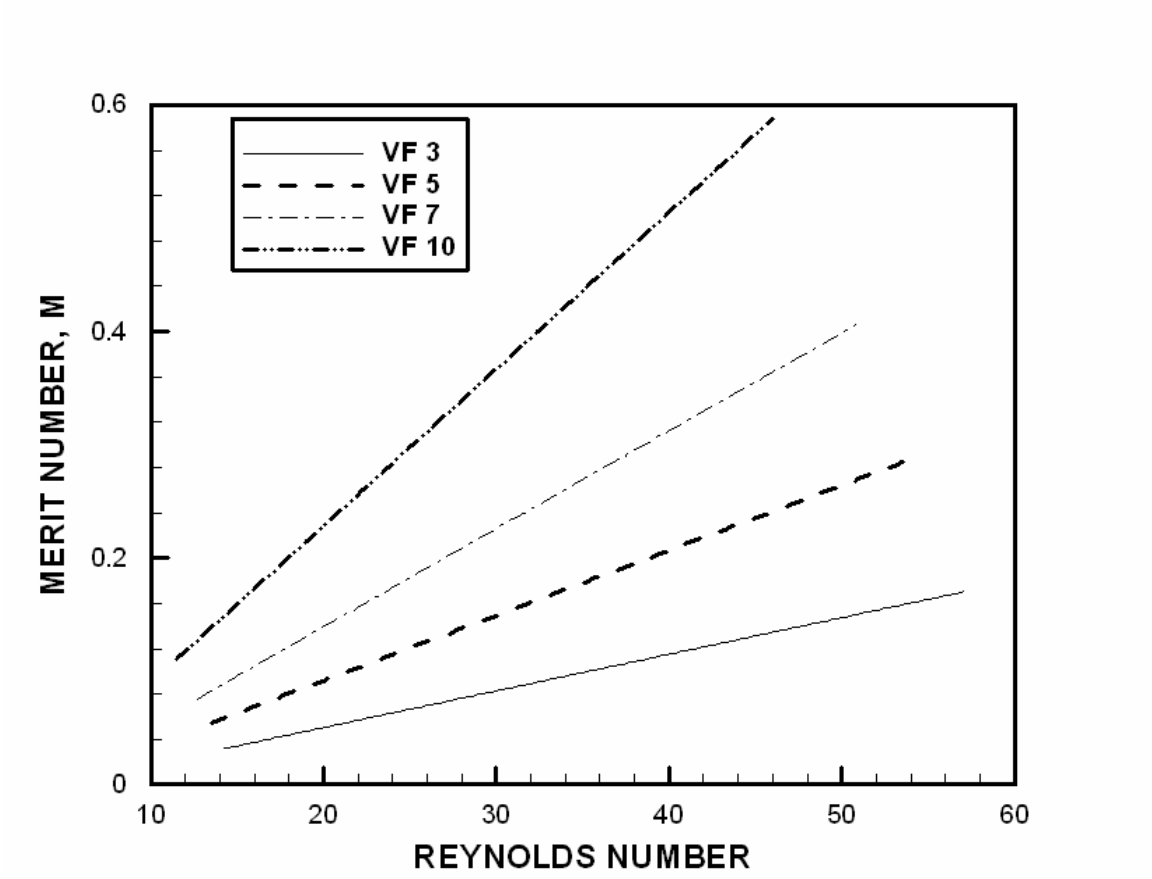

Figure 5.26 Variation of Merit number with Reynolds number for heat flux of 20000 W/m^2, where VF 3, VF 5, VF 7 and VF 10 represents 3%, 5%, 7% and 10% volume concentration of the particles, respectively.

5.3 Volumetric Entropy Generation Rate due to Heat Transfer and Fluid Friction

The influence of particle volume concentration, mass flow rate and heat flux on the volumetric entropy generation rate due to heat transfer and fluid friction is investigated by conducting a parametric study.

At the inlet, the temperature of the particles and carrier fluid is specified as 315 K, which is lower than the melting temperature of the P.C.M. particles. The mass flow rate of the bulk fluid at the inlet is varied from 10^{-5} kg/s to 4 x 10^{-5} kg/s. The heat flux applied at the bottom wall of the microchannel is varied from 8000 W/m^2 to 20000 W/m^2.

5.3.1 Volumetric Entropy Generation Rate due to Heat Transfer

The volumetric entropy generation rate due to heat transfer is defined as

$$S'''_{generation\_h} = \frac{k_b}{T^2}\left[\left(\frac{\partial T}{\partial x}\right)^2 + \left(\frac{\partial T}{\partial y}\right)^2\right] \tag{5.3.1}$$

Figures 5.27 to 5.30 show the variation of volumetric entropy generation rate due to heat transfer, with heat flux, for different mass flow rates and particle volume concentrations. The volumetric entropy generation rate due to heat transfer increases with increasing heat flux. Increasing volume concentration of particles in the bulk fluid, almost always leads to an increase in the volumetric entropy generation rate due to heat transfer. The volumetric entropy generation rate due to heat transfer, in most cases, increases with increasing mass flow rate. Therefore, the highest volumetric entropy generation rate due

to heat transfer is obtained for mass flow rate of 4 x 10^{-5} kg/s, heat flux of 20000 W/m^2 and 10% volume concentration of particles.

Increase in heat flux leads to increase in the temperature rise and the temperature gradients in the microchannel as seen from Figures 5.31 to 5.38. Higher value of heat flux leads to a reduction in phase change region, and therefore $\partial T/\partial x$ also increases. Since, increase in heat flux leads to a much higher rate of increase of temperature gradients in both the axial and transverse directions, as compared to the rate of increase of temperature, therefore, the rate of volumetric entropy generated due to heat transfer increases with increasing heat flux.

In the phase change region, the slope of temperature along the length i.e. $\partial T/\partial x$ reduces as can be seen from Figures 5.31 to 5.34. The phase change region, increases with increasing volume concentration of particles and consequently higher volume concentration of particles leads to a lower value of $\partial T/\partial x$. However, with increase in the volume concentration of particles, the temperature rise in the bulk fluid also reduces, thereby reducing the denominator in the equation for volumetric entropy generation rate. Moreover, the increase in volume concentration of particles in the bulk fluid coupled with decrease in the temperature rise reduce the bulk fluid thermal conductivity, thereby, increasing the temperature gradient along height i.e. $\partial T/\partial y$ as can be seen from Figures 5.35 to 5.38. Therefore, an increase in the volume concentration of particles in the bulk fluid, almost always leads to increase in the volumetric entropy generation rate due to

heat transfer in spite of the reduction in $\partial T/\partial x$. In some cases, with high mass flow rates and low heat flux, increase in volume concentration leads to a reduction in volumetric entropy generation rate due to heat transfer. For mass flow rate of 3 x 10^{-5} kg/s and heat flux of 8000 W/m^2, increase in volume concentration of particles from 3% to 5% leads to a reduction in volumetric entropy generation rate due to heat transfer. Similarly, for mass flow rate of 4 x 10^{-5} kg/s and heat flux of 12000 W/m^2, increase in volume concentration of particles beyond 5% leads to a reduction in volumetric entropy generation rate as compared to the case with 5% volume concentration of particles. For mass flow rate of 2 x 10^{-5} kg/s, heat flux of 8000 W/m^2, and mass flow rate of 4 x 10^{-5} kg/s, heat flux of 16000 W/m^2, increase in volume concentration of particles beyond 7% leads to a reduction in volumetric entropy generation rate due to heat transfer.

Increase in the mass flow rate of the bulk fluid generally increases the volumetric entropy generation rate due to heat transfer, but, at certain volume concentration of particles and for low heat flux and high mass flow rates, further increase in mass flow rates leads to a reduction in volumetric entropy generation rate. For carrier fluid without any P.C.M. particles and for cases with high heat flux, increase in mass flow rate always leads to an increase in the volumetric entropy generation rate due to heat transfer. Increase in mass flow rate leads to a reduction in temperature rise as well as reduction in temperature gradient in the axial direction. However, the temperature gradient in the transverse direction remains almost constant with increase in mass flow rate. Since the temperature gradient in transverse direction is much larger than the temperature gradient in the axial

direction, the volumetric entropy generation rate due to heat transfer increases as the temperature rise decreases with increase in mass flow rate.

In the case of 3% volume concentration of particles in the carrier fluid, increase in mass flow rate always leads to an increase in volumetric entropy generation rate due to heat transfer, except for mass flow rate of 4 x 10^{-5} kg/s and heat flux of 8000 W/m^2. At mass flow rate of 4 x 10^{-5} kg/s and for heat flux of 8000 W/m^2, the volumetric entropy generation rate is slightly higher than the base case of 10^{-5} kg/s, but it is lower compared to the case with mass flow rate of 3 x 10^{-5} kg/s. For 5% volume concentration of particles in the carrier fluid, there are three cases where the volumetric entropy generation rate due to heat transfer decreases with increase in mass flow rate. For heat flux of 8000 W/m^2, increase in mass flow rate beyond 2 x 10^{-5} kg/s leads to a reduction in the volumetric entropy generation rate due to heat transfer. For heat flux of 12000 W/m^2, increase in mass flow rate from 3 x 10^{-5} to 4 x 10^{-5} kg/s reduces the rate of volumetric entropy generation. A similar observation is made for 7% volume concentration of particles. For 10% volume concentration of particles and heat flux of 8000 W/m^2, any increase in mass flow rate beyond 10^{-5} kg/s leads to a reduction in volumetric entropy generation rate. For heat flux of 12000 W/m^2, increase in mass flow rate beyond 2 x 10^{-5} kg/s leads to a reduction in volumetric entropy generation rate. For heat flux of 16000 W/m^2, increase of mass flow rate beyond 3 x 10^{-5} kg/s leads to a reduction in volumetric entropy generation rate.

The above trends in which increase in mass flow rate and volume concentration of bulk fluid lead to reduction in rate of volumetric entropy generation due to heat transfer can be explained as follows:

The region near the bottom wall of the microchannel is at higher temperature compared to the upper region because of heat flux being applied at the bottom wall. Therefore, the P.C.M. particles near the bottom wall of the microchannel exceed the lower phase change temperature (solidus temperature) earlier than the particles in the upper region of the microchannel. At the same time, the region near the top of the microchannel is still below the solidus temperature. Hence, the rate of increase of temperature in the region near bottom wall slows down on exceeding the solidus temperature, but the temperature in the upper region keeps increasing at the same rate; thereby bringing down the temperature gradient in the transverse direction. Once the temperature in the upper region also exceeds the solidus temperature, then the temperature gradient starts to increase again, and reaches a distribution with almost constant upper and lower limits. Towards the end of phase change process, the temperature in the region near the bottom wall exceeds the liquidus temperature earlier and, as a result, starts to increase at a higher rate, while the temperature at the top is still in the melting range and increases slowly. This leads to an increase in the temperature gradient in the transverse direction. Once the temperature in the upper region of the microchannel exceeds the liquidus temperature, then the temperature gradient reduces and again reaches its normal distribution. Therefore, the average value of temperature gradient $\partial T/\partial y$ along the height of the microchannel is

almost constant, except that it varies at the beginning and end of phase change regions. The drop in the magnitude of $\partial T/\partial y$ observed at the beginning of the phase change process is compensated by the increase in its magnitude at the end of phase change process. However, certain mass flow rate, volume concentration, and heat flux combinations lead to incomplete melting of particles. In such cases, the temperature gradient $\partial T/\partial y$ decreases at the beginning of the phase change process, however as the temperature does not exceed the melting range, $\partial T/\partial y$ does not increase towards the end. This causes a net decrease in the temperature gradient $\partial T/\partial y$, and consequently a reduction in the volumetric entropy generation rate due to heat transfer as is observed in the above cases.

The maximum volumetric entropy generation rate is obtained for mass flow rate of 4×10^{-5} kg/s, heat flux of 20000 W/m^2 and 10% volume concentration of particles, and is 15.6% higher than the volumetric entropy generation rate for carrier fluid without P.C.M. particles. The volumetric entropy generation rate due to heat transfer is found to vary with mass flow rate, volume concentration of particles, and heat flux. From the above analysis, it can be concluded that the temperature gradient in the transverse direction, $\partial T/\partial y$, is the controlling factor for volumetric entropy generation rate due to heat transfer. Any significant change in $\partial T/\partial y$ directly effects the volumetric entropy generation rate due to heat transfer.

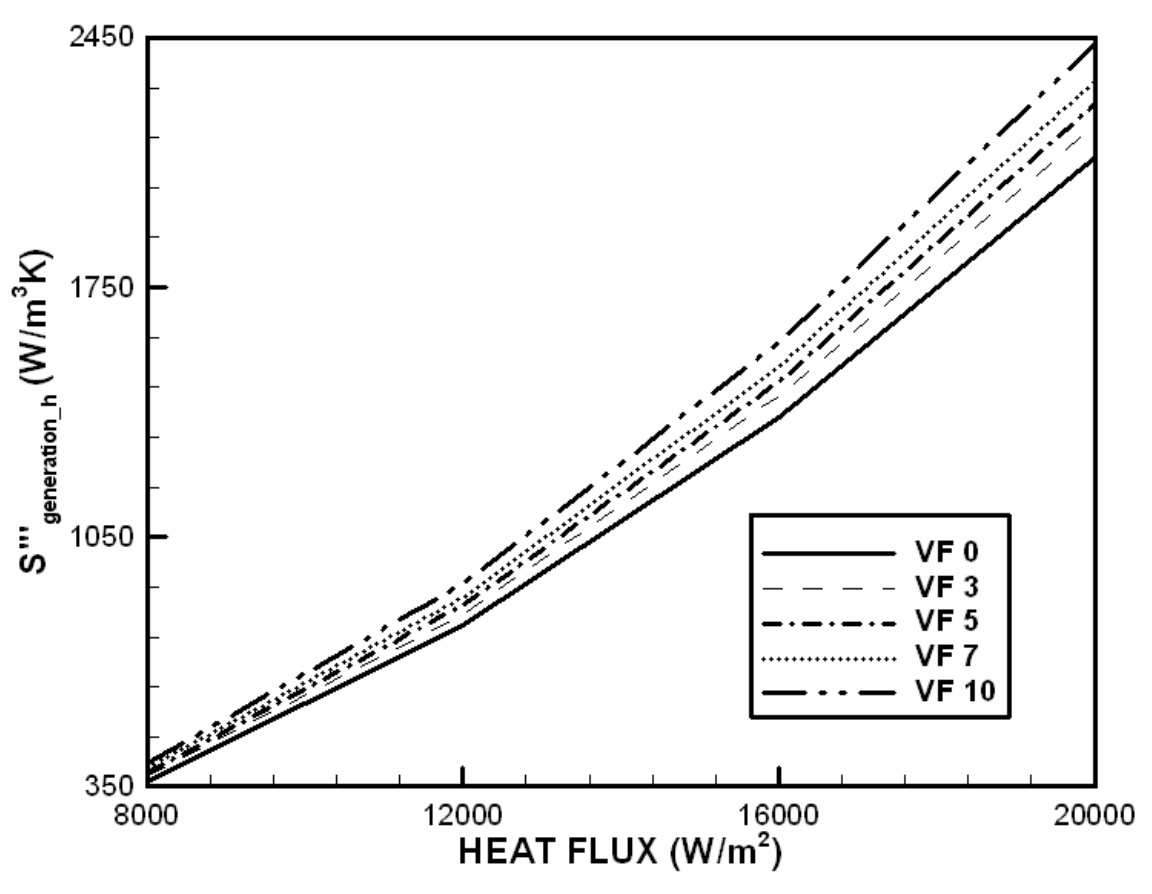

Figure 5.27 Volumetric entropy generation rate due to heat transfer for mass flow rate of 10^{-5} kg/s ; where VF0,VF 3, VF 5, VF 7 and VF 10 represent 0%, 3%, 5%, 7% and 10% volume concentration of the particles, respectively.

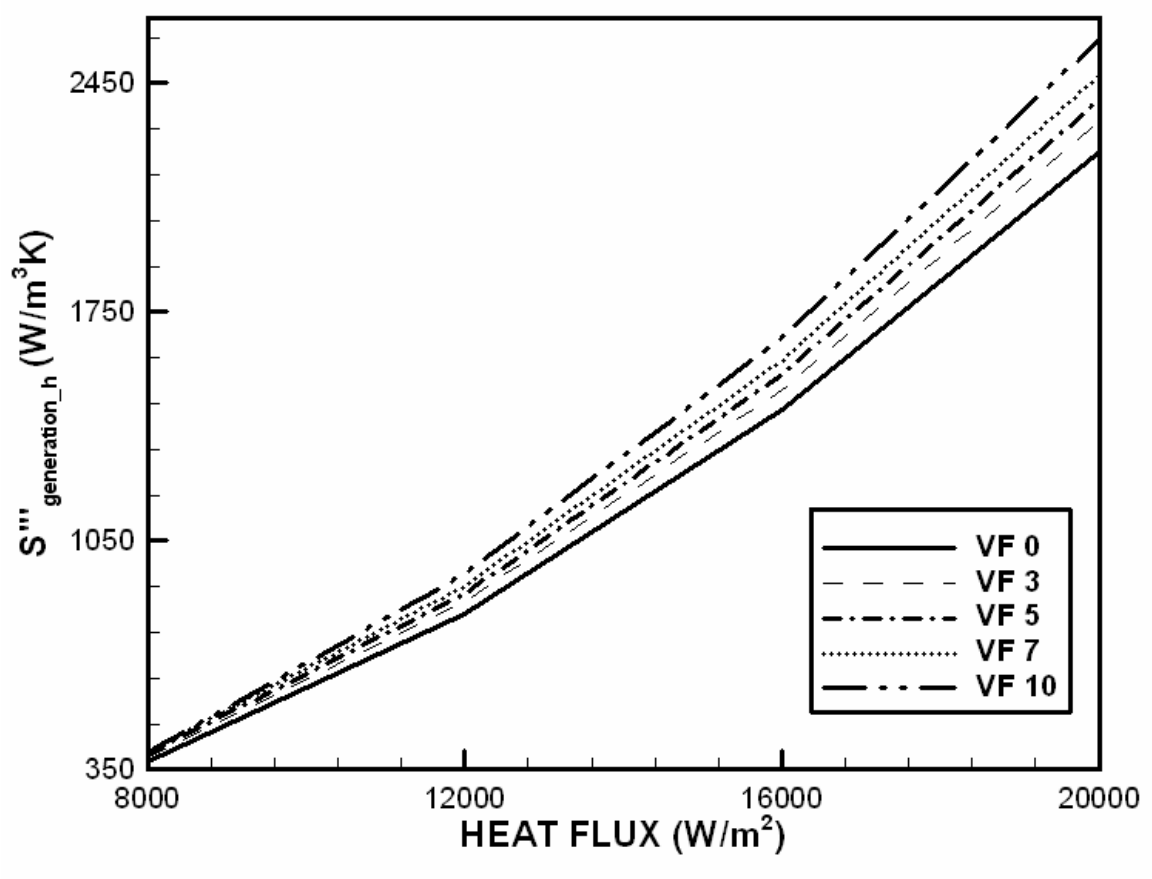

Figure 5.28 Volumetric entropy generation rate due to heat transfer for mass flow rate of 2×10^{-5} kg/s ; where VF0,VF 3, VF 5, VF 7 and VF 10 represent 0%, 3%, 5%, 7% and 10% volume concentration of the particles, respectively

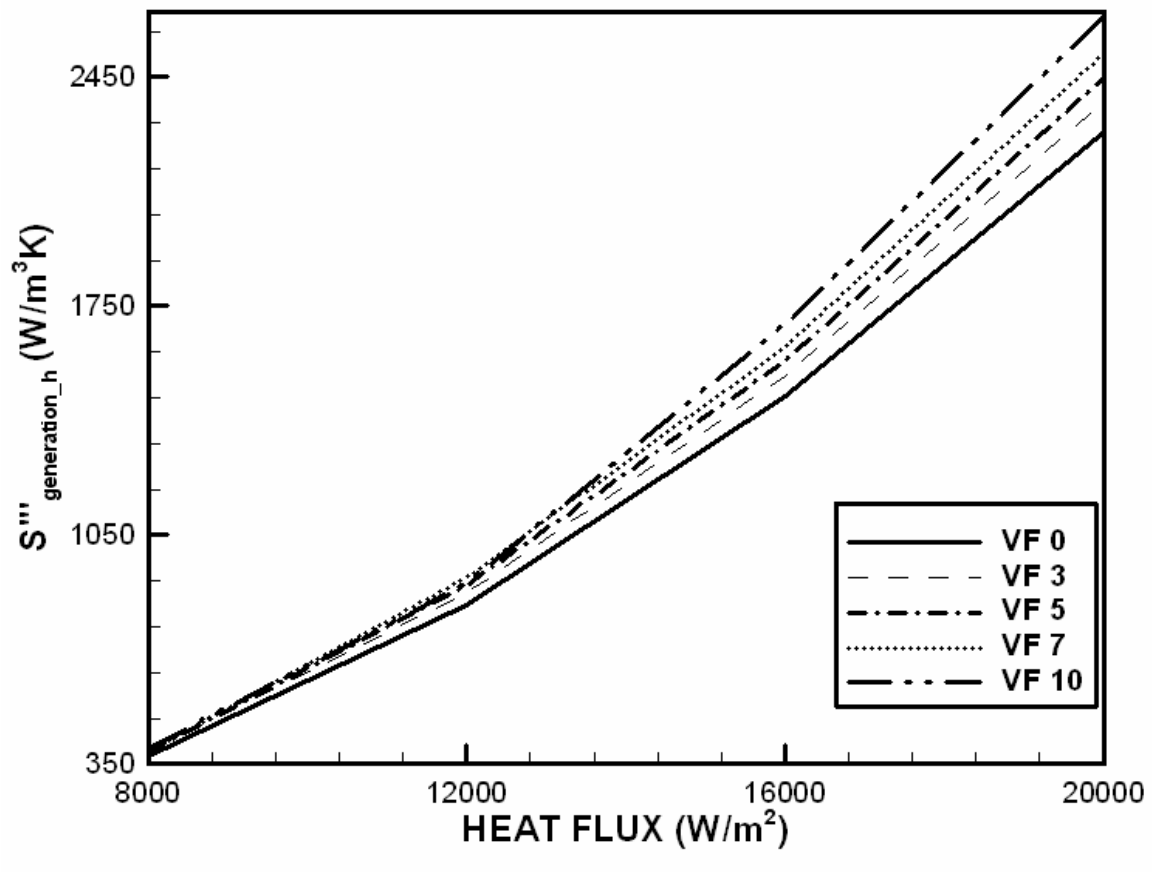

Figure 5.29 Volumetric entropy generation rate due to heat transfer for mass flow rate of 3 x 10^{-5} kg/s ; where VF0,VF 3, VF 5, VF 7 and VF 10 represent 0%, 3%, 5%, 7% and 10% volume concentration of the particles, respectively.

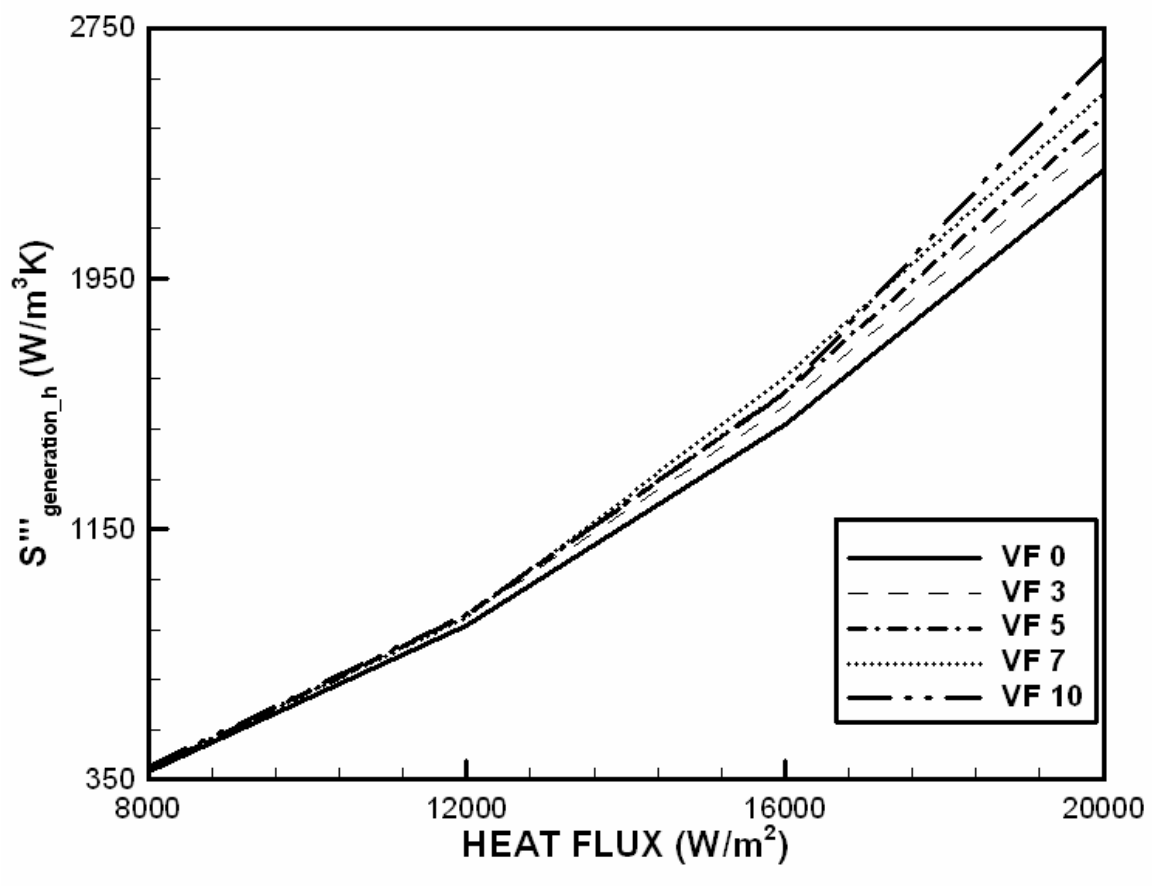

Figure 5.30 Volumetric entropy generation rate due to heat transfer for mass flow rate of 4 x 10^{-5} kg/s ; where VF0,VF 3, VF 5, VF 7 and VF 10 represent 0%, 3%, 5%, 7% and 10% volume concentration of the particles, respectively.

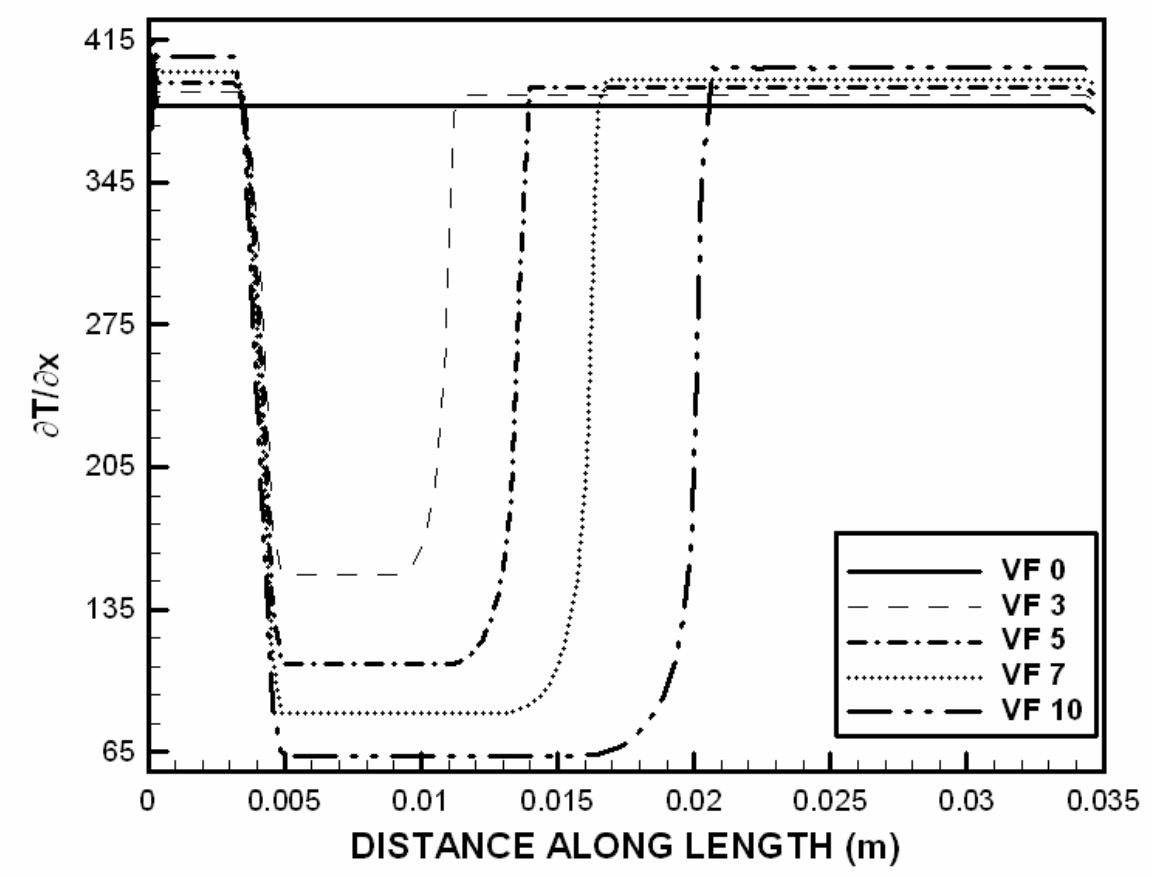

Figure 5.31 Temperature gradient along microchannel length for heat flux of 8000 W/m^2 and mass flow rate of 10^{-5} kg/s ; where VF0,VF 3, VF 5, VF 7 and VF 10 represent 0%, 3%, 5%, 7% and 10% volume concentration of the particles, respectively.

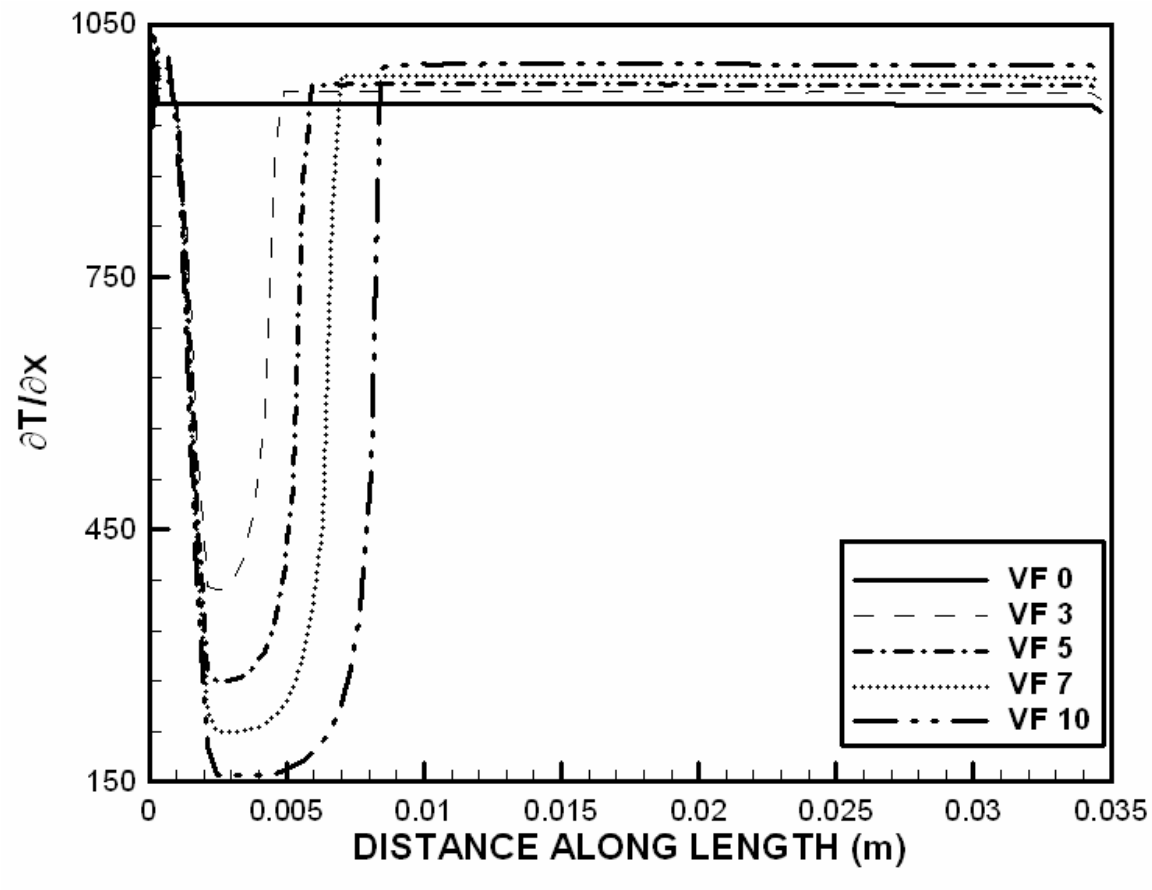

Figure 5.32 Temperature gradient along microchannel length for heat flux of 20000 W/m^2 and mass flow rate of 10^{-5} kg/s ; where VF0,VF 3, VF 5, VF 7 and VF 10 represent 0%, 3%, 5%, 7% and 10% volume concentration of the particles, respectively.

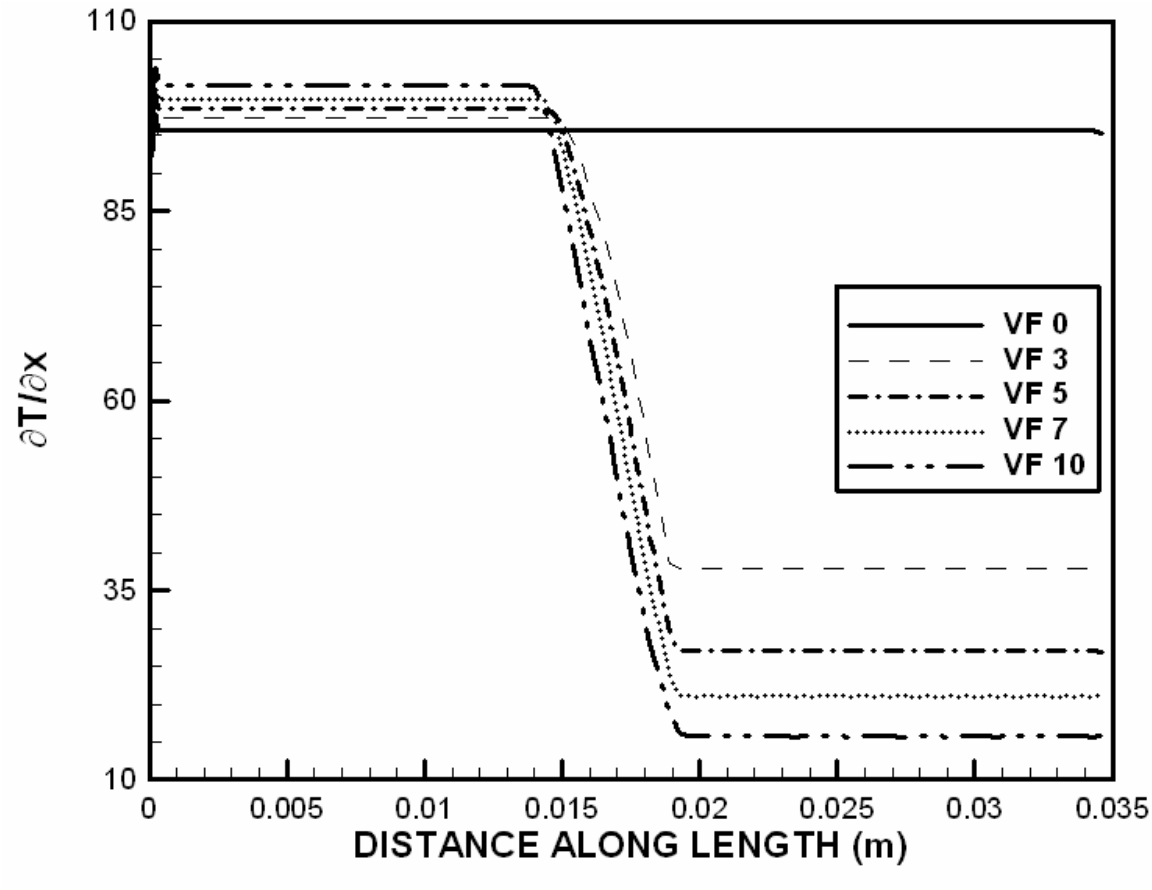

Figure 5.33 Temperature gradient along microchannel length for heat flux of 8000 W/m^2 and mass flow rate of 4 x 10^{-5} kg/s ; where VF0,VF 3, VF 5, VF 7 and VF 10 represent 0%, 3%, 5%, 7% and 10% volume concentration of the particles, respectively.

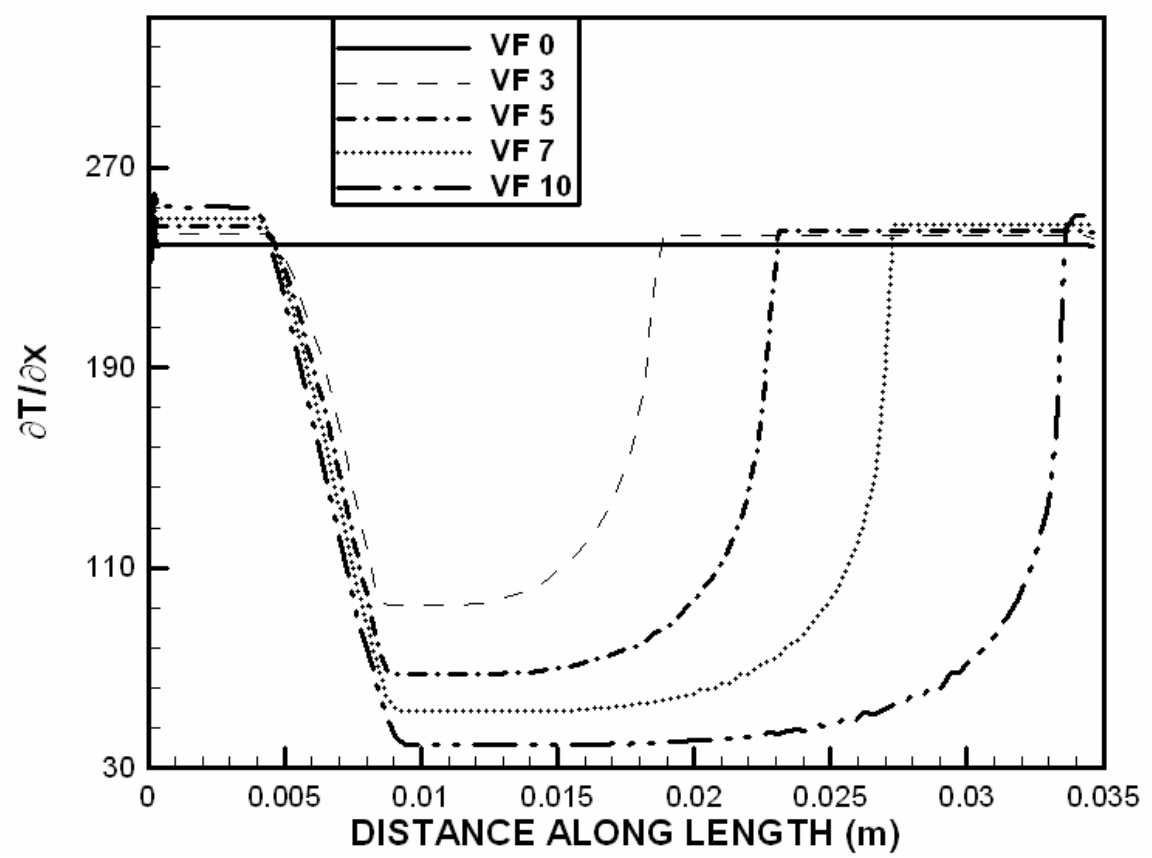

Figure 5.34 Temperature gradient along microchannel length for heat flux of 20000 W/m^2 and mass flow rate of 4 x 10^{-5} kg/s ; where VF0,VF 3, VF 5, VF 7 and VF 10 represent 0%, 3%, 5%, 7% and 10% volume concentration of the particles, respectively.

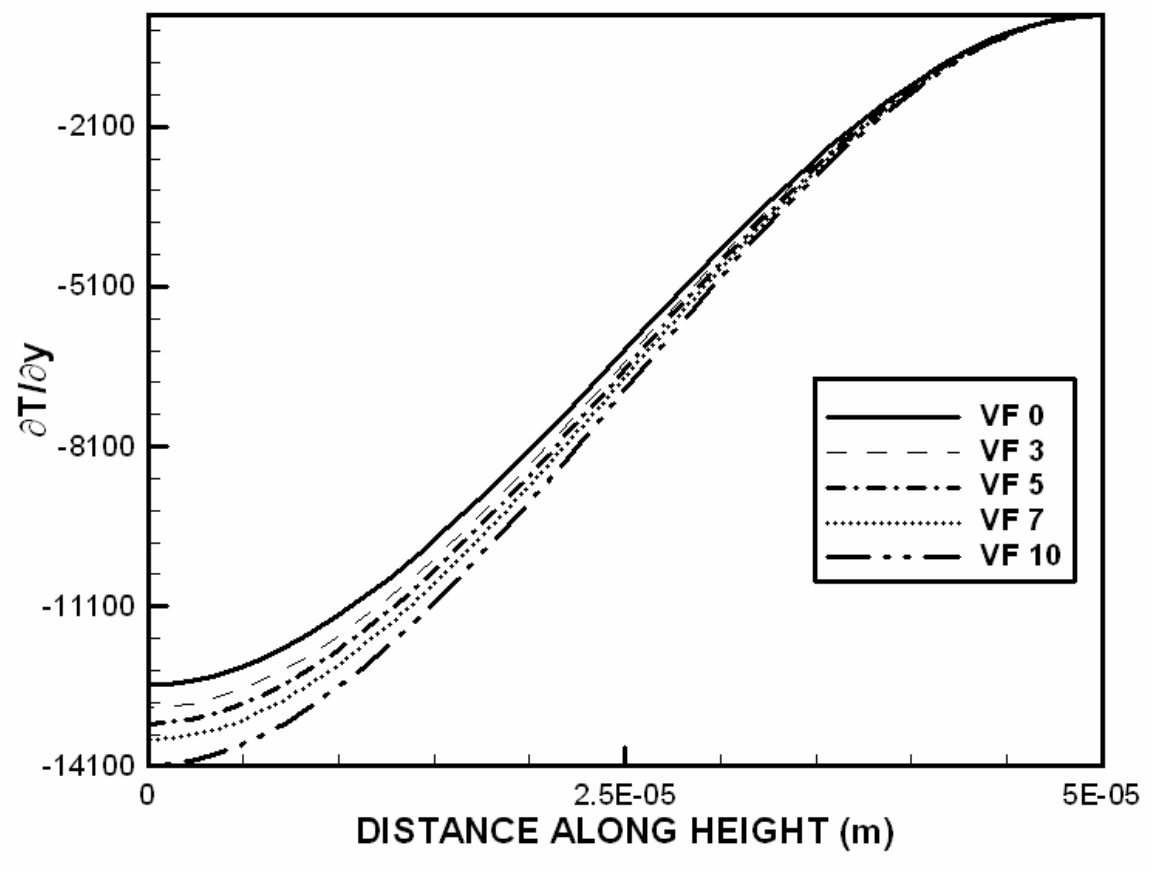

Figure 5.35 Temperature gradient along microchannel height at axial distance of 0.0345 m from inlet, for heat flux of 8000 W/m^2 and mass flow rate of 10^{-5} kg/s ; where VF0,VF 3, VF 5, VF 7 and VF 10 represent 0%, 3%, 5%, 7% and 10% volume concentration of the particles, respectively.

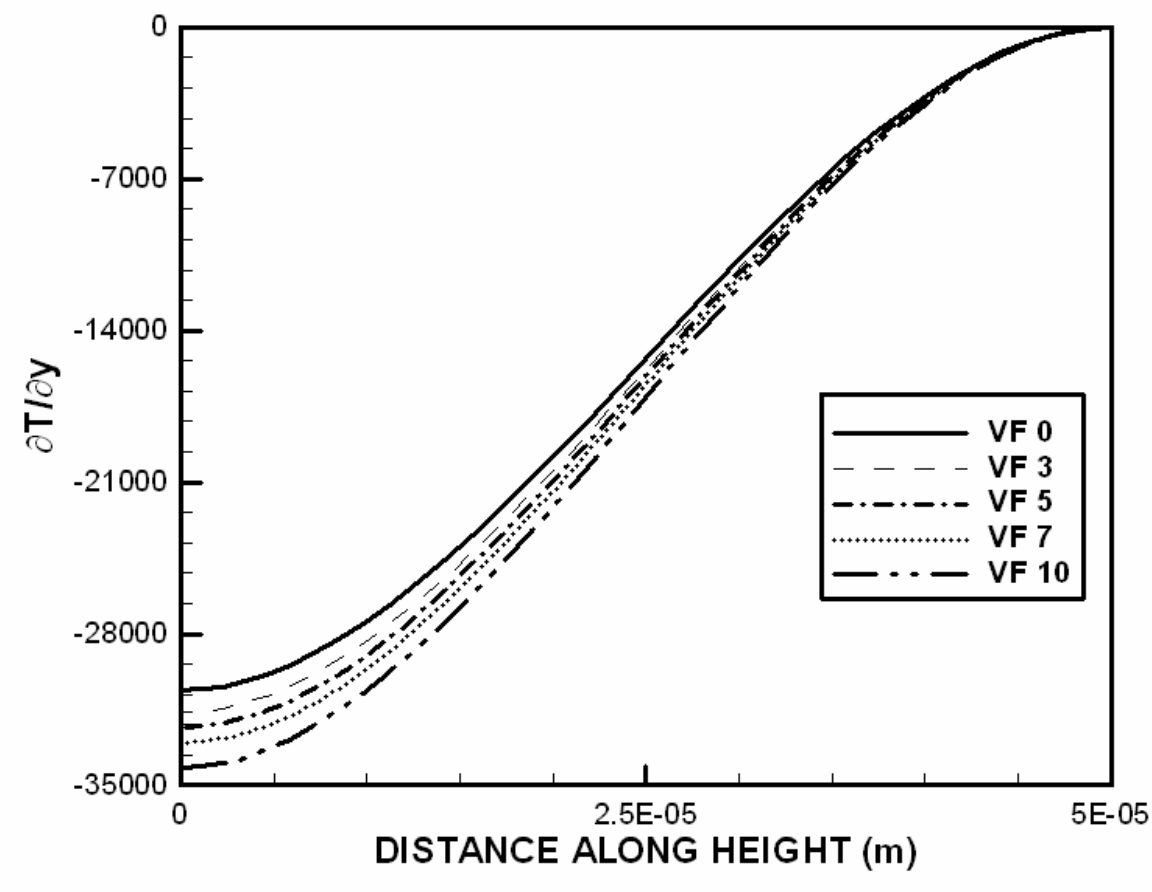

Figure 5.36 Temperature gradient along microchannel height at axial distance of 0.0345 m from inlet,for heat flux of 20000 W/m^2 and mass flow rate of 10^{-5} kg/s ; where VF0,VF 3, VF 5, VF 7 and VF 10 represent 0%, 3%, 5%, 7% and 10% volume concentration of the particles, respectively.

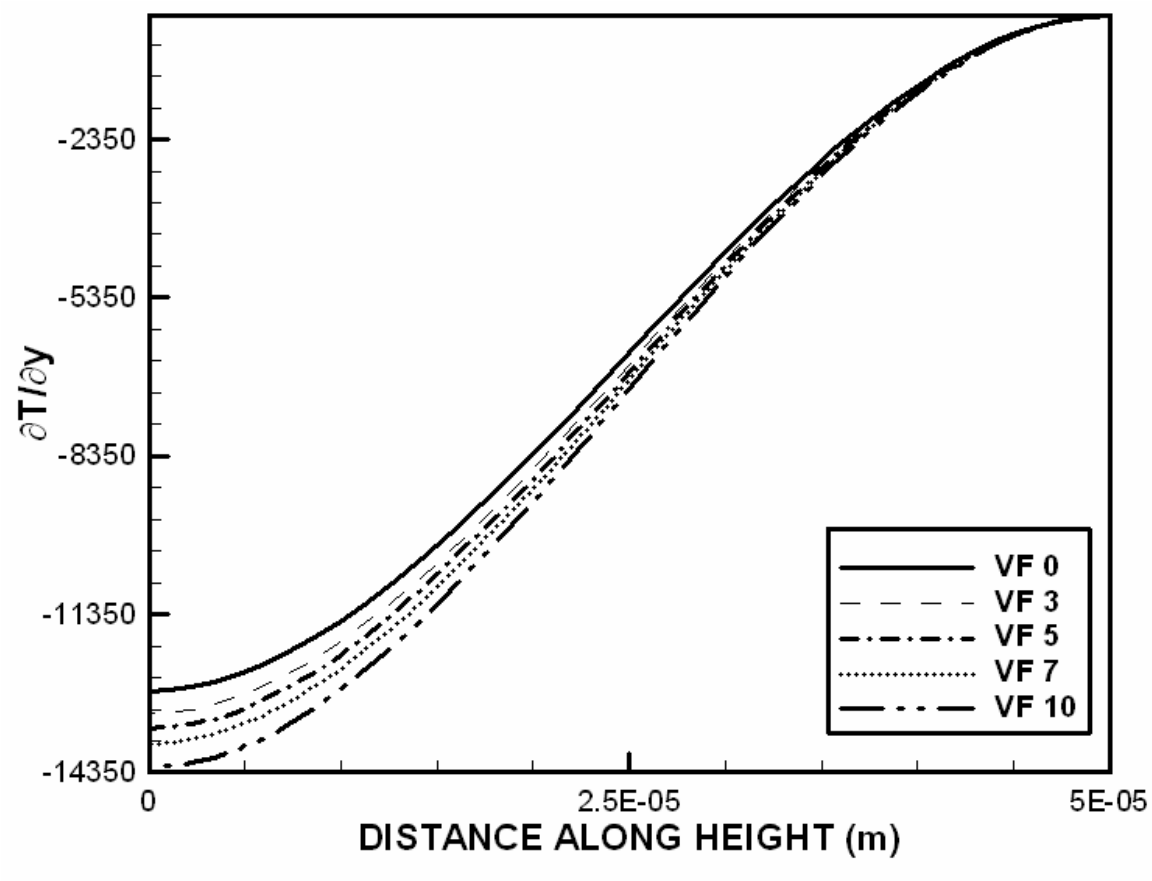

Figure 5.37 Temperature gradient along microchannel height at axial distance of 0.0345 m from inlet,for heat flux of 8000 W/m^2 and mass flow rate of 4 x 10^{-5} kg/s ; where VF0,VF 3, VF 5, VF 7 and VF 10 represent 0%, 3%, 5%, 7% and 10% volume concentration of the particles, respectively.

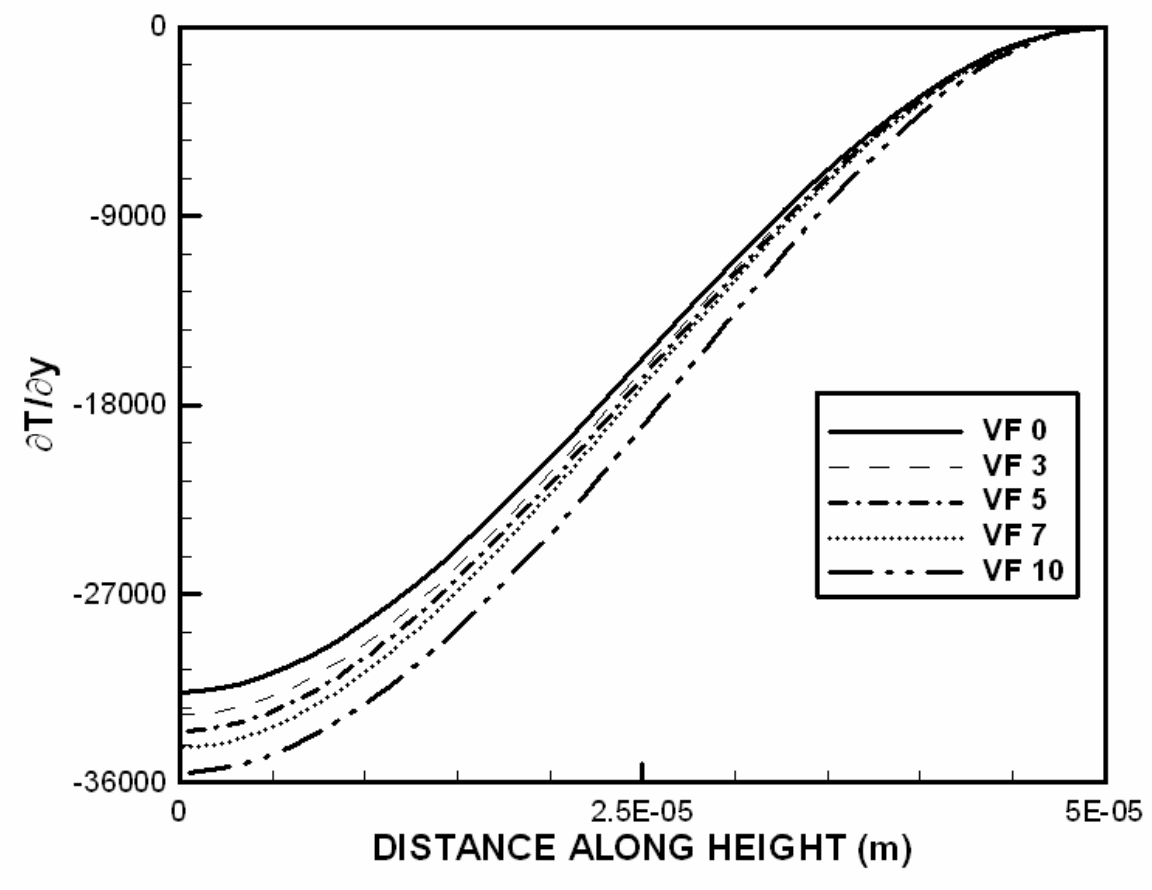

Figure 5.38 Temperature gradient along microchannel height at axial distance of 0.0345 m from inlet,for heat flux of 20000 W/m^2 and mass flow rate of 4 x 10^{-5} kg/s ; where VF0,VF 3, VF 5, VF 7 and VF 10 represent 0%, 3%, 5%, 7% and 10% volume concentration of the particles, respectively.

5.3.2 Volumetric Entropy Generation Rate due to Fluid Friction

The volumetric entropy generation rate due to fluid friction is defined as:

$$S'''_{generation\_f} = \frac{\mu_b}{T}\left(\frac{\partial u}{\partial y}\right)^2 \tag{5.3.2}$$

Figures 5.39 to 5.42 show the variation of volumetric entropy generation rate due to fluid friction, with heat flux, for different mass flow rates and particle volume concentrations. Figures 5.43 and 5.44 show the effect of increasing volume concentration of particles and heat flux on the pressure drop in the microchannel. The volumetric entropy generation rate due to fluid friction decreases with increasing heat flux, but the rate of decrease reduces at high mass flow rates as shown in Figures 5.41 and 5.42. Increasing the mass flow rate and volume concentration of particles in the bulk fluid leads to an increase in the volumetric entropy generation rate due to fluid friction. Therefore, the highest volumetric entropy generation rate due to fluid friction is obtained for mass flow rate of 4×10^{-5} kg/s, heat flux of 8000 W/m^2 and 10% volume concentration of particles.

Increase in the heat flux leads to an increase in the temperature and consequently a decrease in viscosity of the bulk fluid. Therefore with increase in heat flux, the volumetric entropy generation rate due to fluid friction keeps decreasing. Increase in the mass flow rate of the bulk fluid leads to an increase in the velocity gradient in the transverse direction. Increase in mass flow rate also reduces the temperature and increases the viscosity, therefore, the volumetric entropy generation rate due to fluid friction increases with increasing mass flow rate. Increase in the volume concentration of

particles leads to an increase in the viscosity of the bulk fluid as well as reduction in its temperature. Therefore, increasing volume concentration of particles leads to an increase in the volumetric entropy generation rate due to fluid friction.

The highest volumetric entropy generation rate due to fluid friction is obtained for mass flow rate of 4 x 10^{-5} kg/s, heat flux of 8000 W/m^2 and 10% volume concentration of particles and is 35% higher than the volumetric entropy generation rate for carrier fluid without P.C.M. particles. At low mass flow rates, the volumetric entropy generation rate due to heat transfer is much higher than the volumetric entropy generation rate due to fluid friction. However, at mass flow rate of 4 x 10^{-5} kg/s, the volumetric entropy generation rate due to heat transfer and due to fluid friction become comparable. Therefore, the total volumetric entropy generation rate is highest at mass flow rate of 4 x 10^{-5} kg/s, heat flux of 20000 W/m^2 and 10% volume concentration of particles.

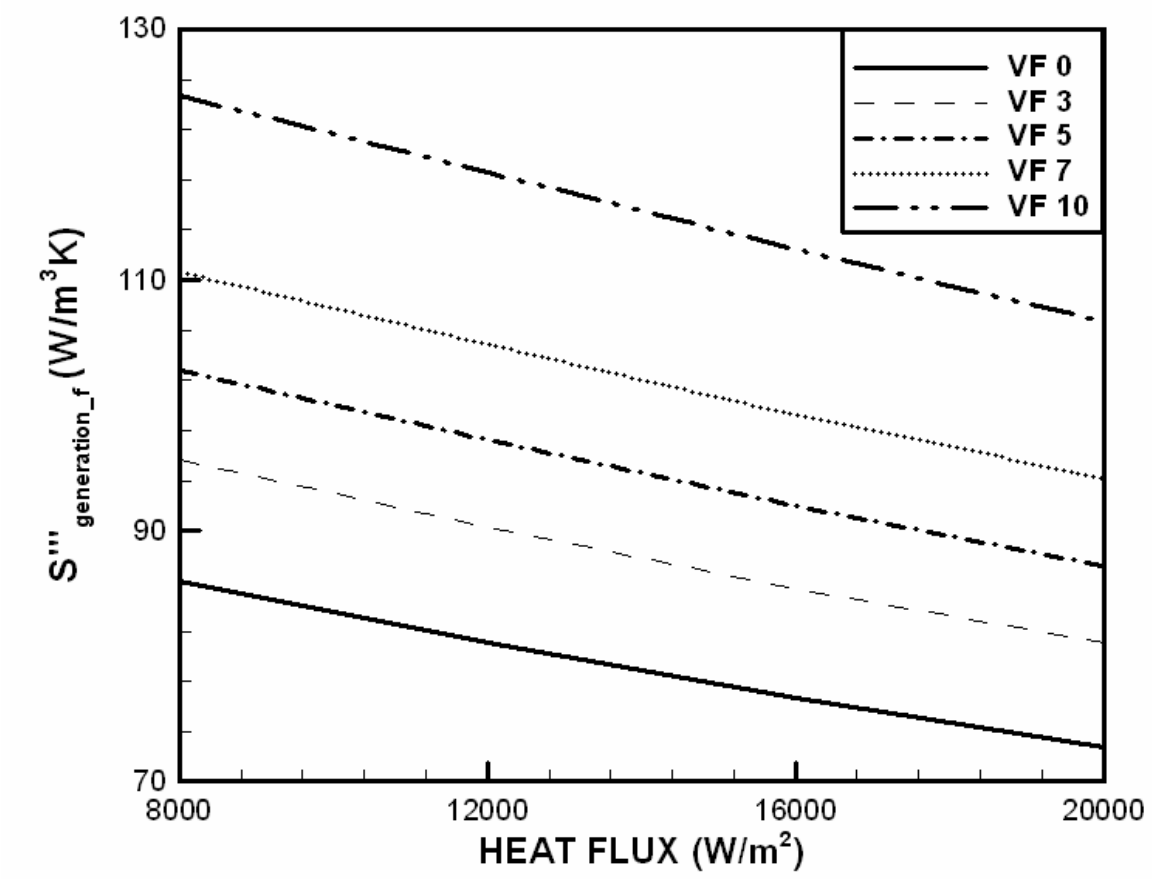

Figure 5.39 Volumetric entropy generation rate due to fluid friction for mass flow rate of 10^{-5} kg/s ; where VF0,VF 3, VF 5, VF 7 and VF 10 represent 0%, 3%, 5%, 7% and 10% volume concentration of the particles, respectively.

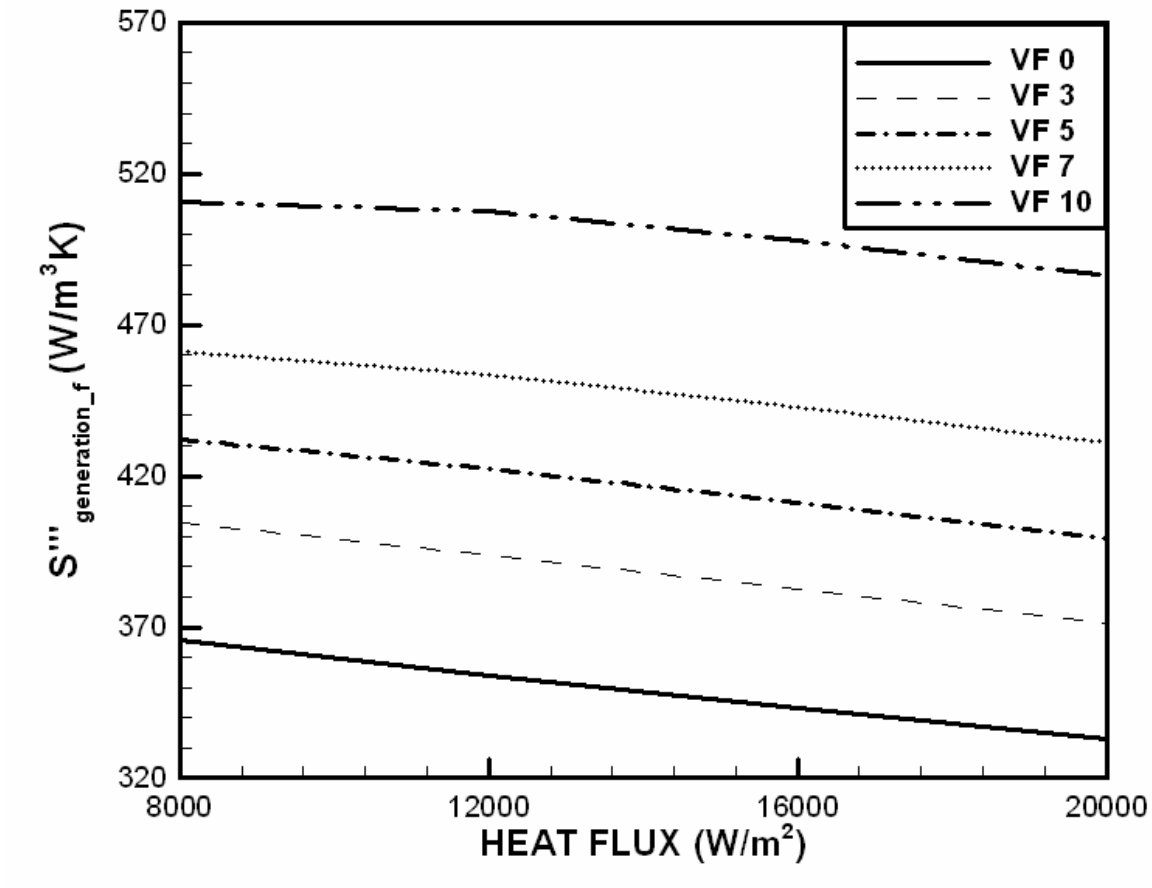

Figure 5.40 Volumetric entropy generation rate due to fluid friction for mass flow rate of 2 x 10^{-5} kg/s ; where VF0,VF 3, VF 5, VF 7 and VF 10 represent 0%, 3%, 5%, 7% and 10% volume concentration of the particles, respectively.

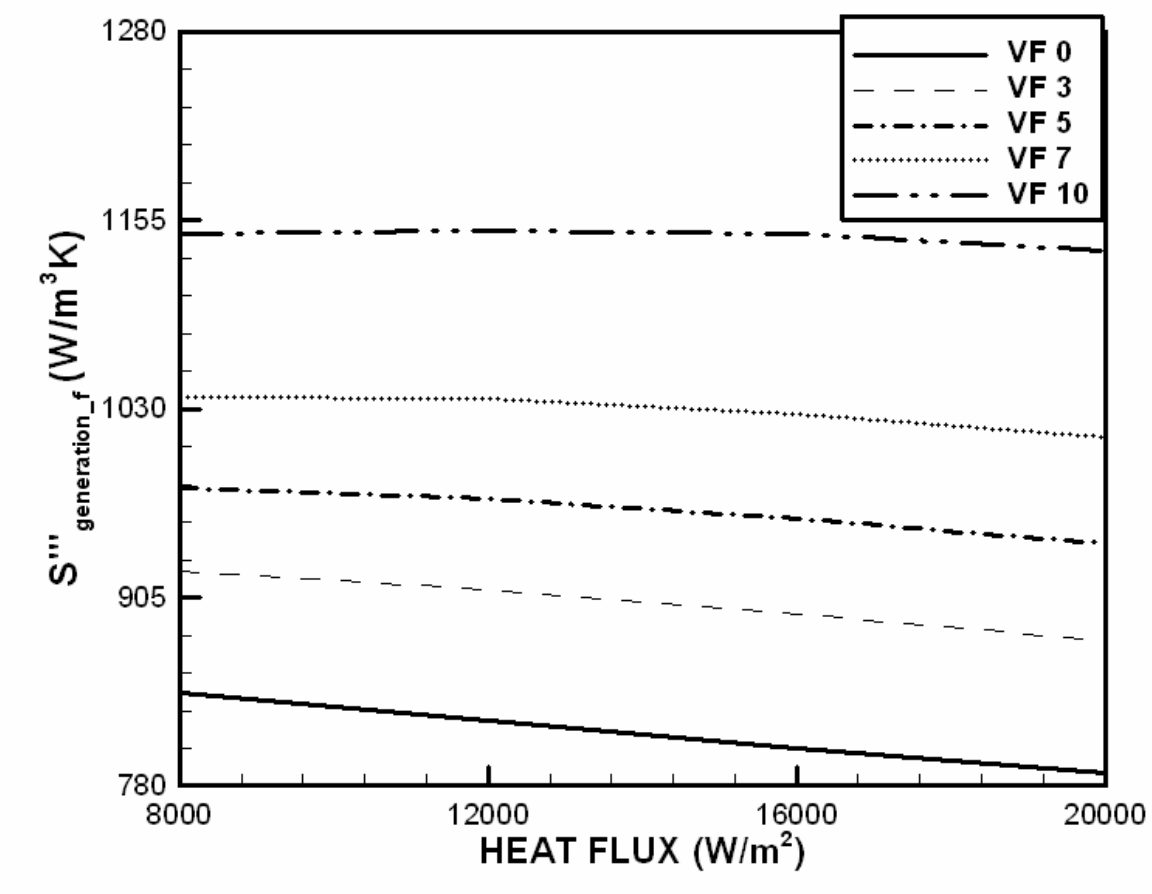

Figure 5.41 Volumetric entropy generation rate due to fluid friction for mass flow rate of 3 x 10^{-5} kg/s ; where VF0,VF 3, VF 5, VF 7 and VF 10 represent 0%, 3%, 5%, 7% and 10% volume concentration of the particles, respectively.

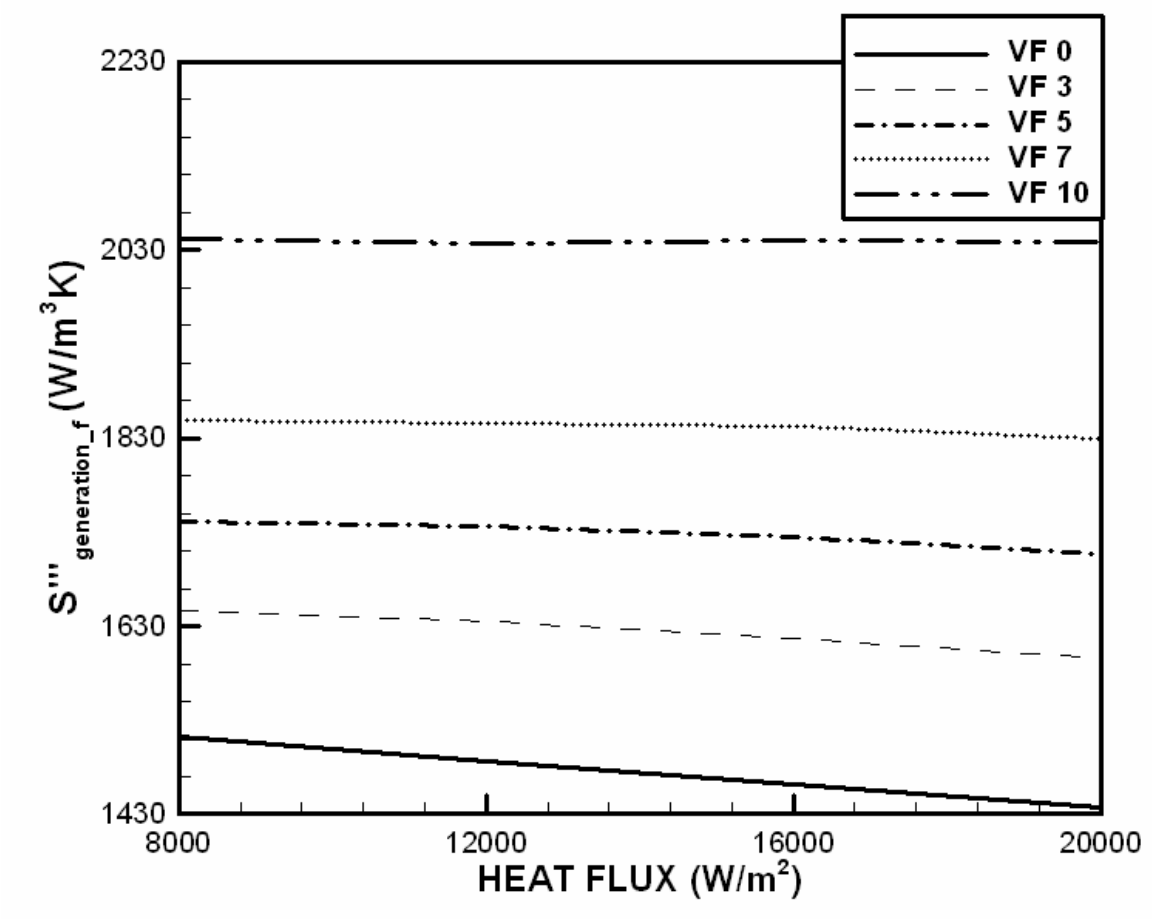

Figure 5.42 Volumetric entropy generation rate due to fluid friction for mass flow rate of 4 x 10^{-5} kg/s ; where VF0,VF 3, VF 5, VF 7 and VF 10 represent 0%, 3%, 5%, 7% and 10% volume concentration of the particles, respectively.

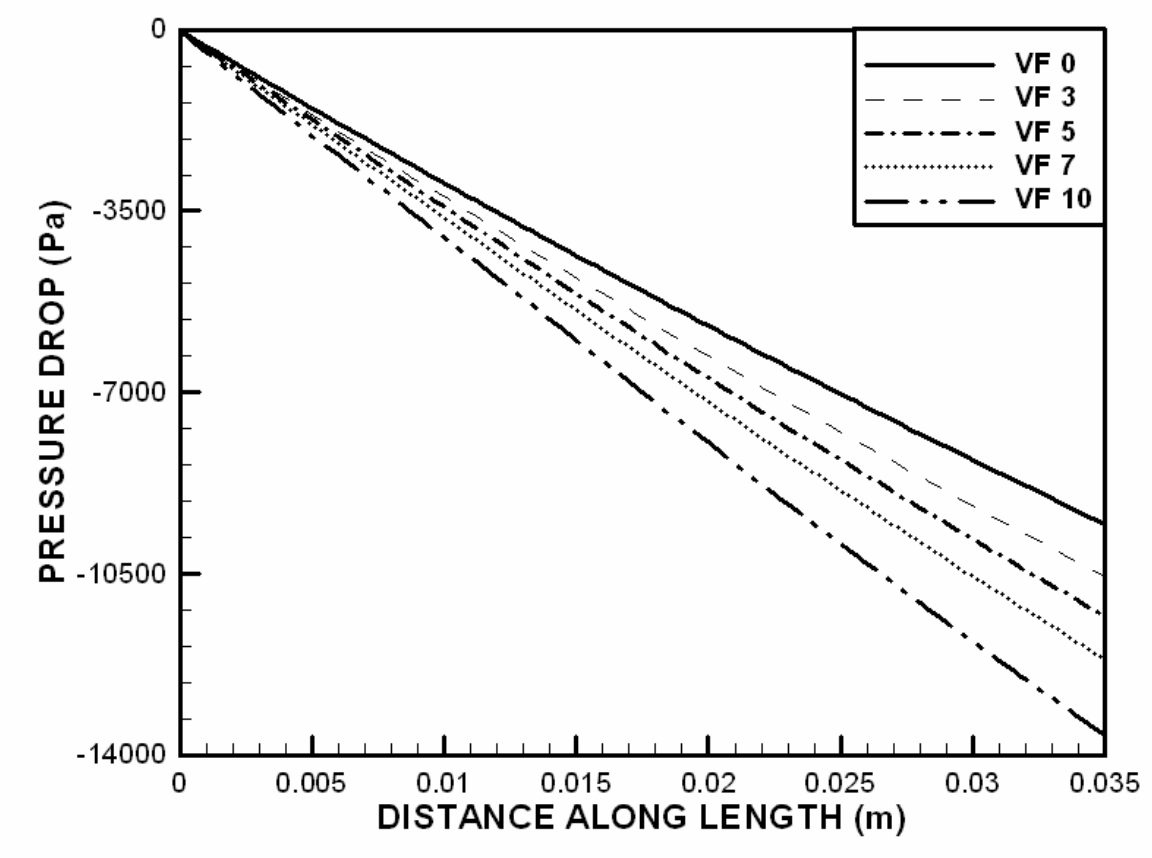

Figure 5.43 Pressure drop along microchannel length for heat flux of 8000 W/m^2 and mass flow rate of 10^{-5} kg/s ; where VF0,VF 3, VF 5, VF 7 and VF 10 represent 0%, 3%, 5%, 7% and 10% volume concentration of the particles, respectively.

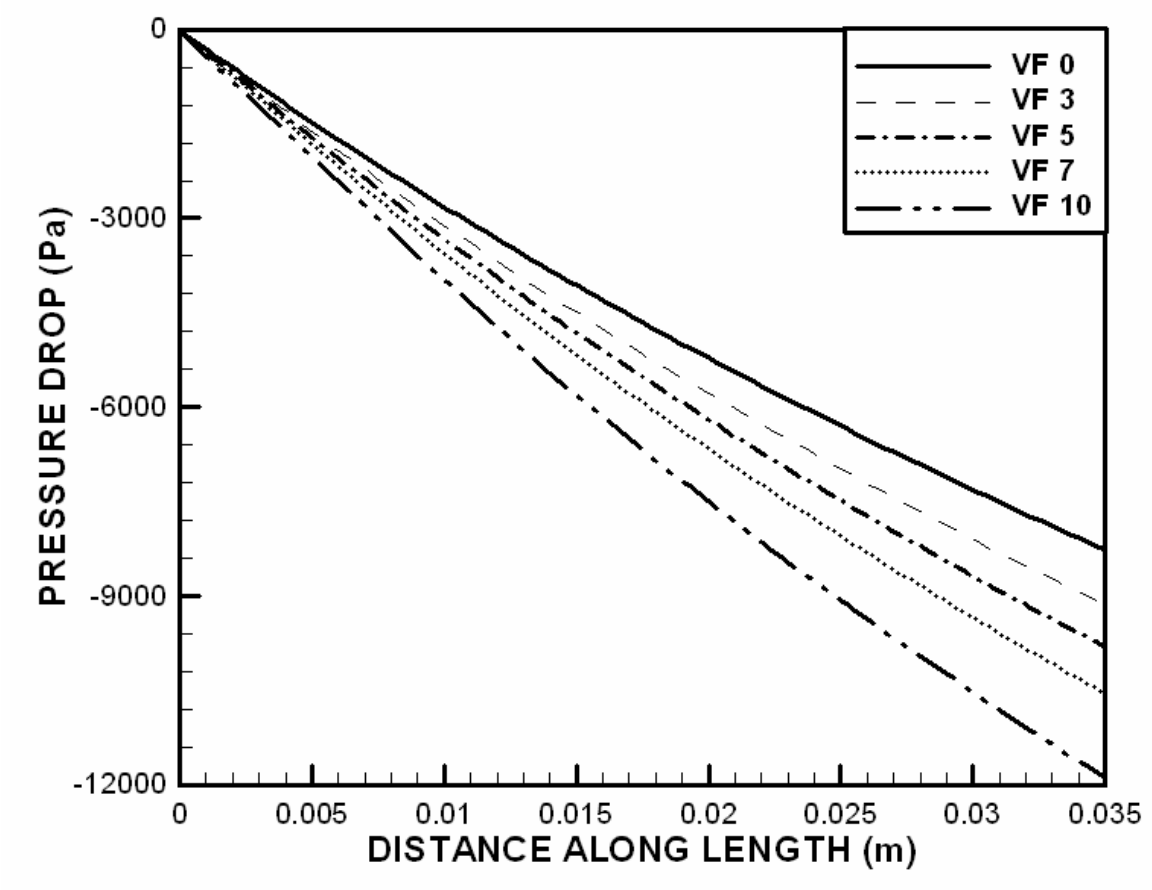

Figure 5.44 Pressure drop along microchannel length for heat flux of 20000 W/m^2 and mass flow rate of 10^{-5} kg/s ; where VF0,VF 3, VF 5, VF 7 and VF 10 represent 0%, 3%, 5%, 7% and 10% volume concentration of the particles, respectively.

5.4 Normalized Length of Phase Change and Total Phase Change Length

In this section, a parametric study is conducted to investigate the effect of particle volume concentration, mass flow rate and heat flux on the normalized length of phase change and normalized total phase change length in the microchannel.

The normalized length of phase change is defined as the ratio of the length of the microchannel in which phase change of P.C.M. particles takes place to the total length of the microchannel. Total phase change length is defined as the axial distance from the inlet of the microchannel to the axial location at which the phase change of P.C.M. particles is complete. Therefore, the normalized total phase change length is defined as the ratio of total phase change length to the total length of the microchannel.

At the inlet of the microchannel, the mass flow rate of the bulk fluid is varied between 10^{-5} kg/s to 2 x 10^{-5} kg/s. The range of mass flow rates is selected to ensure that the phase change of particles is complete, even at the highest mass flow rate and lowest heat flux. The heat flux at the bottom wall of the microchannel is varied between 10000 W/m^2 to 20000 W/m^2. The temperature of the particles and carrier fluid is specified as 315 K at the inlet, which is less than the melting temperature of the P.C.M. particles.

5.4.1 Normalized Length of Phase Change

Figures 5.45 to 5.47 show the variation of normalized length of phase change with heat flux for different particle volume concentrations and mass flow rates. Figures 5.48 to 5.52

show the variation of normalized length of phase change with mass flow rate for different particle volume concentrations and heat flux. Figures 5.45 to 5.47 show that for all particle volume concentrations, the maximum normalized length of phase change is obtained for the lowest heat flux of 10000 W/m^2. From Figures 5.45 to 5.47, it can be observed that increasing the mass flow rate and volume concentration of the bulk fluid increases the value of normalized length of phase change. The observed trends in the magnitude of normalized length of phase change can be explained as follows:

The normalized length of phase change is proportional to the ratio of latent heating of the bulk fluid to the heat input into the microchannel. Latent heat to heat input ratio is written as

$$\frac{\dot{m}c_{p,b}\left(T_{liquidus}-T_{solidus}\right)}{\dot{Q}_{in}} \tag{5.4.1}$$

where $\dot{Q}_{in}$ is the heat transferred to the microchannel at its bottom wall.

For a given heat input to the microchannel, increase in mass flow rate will not affect the value of specific heat of the bulk fluid, but will reduce the sensible heating of the bulk fluid inside the microchannel. Consequently, for a given heat input to the microchannel, increase in mass flow rate will result in a linear increase in the ratio of latent heat to heat input, therefore an increase in the normalized length of phase change, as is observed in Figures 5.48 to 5.52. The slope of the line showing the variation of normalized length of phase change with mass flow rate varies with volume concentration of particles. Increase

in the volume concentration of particles in the bulk fluid will increase the heat storage capacity of the bulk fluid linearly. Therefore, increase in volume concentration of the particles for a given heat input and given mass flow rate will increase the normalized length of phase change linearly. Consequently, an increase in the volume concentration of particles in the bulk fluid corresponds to an increase in the normalized length of phase change.

Increase in heat flux for a given mass flow rate and volume concentration of particles leads to a decrease in the normalized length of phase change. When the mass flow rate and volume concentration of particles in the bulk fluid is fixed, increase in heat flux will lead to increase in the sensible heating of the bulk fluid inside the microchannel. The increase in sensible heating of the bulk fluid leads to a decrease in the ratio of latent heat to heat input, and as a result the normalized length of phase change decreases.

The maximum normalized length of phase change of 0.77 is obtained for mass flow rate of 2×10^{-5} kg/s, heat flux of 10000 W/m^2, and particle volume concentration of 10%. The maximum value of the normalized length of phase change of 0.77 indicates that phase change takes place in 77% of the length of microchannel. Figures 5.45 to 5.47 show that increasing the mass flow rate of the bulk fluid increases the value of maximum normalized length of phase change. From Figures 5.45 to 5.47 it can be concluded that for a given volume concentration of particles, increase in heat flux reduces the normalized length of phase change, while increase in mass flow rate increases the normalized length of phase change. More importantly, Figures 5.45 to 5.52 guide the

designer regarding the optimum operating conditions to be used for a given length of the microchannel to get maximum enhancement in heat storage capacity. Normalized length of phase change is the minimum length required for the phase change to be complete and can be used to decide the operating conditions when the temperature of the carrier fluid and the P.C.M. particles at the inlet is equal to the solidus temperature. In case of constraints in terms of mass flow rate due to maximum allowable pressure drop in the microchannel or if the heat flux required to be dissipated is known beforehand, Figures 5.45 to 5.52 can also be used to calculate the length of the microchannel required to obtain maximum gain in heat storage capacity by the addition of P.C.M. particles. Figures 5.45 to 5.52 can be used to decide the length of the microchannel when the temperature at the inlet of the microchannel is equal to the solidus temperature of the P.C.M. particles.

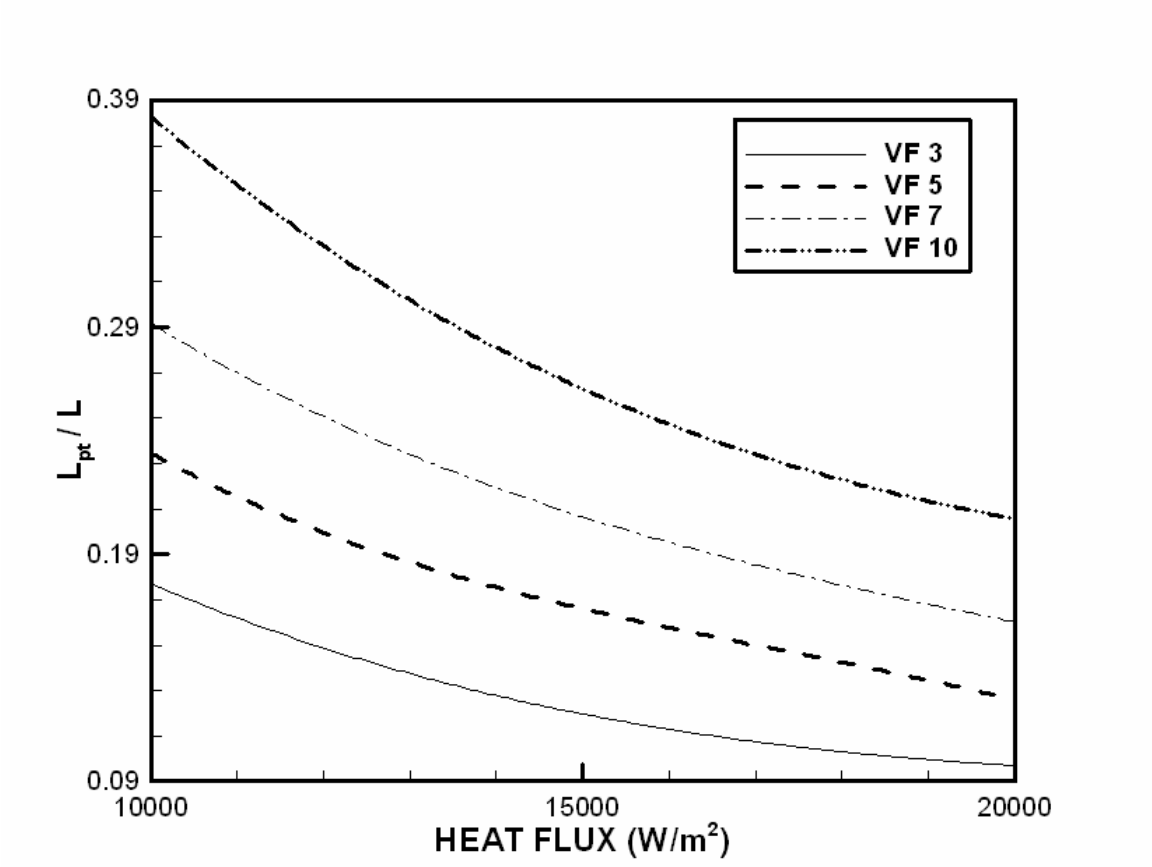

Figure 5.45 Normalized length of phase change for mass flow rate of 10^{-5} kg/s, where VF 3, VF 5, VF 7 and VF 10 represents 3%, 5%, 7% and 10% volume concentration of the particles, respectively.

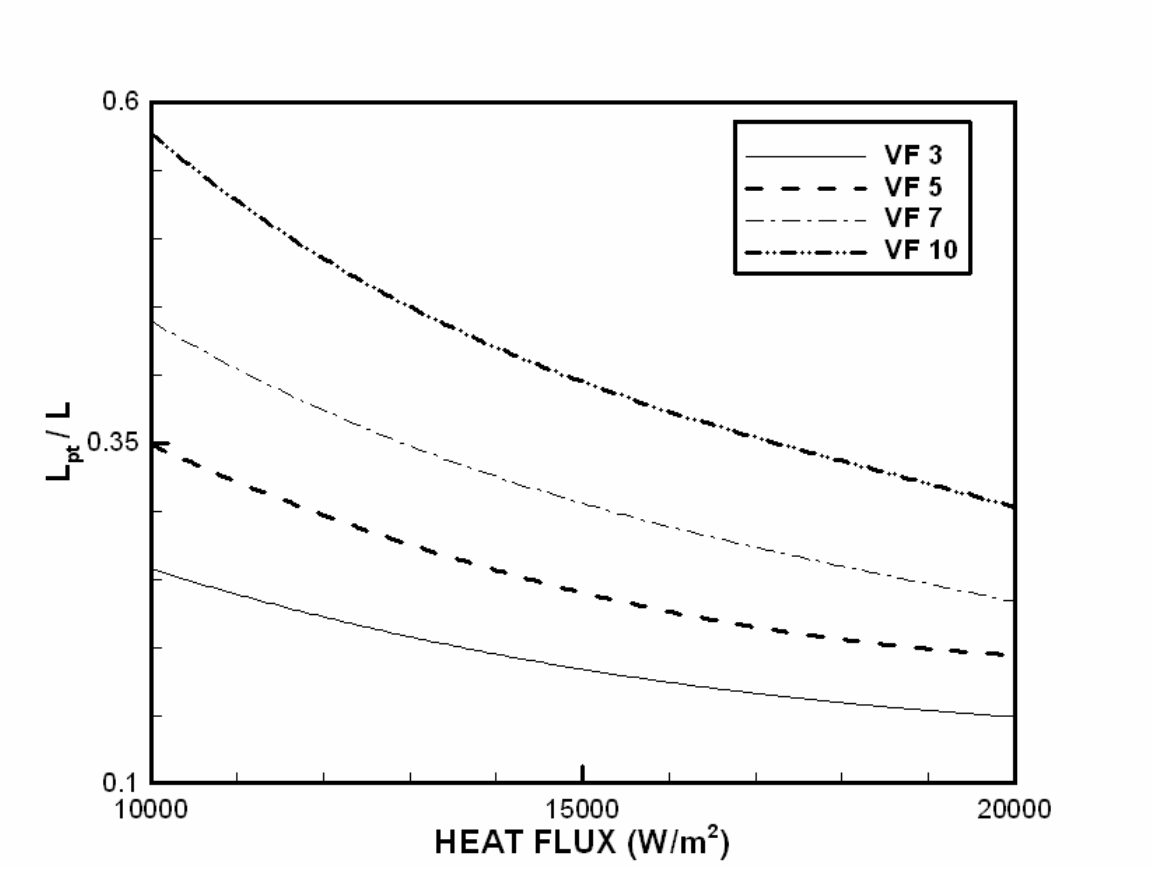

Figure 5.46 Normalized length of phase change for mass flow rate of 1.5 x 10^{-5} kg/s, where VF 3, VF 5, VF 7 and VF 10 represents 3%, 5%, 7% and 10% volume concentration of the particles, respectively.

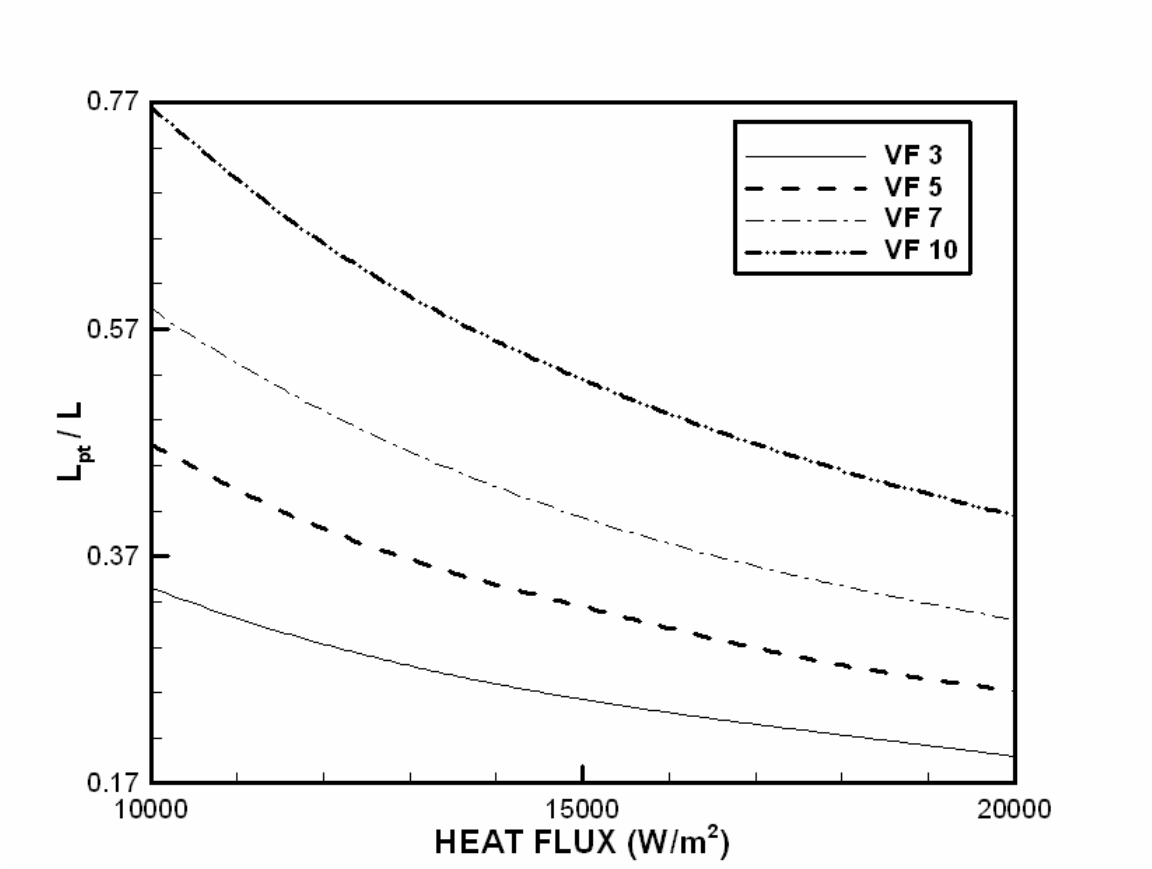

Figure 5.47 Normalized length of phase change for mass flow rate of 2 x 10^{-5} kg/s, where VF 3, VF 5, VF 7 and VF 10 represents 3%, 5%, 7% and 10% volume concentration of the particles, respectively.

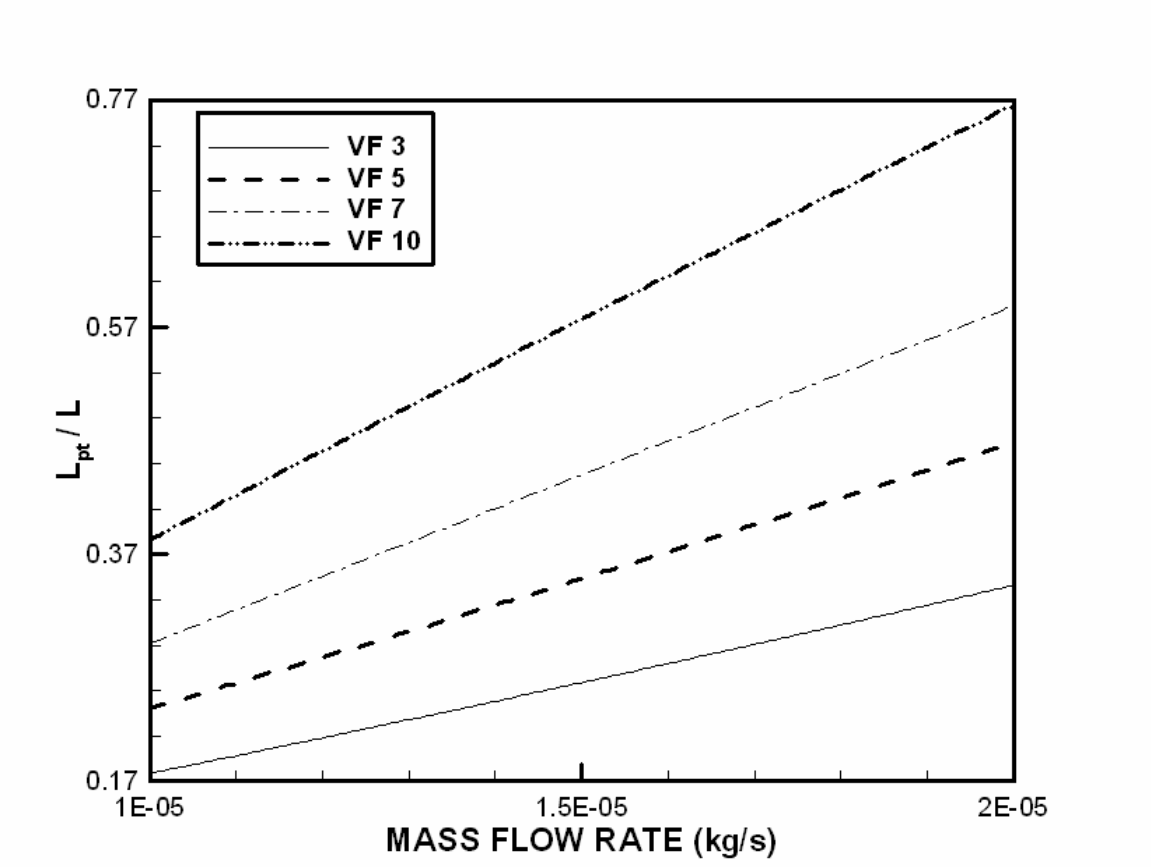

Figure 5.48 Normalized length of phase change for heat flux of 10000 W/m^2, where VF 3, VF 5, VF 7 and VF 10 represents 3%, 5%, 7% and 10% volume concentration of the particles, respectively.

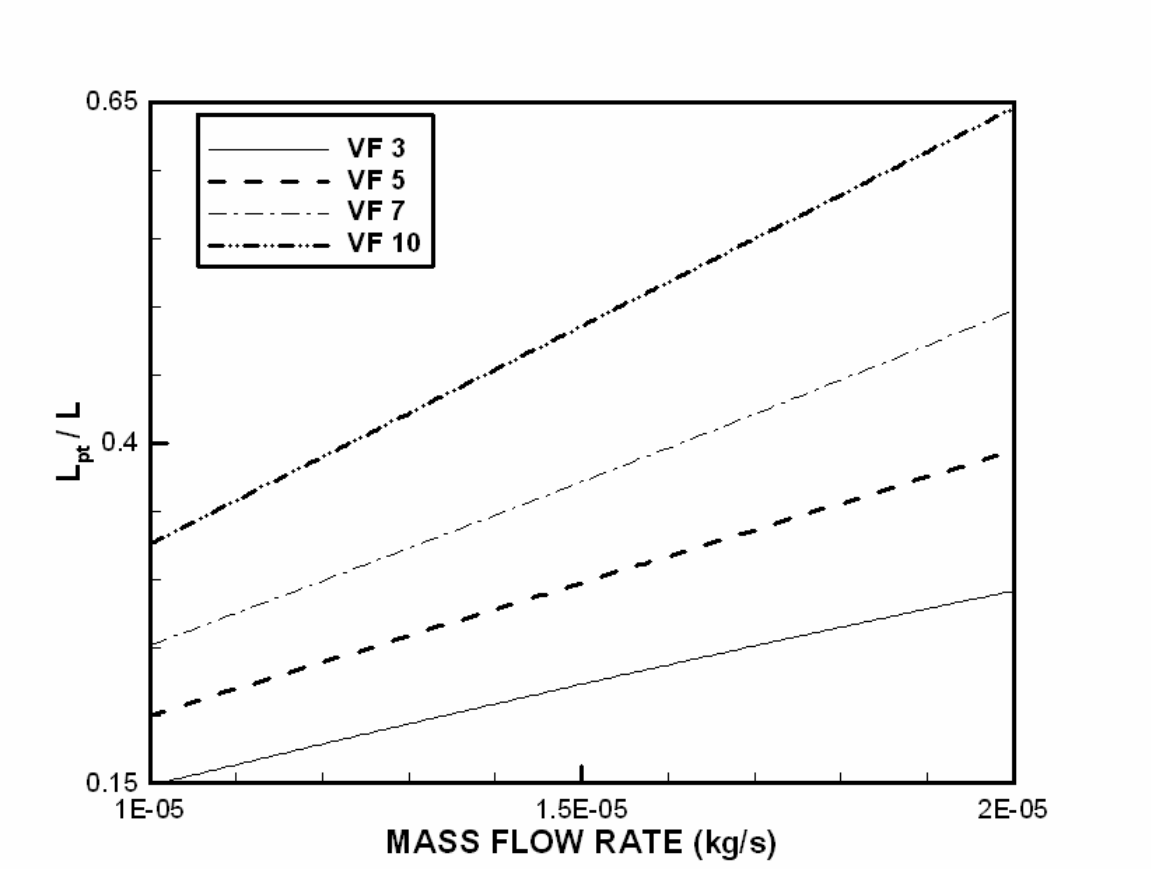

Figure 5.49 Normalized length of phase change for heat flux of 12000 W/m^2, where VF 3, VF 5, VF 7 and VF 10 represents 3%, 5%, 7% and 10% volume concentration of the particles, respectively.

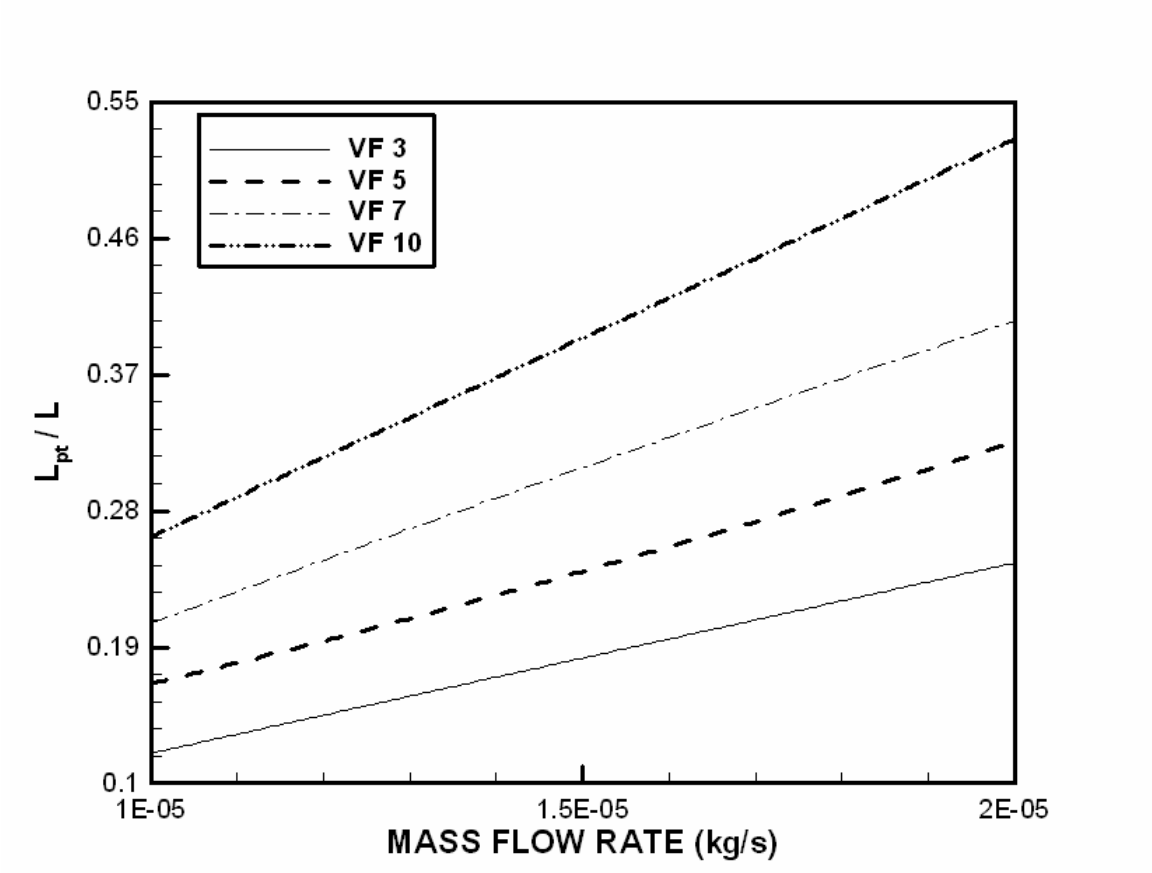

Figure 5.50 Normalized length of phase change for heat flux of 15000 W/m^2, where VF 3, VF 5, VF 7 and VF 10 represents 3%, 5%, 7% and 10% volume concentration of the particles, respectively.

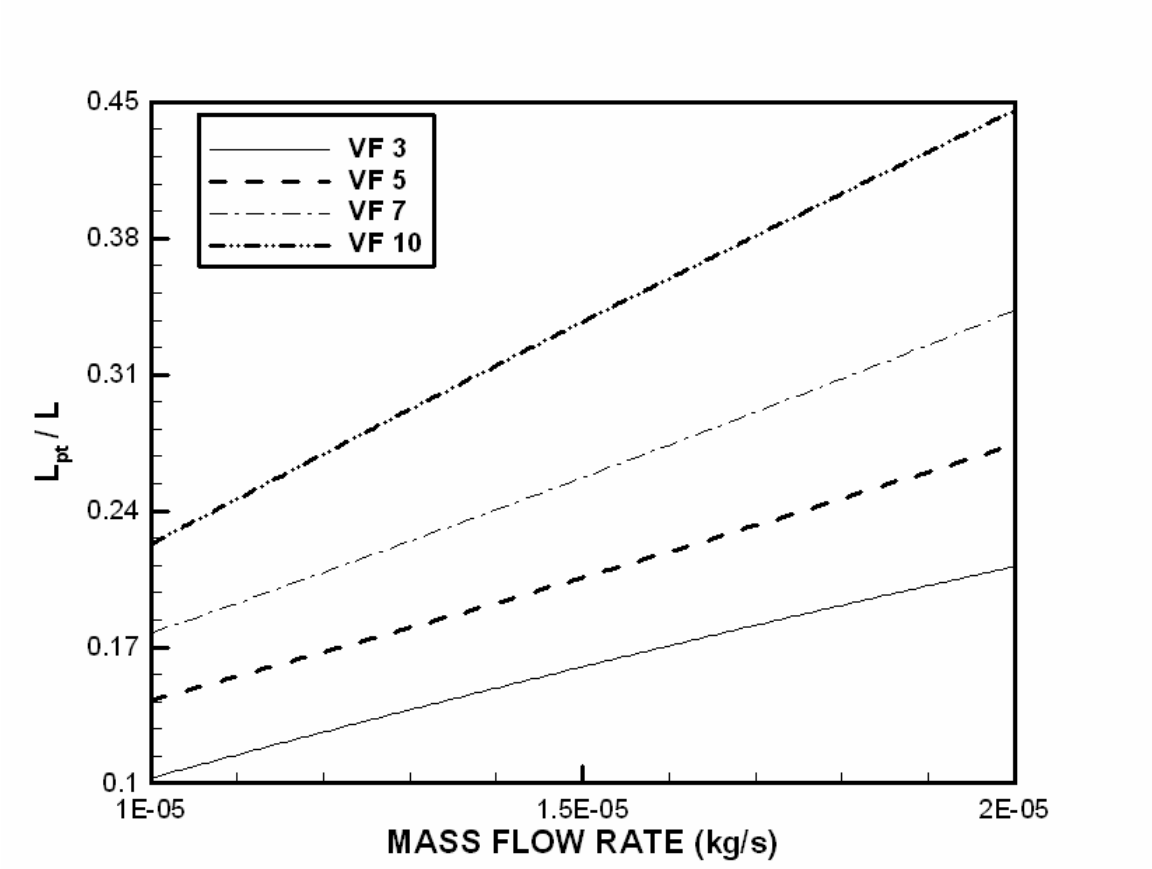

Figure 5.51 Normalized length of phase change for heat flux of 18000 W/m^2, where VF 3, VF 5, VF 7 and VF 10 represents 3%, 5%, 7% and 10% volume concentration of the particles, respectively.

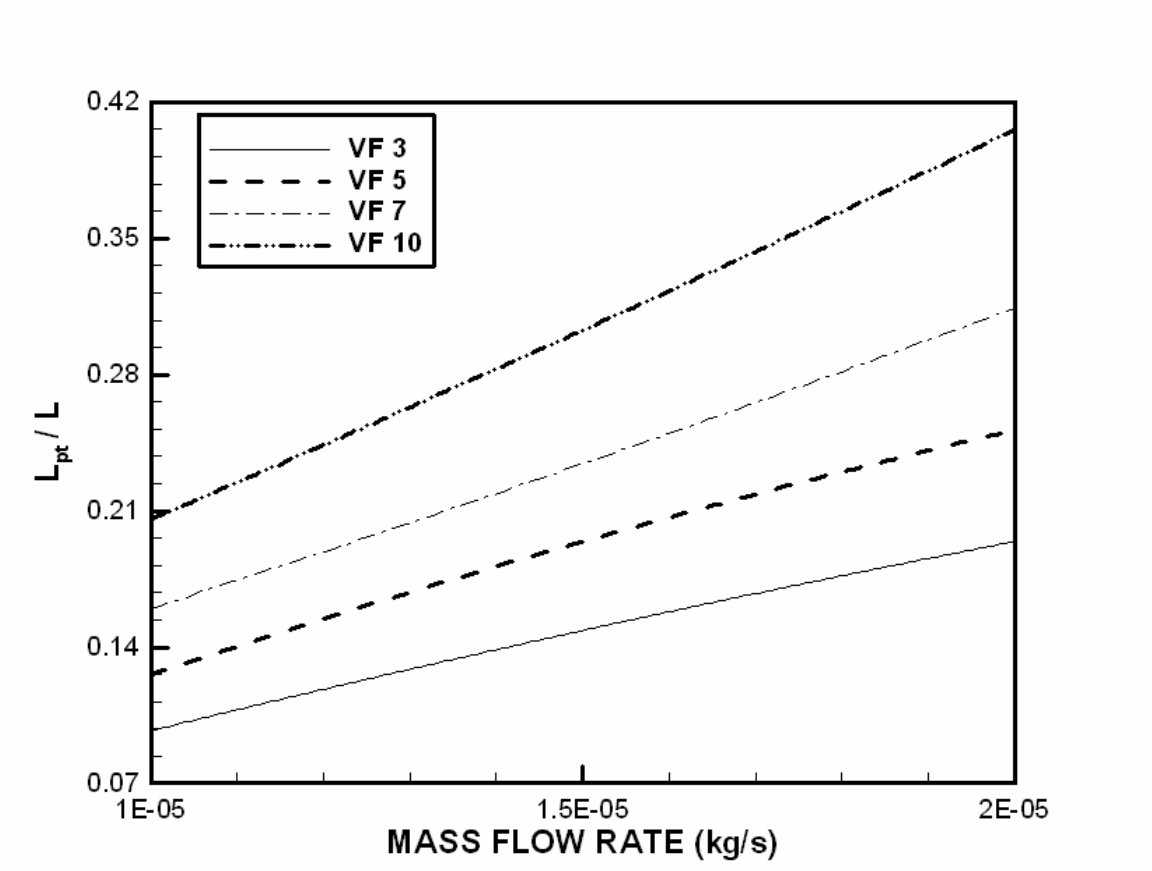

Figure 5.52 Normalized length of phase change for heat flux of 20000 W/m^2, where VF 3, VF 5, VF 7 and VF 10 represents 3%, 5%, 7% and 10% volume concentration of the particles, respectively.

5.4.2 Normalized Total Phase Change Length

Figures 5.53 to 5.55 show the variation of normalized total phase change length with heat flux for different particle volume concentrations and mass flow rates. Figures 5.56 to 5.60 show the variation of normalized total phase change length with mass flow rate for different particle volume concentrations and heat flux. The normalized total phase change length follows the same trend as normalized length of phase change for the mass flow rates, heat flux, and volume concentrations considered. The normalized total phase change length for 10% volume concentration of particles is also the highest for all heat flux and mass flow rates considered in the simulations. This shows that the length of the microchannel from the inlet to the axial distance at which phase change starts is negligible compared to the length of phase change for all mass flow rates and heat fluxes considered. In this case, the highest normalized total phase change length of 0.92 is obtained for bulk fluid mass flow rate of 2×10^{-5} kg/s, heat flux of 10000 W/m^2, and particle volume concentration of 10%. The maximum value of normalized total phase change length of 0.92 shows that 92% length of the microchannel is required for the phase change to complete when the total distance from inlet of microchannel is measured. From Figures 5.53 to 5.55 it can be concluded that for a given volume concentration of particles, increase in heat flux reduces the normalized total phase change length, while increase in mass flow rate increases it.

The normalized total phase change length can be used to determine optimum operating conditions required to obtain maximum enhancement in heat storage capacity for a given

microchannel length when the temperature at the inlet is below solidus temperature. Example: For a microchannel length of 17.5 mm, Figures 5.53 to 5.60 show that a mass flow rate of 1.5x 10^{-5} kg/s and a heat flux of 14000 W/m^2, or a mass flow rate of 2 x 10^{-5} kg/s and heat flux of 16500 W/m^2 should be used for 10% volume concentration of particles to obtain the best enhancement in heat storage capacity. It can also be observed that using mass flow rate of 10^{-5} kg/s will lead to sensible heating of bulk fluid after the completion of phase change as the maximum value of normalized total phase change length is less than 0.5 even for 10% volume concentration of P.C.M. particles. Therefore, for a microchannel of given length, the normalized total phase change length can be used to determine the optimum operating conditions to be used such that phase change is completed just at the end of the microchannel and maximum enhancement in heat storage capacity is obtained.

The normalized total phase change length can also be used to calculate the optimum length of the microchannel if the operating conditions like mass flow rate and heat flux required to be dissipated is known beforehand. In such a case, Figures 5.53 to 5.60 can be used to calculate the length of the microchannel required to obtain maximum gain by the use of P.C.M. particles if the temperature at the inlet is below the solidus temperature of the P.C.M. particles.

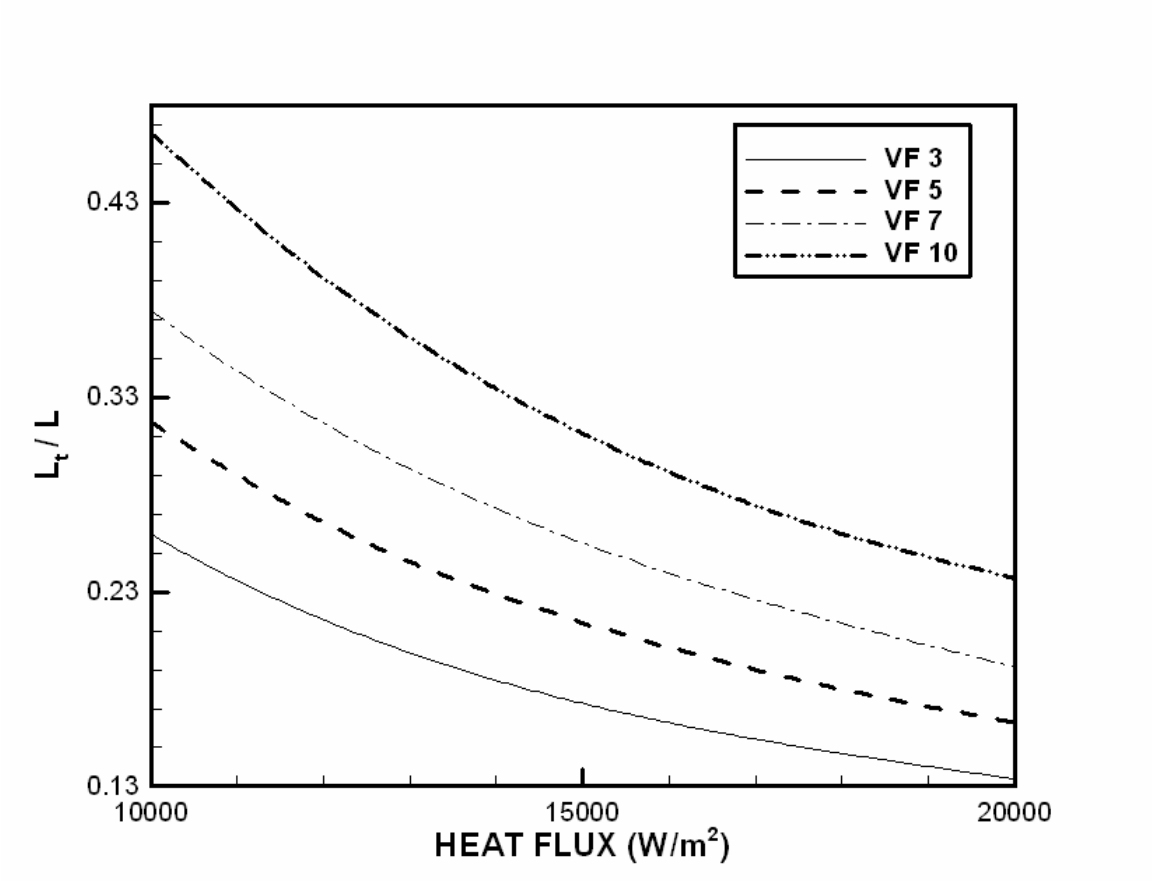

Figure 5.53 Normalized total phase change length for mass flow rate of 10^{-5} kg/s, where VF 3, VF 5, VF 7 and VF 10 represents 3%, 5%, 7% and 10% volume concentration of the particles, respectively.

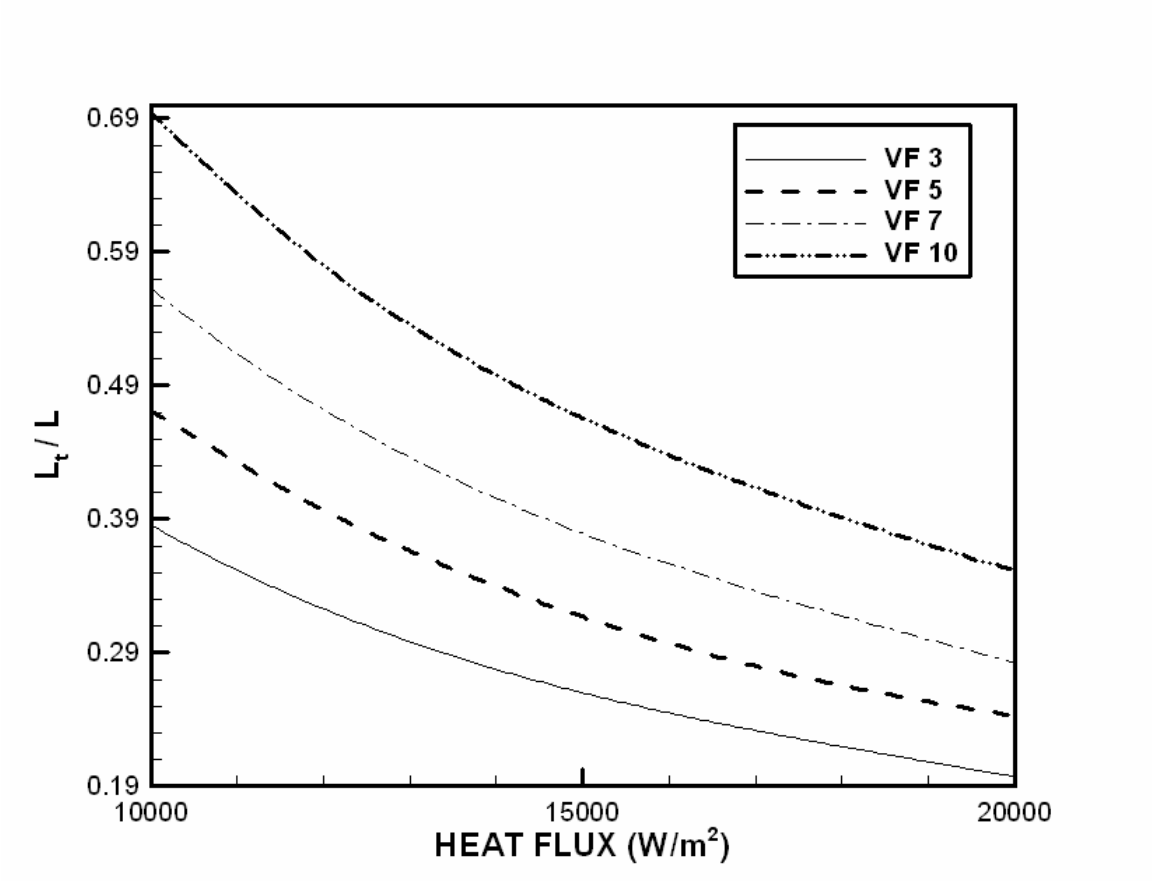

Figure 5.54 Normalized total phase change length for mass flow rate of 1.5 x 10^{-5} kg/s, where VF 3, VF 5, VF 7 and VF 10 represents 3%, 5%, 7% and 10% volume concentration of the particles, respectively.

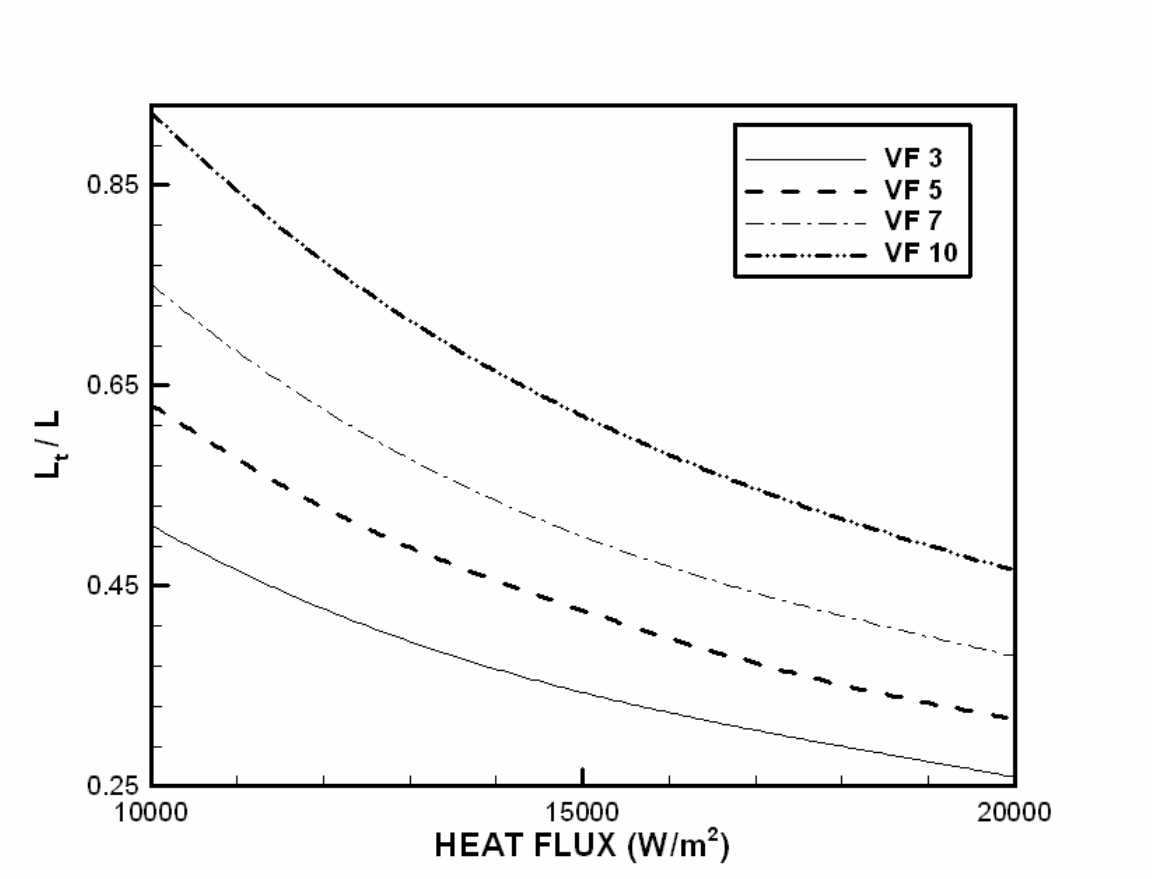

Figure 5.55 Normalized total phase change length for mass flow rate of 2 x 10^{-5} kg/s, where VF 3, VF 5, VF 7 and VF 10 represents 3%, 5%, 7% and 10% volume concentration of the particles, respectively.

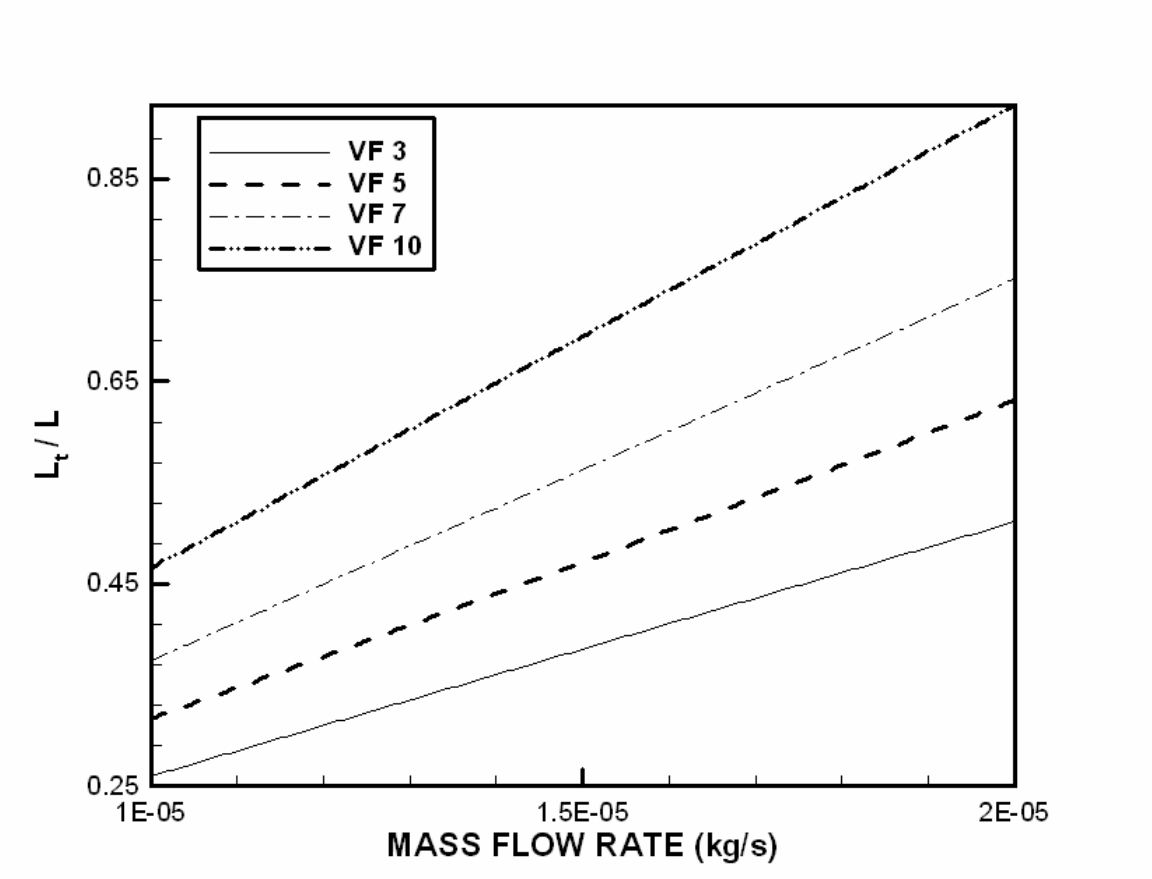

Figure 5.56 Normalized total phase change length for heat flux of 10000 W/m^2, where VF 3, VF 5, VF 7 and VF 10 represents 3%, 5%, 7% and 10% volume concentration of the particles, respectively.

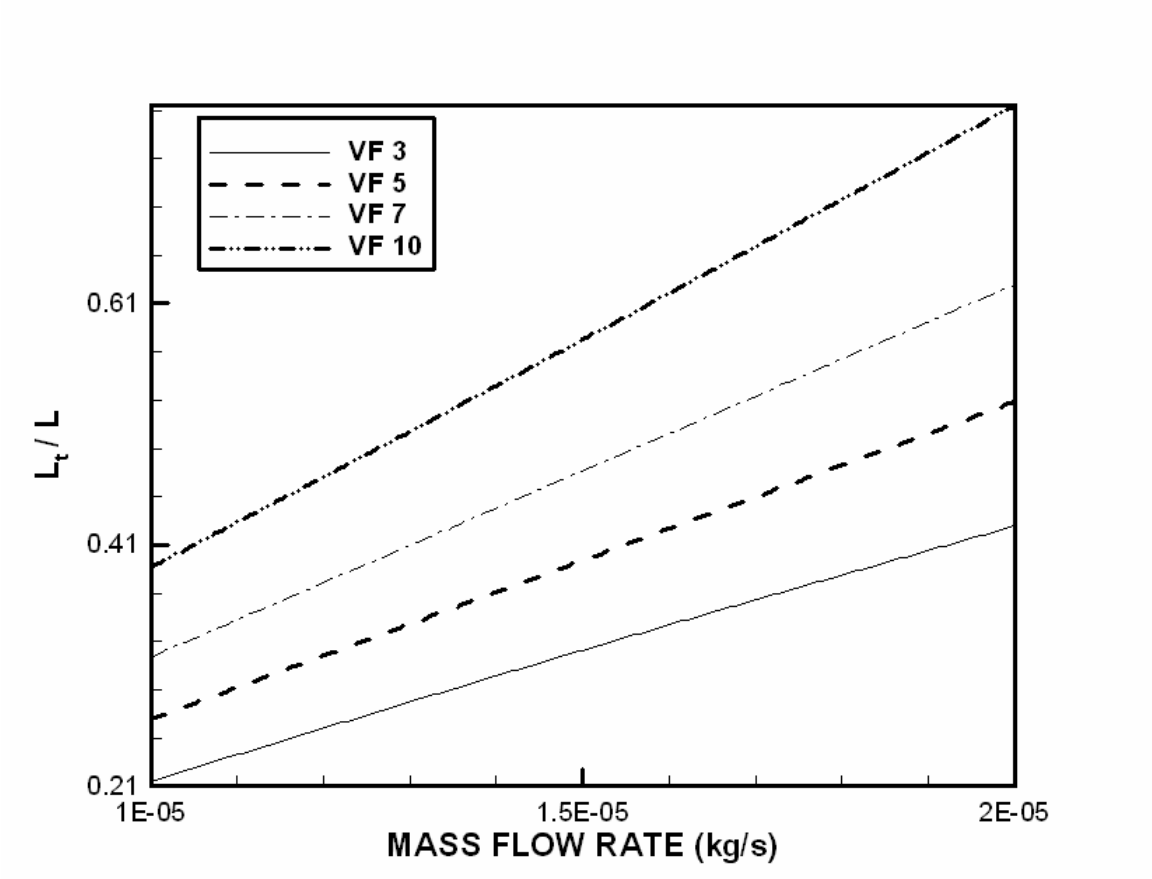

Figure 5.57 Normalized total phase change length for heat flux of 12000 W/m^2, where VF 3, VF 5, VF 7 and VF 10 represents 3%, 5%, 7% and 10% volume concentration of the particles, respectively.

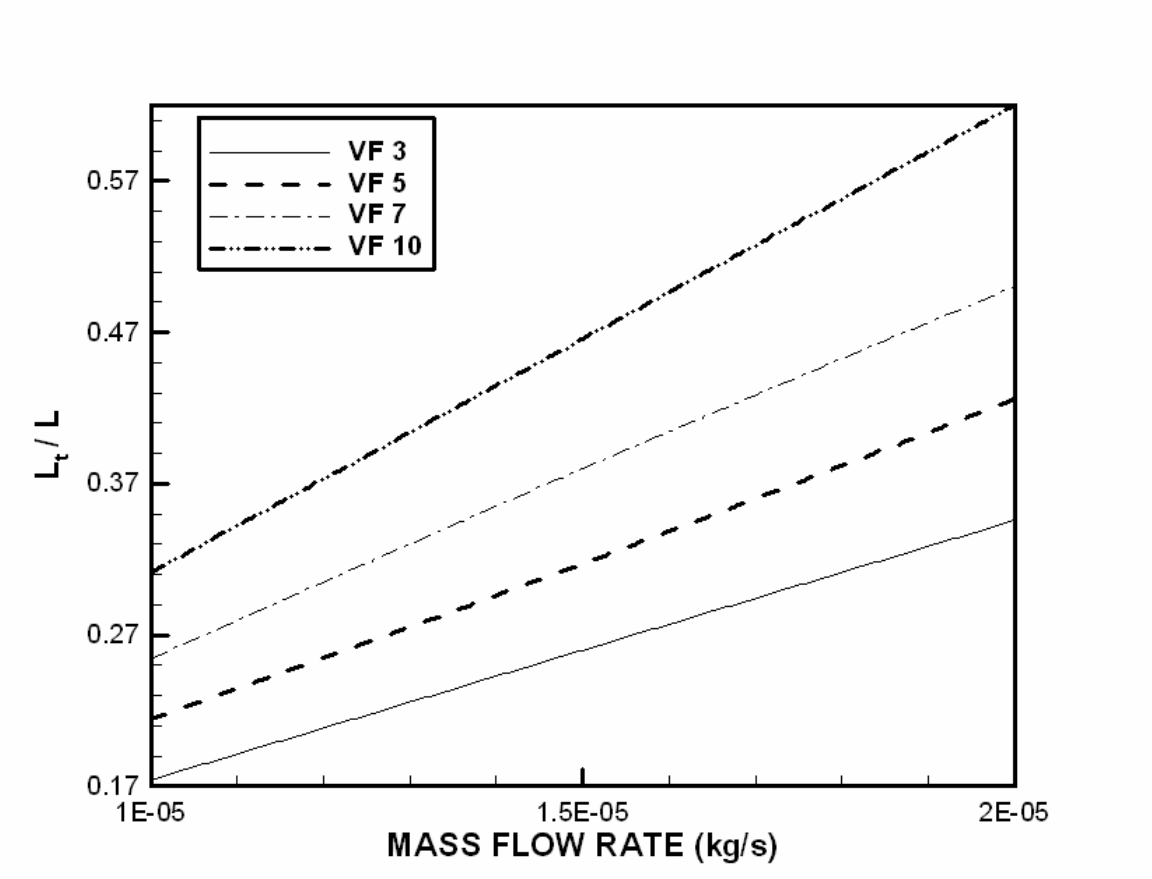

Figure 5.58 Normalized total phase change length for heat flux of 15000 W/m^2, where VF 3, VF 5, VF 7 and VF 10 represents 3%, 5%, 7% and 10% volume concentration of the particles, respectively.

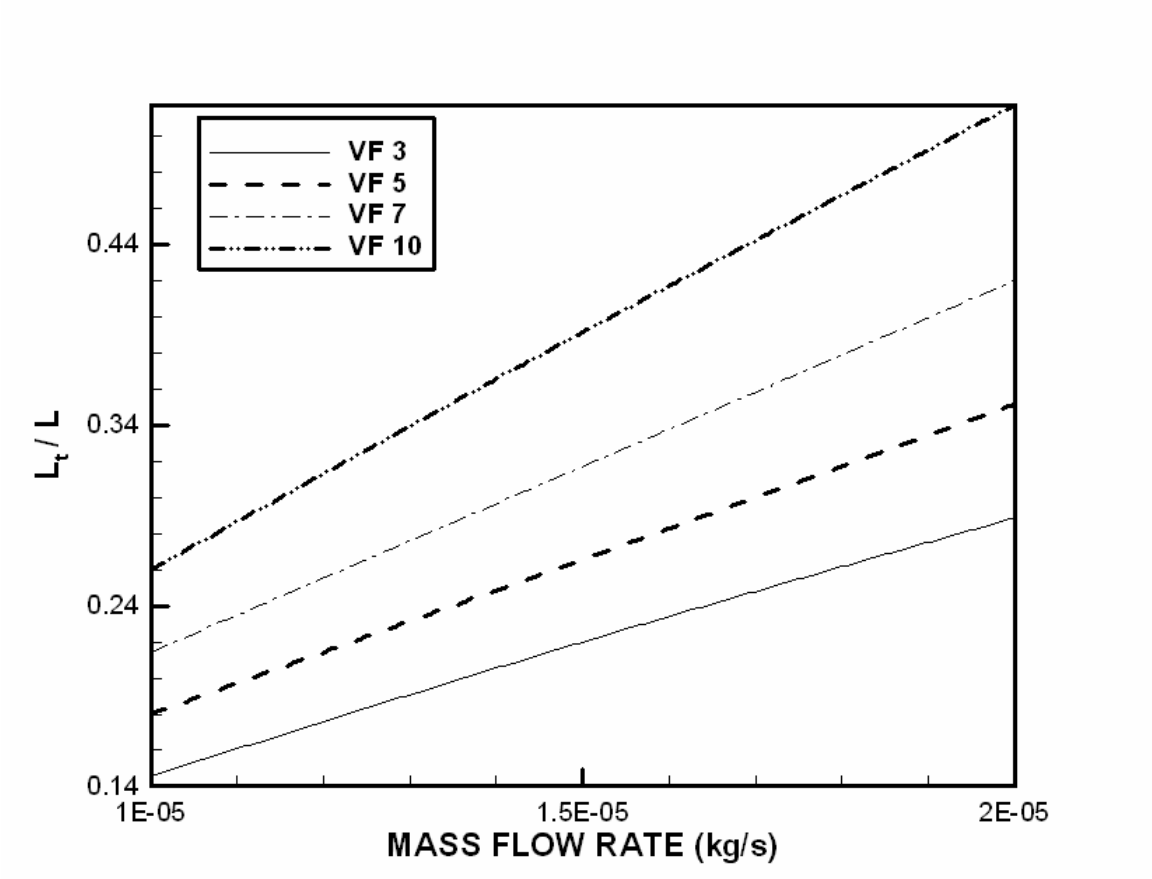

Figure 5.59 Normalized total phase change length for heat flux of 18000 W/m^2, where VF 3, VF 5, VF 7 and VF 10 represents 3%, 5%, 7% and 10% volume concentration of the particles, respectively.

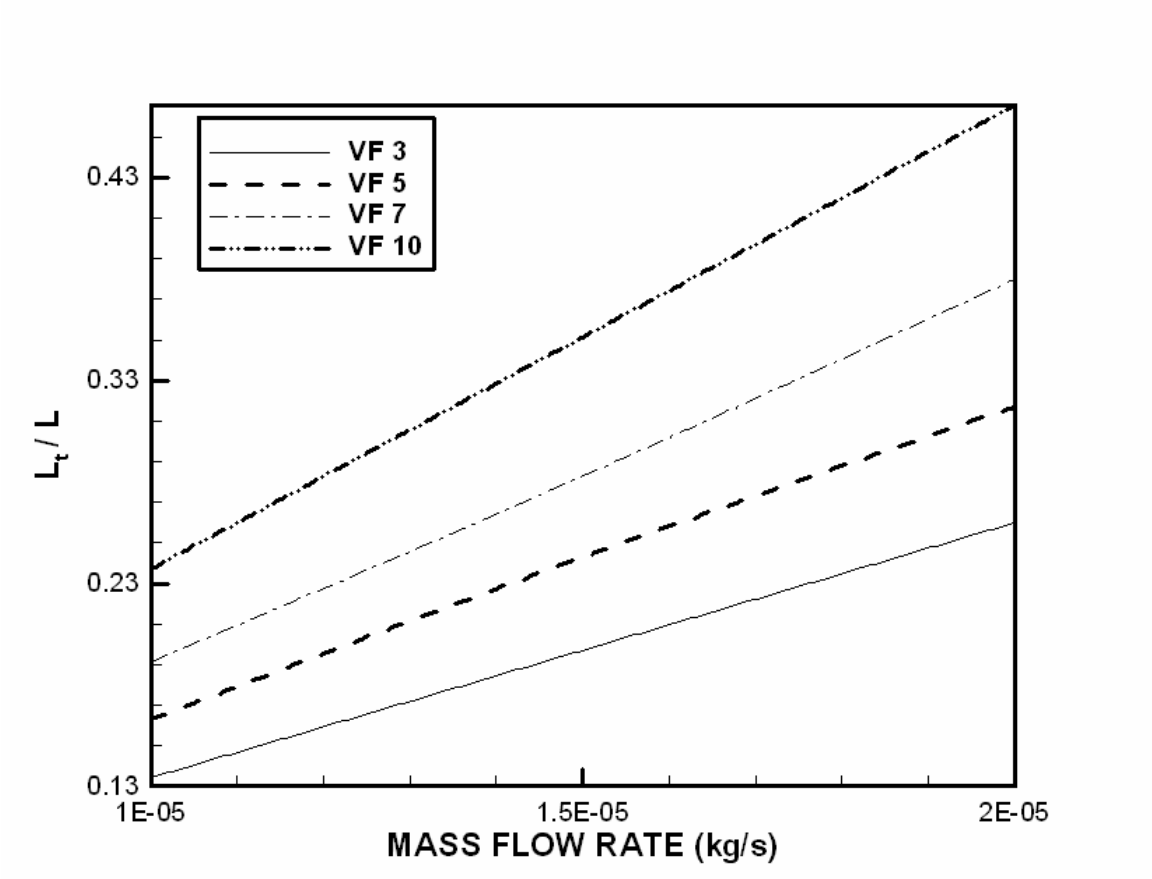

Figure 5.60 Normalized total phase change length for heat flux of 20000 W/m^2, where VF 3, VF 5, VF 7 and VF 10 represents 3%, 5%, 7% and 10% volume concentration of the particles, respectively.

As mentioned earlier, the enhancement in heat storage capacity due to the addition of P.C.M. particles is significant when the phase change of P.C.M. particles completes just at the exit of the microchannel. The length required for the phase change of P.C.M. particles, defined as total phase change length, depends on the heat flux applied, the mass flow rate of the P.C.M. slurry as well as the volume concentration of P.C.M. particles in the slurry. Figure 5.61 shows the variation of L_t/D_h with the different values of operating parameters. It can be observed that increasing the mass flow rate of the P.C.M. slurry, while keeping volume concentration of P.C.M. particles and heat flux constant increases the length required for phase change. Increase in volume concentration of P.C.M. particles while keeping other parameters constant also leads to increase in the phase change length. Increase in heat flux applied to the P.C.M .slurry always decreases the magnitude of phase change length. Therefore, Figure 5.61 can be used in the design of microchannels when operating conditions are known beforehand.

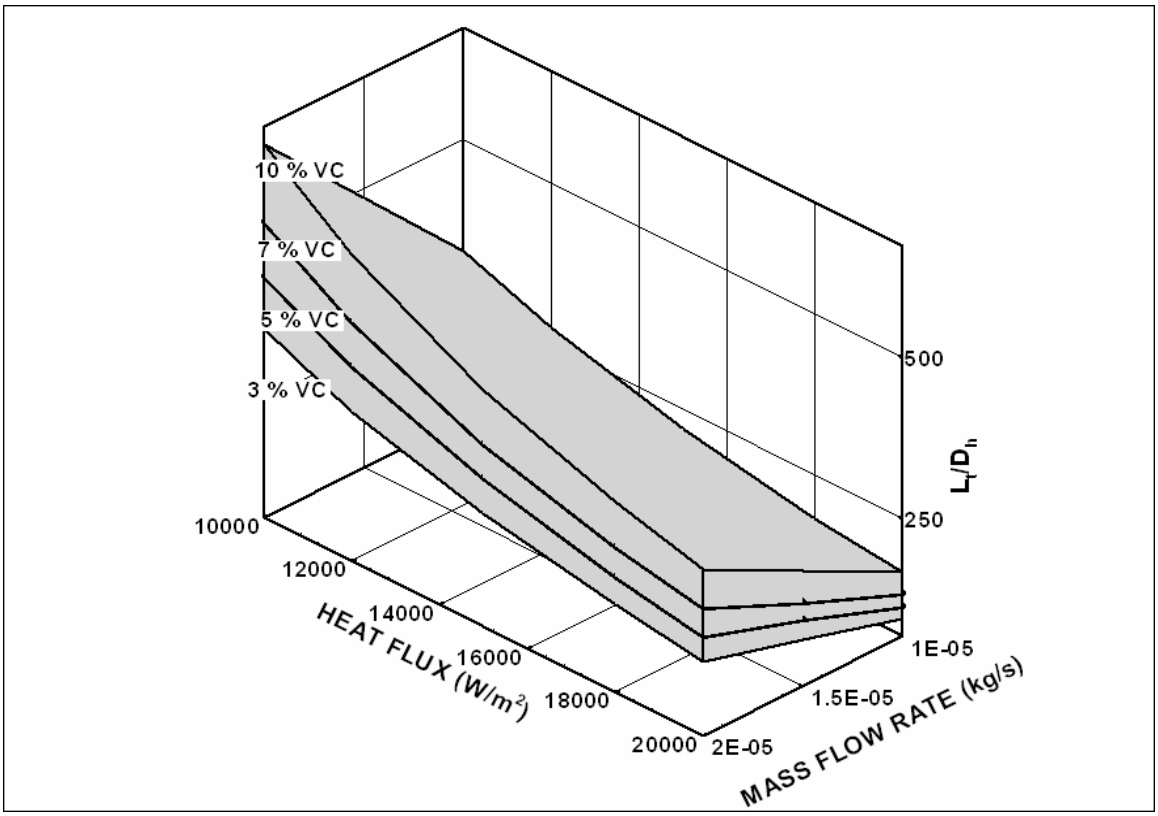

Figure 5.61 Variation of L_t/D_h with operating conditions.

CHAPTER 6

CONCLUSION AND FUTURE WORK

This chapter of the thesis is divided into five sections. In the first four sections, the conclusions corresponding to the results in the previous chapter are presented. In the last section, some of the directions in which this thesis work can be extended are discussed.

6.1 Identification of a Unified Model

Microchannel flow with water as a carrier fluid in the presence of nanosized lauric acid P.C.M. particles using D.P.M. and homogeneous fluid model is investigated. The D.P.M. indicates that presence of 10% volume concentration of P.C.M. particles does not cause an increase in the pressure drop along the microchannel length. However, prediction from the homogeneous model shows an increase in the pressure drop due to the addition of nanoparticles in such a way that 10% volume concentration of particles causes 34.4% increase in pressure drop. The D.P.M and the homogeneous models, however, predicted an improvement in the heat storage capacity due to the addition of P.C.M. nanoparticles. Increasing concentration of P.C.M. particles improves the heat storage capacity of the carrier fluid through the phase change of P.C.M. particles as temperature rise is found to

reduce by 34.6 % in the presence of 10% volume concentration of P.C.M. particles. The D.P.M. is good at predicting the heat transfer due to the addition of nanoparticles, but it fails to predict accurately the pressure drop when nanoparticles are added to the carrier fluid. Based on the results obtained in this study, it is decided to use homogeneous model to investigate the flow of P.C.M. slurry in microchannels.

6.2 Effectiveness Ratio, Performance Index and Merit Number

The flow of P.C.M. slurry in a microchannel is investigated using the homogeneous model. A parametric study is carried out through varying the mass flow rate, heat flux and particle volume concentration of the bulk fluid. It is found that there exists a unique heat flux to mass flow rate ratio for a given volume concentration of particles at which the effectiveness ratio, the performance index, and the Merit number are the maximum. The effectiveness ratio is greater than 1 for all cases and it reaches a maximum value of 2.75. This indicates that for the same temperature rise, the bulk fluid can absorb 175% more heat as compared to carrier fluid without particles. The performance index is lower than 1 for all heat flux to mass flow rate ratios for the P.C.M. slurry of 3% particle volume concentration. The maximum value of the performance index is 1.37, which reflects a 37% increase in heat transfer rate to fluid pumping power ratio of the bulk fluid as compared to carrier fluid. The Merit number follows the same trend as the effectiveness ratio, which indicates that the increase in irreversibility due to addition of P.C.M. particles is offset by the gain in heat transfer. The effectiveness ratio,

performance index and the Merit number have the same corresponding value of optimum heat flux to mass flow rate ratio for a given particle concentration. The ratios calculated in this study, namely, effectiveness ratio, performance index and Merit number guide the designer regarding the conditions to be used in order to obtain the maximum benefit in terms of heat storage capacity by the addition of P.C.M. particles.

6.3 Volumetric Entropy Generation Rate due to Heat Transfer and Fluid Friction

In the present study, an investigation is done on microchannel flow with water in the presence of nanosized lauric acid P.C.M. particles using the homogeneous fluid model. The homogeneous model and the calculation of volumetric entropy generation rate using the C.F.D. code FLUENT^{TM} is validated by comparing with experimental and analytical results respectively. A parametric analysis is carried out through varying the particle volume concentration, mass flow rate and heat flux of the bulk fluid. It is observed that for bulk fluid mass flow rate of 4 x 10^{-5} kg/s, heat flux of 20000 W/m^2, and particle volume concentration of 10%, the volumetric entropy generation rate due to heat transfer and the total volumetric entropy generation rate are the maximum. The volumetric entropy generation rate due to heat transfer always increases with increasing heat flux. Increase in mass flow rate and volume concentration of particles, generally lead to increase in volumetric entropy generation rate due to heat transfer but the change is less than 16% for all cases. Among the three parameters studied, heat flux has the highest impact on the volumetric entropy generation rate due to heat transfer. The volumetric

entropy generation rate due to fluid friction is found to increase with increasing mass flow rate and volume concentration of particles, and reduces with increasing heat flux. Therefore, the highest value of volumetric entropy generation rate due to fluid friction is obtained at mass flow rate of 4 x 10^{-5} kg/s, heat flux of 8000 W/m^2, and particle volume concentration of 10%. Among the three parameters studied, mass flow rate has the highest impact on the volumetric entropy generation rate due to fluid friction. At low mass flow rates, the volumetric entropy generation rate due to heat transfer is much higher than the volumetric entropy generation rate due to fluid friction. However, at mass flow rate of 4 x 10^{-5} kg/s, the volumetric entropy generation rate due to heat transfer and due to fluid friction become comparable. Volumetric entropy generation rate due to heat transfer and due to fluid friction guide the designer regarding the conditions to be used in order to minimize the losses in terms of irreversibility caused by the addition of P.C.M. particles.

6.4 Normalized Length of Phase Change and Total Phase Change Length

Laminar flow of water in a microchannel in the presence of nanosized lauric acid P.C.M. particles is investigated using the homogeneous model. A parametric study is conducted by varying the mass flow rate, heat flux and particle volume concentration of the bulk fluid. The results presented in this thesis guide the designer regarding the operating conditions to be used for obtaining maximum enhancement in heat storage capacity for a given microchannel length. In case of the operating conditions being known beforehand,

the results guide the designer regarding the required length to diameter ratio of the microchannel in order to get maximum benefit in terms of heat storage capacity. It is found that the normalized length of phase change and normalized total phase change length increase with increasing volume concentration of particles and with increasing mass flow rate of the P.C.M. slurry. Increase in heat flux reduces the normalized length of phase change and normalized total phase change length. For bulk fluid mass flow rate of 2×10^{-5} kg/s, heat flux of 10000 W/m^2, and particle volume concentration of 10%, the normalized length of phase change and normalized total phase change length is the maximum. The maximum value of the normalized length of phase change is 0.77, which indicates that phase change take place in 77% of the length of microchannel. The maximum value of normalized total phase change length is 0.92, which shows that within 92% length of the microchannel the phase change is complete when the total distance from inlet of microchannel is measured.

6.5 Future Work

The flow of P.C.M. slurry through microchannels is investigated thoroughly in this thesis work. However, there are certain directions in which the work can be extended if experimental validation is available.

The addition of P.C.M. particles into carrier fluid water reduces the thermal conductivity of the slurry due to the lower thermal conductivity of P.C.M. particles. Therefore, metallic nanosized particles like alumina can be added along with P.C.M. particles so that

the enhancement in heat storage capacity by the addition of P.C.M. particles does not decrease the bulk thermal conductivity. Preliminary numerical results showed that the addition of 3% volume concentration of Alumina nanoparticles into P.C.M. slurry increases the heat transfer coefficient by 8.6%. However, the effective thermal conductivity of the slurry containing P.C.M. and alumina nanosized particles had to be calculated in two steps due to the lack of theoretical model for three component mixtures. Due to lack of supporting experimental data for carrier fluid containing nanosized particles of two different materials, it is not possible to be entirely confident about the correctness of the method used for calculating the effective thermal conductivity.

Another interesting direction in which this work can be extended is by focusing the P.C.M. particles near the heated wall. Uniform distribution of P.C.M. particles in the microchannel leads to an increase in Nusselt number at the beginning of phase change and a reduction in Nusselt number towards the end of phase change process. The increase and decrease in Nusselt number tend to nullify each other and the net increase in Nusselt number is less than 1%. The reduction of Nusselt number towards the end of phase change process can be avoided by focusing the P.C.M. particles near the wall subjected to uniform heat flux. Initial results obtained by focusing the P.C.M. particles near the heated wall show a significant enhancement in Nusselt number when the particles are focused in the bottom 40% of the microchannel. The enhancement in Nusselt number also depends on the height of the microchannel in which the particles are focused. However, there are two major problems associated with this idea. When the

particles are uniformly distributed along the microchannel height, the exact nature of phase change process is not very important in the modeling of melting of P.C.M. particles. For uniform distribution of P.C.M. particles, when different specific heat functions were used for modeling the melting of P.C.M. particles, negligible differences in the final result were observed [23]. However, when the particles are focused near the heated wall, the Nusselt number profile tends to follow the specific heat function used for the modeling of phase change of P.C.M. particles. Therefore, it is necessary to experimentally measure the temperature variation of specific heat of P.C.M. slurry before modeling the phase change process. The other major issue is the difficulty involved in the focusing of particles within a required height of the microchannel in an experimental setup. The reduction in the density of P.C.M. particles on melting can lead to migration of some particles near the top of the microchannel and can increase the difficulty in concentrating the particles under a specific height of the microchannel.

Nomenclature

A	cross-sectional area of the microchannel [m^2]
c	volume concentration of nano particles
c_p	specific heat [J kg^{-1} K^{-1}]
$c_{p,S}$	specific heat of particles in solid state[J kg^{-1} K^{-1}]
$c_{p,L}$	specific heat of particles in liquid state [J kg^{-1} K^{-1}]
D_h	hydraulic diameter of the microchannel [m]
E	energy per unit mass [J kg^{-1}]
$\dot{I}$	rate of irreversibility [W]
k	thermal conductivity [W m^{-1} K^{-1}]
L	length of the microchannel [m]
L_{fusion}	latent heat of fusion of P.C.M. particles [J kg^{-1}]
L_{pt}	length of the microchannel in which phase change occurs [m]
L_t	total phase change length [m]
$\dot{m}$	mass flow rate [kg s^{-1}]

p	pressure [Pa]
q''	heat flux [W m^{-2}]
$\dot{Q}$	heat transfer rate [W]
$\dot{Q}_{in}$	heat input to the slurry [W]
r	distance along the radial direction [m]
r_0	radius of the tube [m]
S'''_{gen}	volumetric entropy generation rate [W m^{-3} K^{-1}]
$S'''_{gen,avg}$	averaged volumetric entropy generation rate [W m^{-3} K^{-1}]
$S'''_{generation\_f}$	volumetric entropy generation rate due to fluid friction [W m^{-3} K^{-1}]
$S'''_{generation\_h}$	volumetric entropy generation rate due to heat transfer [W m^{-3} K^{-1}]
T	temperature [K]
T_{in}	temperature at inlet of control volume [K]
T_{out}	temperature at exit of control volume [K]
T_r	reference temperature taken as 298 K
$T_{solidus}$	lower melting temperature [K]

$T_{liquidus}$ upper melting temperature [K]

T_w wall temperature [K]

u x-component of velocity [m s^{-1}]

v velocity [m s^{-1}]

Greek Symbols

μ dynamic viscosity [N s m^{-2}]

ρ density [kg m^{-3}]

τ shear stress [N m^{-2}]

Subscripts

b bulk fluid

f carrier fluid

p Particle

References

[1] Kandlikar S. G., 2006, Heat transfer and fluid flow in minichannels and microchannels, Elsevier Science.

[2] Tuckerman D. B., and Pease R. F. W., 1981, "High-performance heat sinking for VLSI," Electron Device Letters, IEEE, **2**(5), pp. 126-129.

[3] Kandlikar S. G., and Grande W. J., 2003, "Evolution of Microchannel Flow Passages--Thermohydraulic Performance and Fabrication Technology," Heat Transfer Engineering, **24**(1), pp. 3-17.

[4] Pfahler J., Harley J., Bau H., and Zemel J., 1989, "Liquid transport in micron and submicron channels," Sensors and Actuators A: Physical, **22**(1-3), pp. 431-434.

[5] Richter M., and Woias P., others, 1997, "Microchannels for applications in liquid dosing and flow-rate measurement," Sensors and Actuators A: Physical, **62**(1-3), pp. 480-483.

[6] Phillips R. J., Glicksman L. R., and Larson R., 1988, "Forced-convection, liquid-cooled, microchannel heat sinks for high-power-density microelectronics," Cooling Technology for Electronic Equipment, pp. 295-316.

[7] Kandlikar S. G., Steinke M. E., and Balasubramanian P., 2002, "Single-phase flow characteristics and effect of dissolved gases on heat transfer near saturation conditions in microchannels," Proceedings of IMECE02, New Orleans, LA.

[8] Xiangqi W., 2007, "New Approaches to Micro-Electronic Component Cooling."

[9] Xing K., 2007, "Numerical Investigation on the Heat Transfer Enhancement Using Micro / Nano Phase-Change Particulate Flow."

[10] Sharma A., Tyagi V. V., Chen C. R., and Buddhi D., 2009, "Review on thermal energy storage with phase change materials and applications," Renewable and Sustainable Energy Reviews, **13**(2), pp. 318-345.

[11] Ravi G., 2008, "Study of Laminar Flow Forced Convection Heat Transfer Behaviour of a Phase Change Material Fluid."

[12] Mehalick E. M., and Tweedie A. T., 1975, "Two component thermal energy storage material," Final Report General Electric Co., Philadelphia, PA. Space Div., **1**.

[13] Trisaksri V., and Wongwises S., 2007, "Critical review of heat transfer characteristics of nanofluids," Renewable and sustainable energy reviews, **11**(3), pp. 512-523.

[14] Fang Y., Kuang S., Gao X., and Zhang Z., 2009, "Preparation of nanoencapsulated phase change material as latent functionally thermal fluid," Journal of Physics D: Applied Physics, **42**(3), p. 035407.

[15] Product Documentation, Fluent 12.1., ANSYS Inc.

[16] Colvin D. P., 1986, "Spacecraft Heat Rejection Methods: Active and Passive Heat Transfer for Electronic Systems."

[17] Charunyakorn P., Sengupta S., and Roy S. K., 1991, "Forced convection heat transfer in microencapsulated phase change material slurries : flow in circular ducts," Int. J. Heat Mass Transfer, **34**(3), pp. 819-833.

[18] Roy S. K., and Sengupta S., 1991, "An evaluation of phase change microcapsules for use in enhanced heat transfer fluids," International communications in heat and mass transfer, **18**(4), pp. 495-507.

[19] Choi E., Cho Y. I., and Lorsch H. G., 1994, "Forced convection heat transfer with phase-change-material slurries:turbulent flow in a circular tube," Int J. Heat Mass Transfer, **37**(2), pp. 207-215.

[20] Goel M., Roy S. K., and Sengupta S., 1994, "Laminar forced convection heat transfer in microcapsulated phase change material suspensions," International journal of heat and mass transfer, **37**(4), pp. 593-604.

[21] Zhang Y., and Faghri A., 1995, "Analysis of forced convection heat transfer in microencapsulated phase change material suspensions," Journal of thermophysics and heat transfer, **9**(4), pp. 727-732.

[22] Roy S. K., and Avanic B. L., 1997, "Laminar Forced Convection Heat Transfer With Phase Change Material Emulsions," Int. Comm. Heat Mass Transfer, **24**(5), pp. 653-662.

[23] Alisetti E. L., and Roy S. K., 1999, "Forced Convection Heat Transfer to Phase Change Material Slurries in Circular Ducts," J. Thermophysics, **14**(1), pp. 115-118.

[24] Yamagishi Y., Takeuchi H., Pyatenko A. T., and Kayukawa N., 1999, "Characteristics of microencapsulated PCM slurry as a heat-transfer fluid," AichE journal, **45**(4), pp. 696-707.

[25] Roy S. K., and Avanic B. L., 2001, "Laminar Forced Convection Heat Transfer with Phase Change Material Suspensions," Int. Comm. Heat Mass Transfer, **28**(7), pp. 895-904.

[26] Hu X., and Zhang Y., 2002, "Novel insight and numerical analysis of convective heat transfer enhancement with microencapsulated phase change material slurries : laminar flow in a circular tube with constant heat flux," International Journal of Heat and Mass Transfer, **45**, pp. 3163-3172.

[27] Zhang Y., Hu X., and Wang X., 2003, "Theoretical analysis of convective heat transfer enhancement of microencapsulated phase change material slurries," Heat and mass transfer, **40**(1), pp. 59-66.

[28] Chen B., Wang X., and Zhang Y., 2006, "Experimental research on laminar flow performance of phase change emulsion," Applied Thermal Engineering, **26**, pp. 1238-1245.

[29] Alvarado J. L., Marsh C., Sohn C., Phetteplace G., and Newell T., 2007, "Thermal performance of microencapsulated phase change material slurry in turbulent flow under constant heat flux," International journal of heat and mass transfer, **50**(9-10), pp. 1938-1952.

[30] Wang X., Niu J., Li Y., Wang X., Chen B., Zeng R., Song Q., and Zhang Y., 2007, "Flow and heat transfer behaviors of phase change material slurries in a horizontal circular tube," International journal of heat and mass transfer, **50**(13-14), pp. 2480-2491.

[31] Rao Y., Dammel F., Stephan P., and Lin G., 2007, "Convective heat transfer characteristics of microencapsulated phase change material suspensions in minichannels," Heat and Mass transfer, **44**(2), pp. 175-186.

[32] Wang X., Niu J., Li Y., Zhang Y., Wang X., Chen B., Zeng R., and Song Q., 2008, "Heat transfer of microencapsulated PCM slurry flow in a circular tube," AIChE Journal, **54**(4), pp. 1110-1120.

[33] Chen B., Wang X., Zeng R., Zhang Y., Wang X., Niu J., Li Y., and Di H., 2008, "An experimental study of convective heat transfer with microencapsulated phase change material suspension : Laminar flow in a circular tube under constant heat flux," Experimental Thermal and Fluid Science, **32**, pp. 1638-1646.

[34] Zeng R., Wang X., Chen B., Zhang Y., Niu J., Wang X., and Di H., 2009, "Heat transfer characteristics of microencapsulated phase change material slurry in laminar flow under constant heat flux," Applied Energy, **86**(12), pp. 2661-2670.

[35] Xing K. Q., Tao Y.-X., and Hao Y. L., 2005, "Performance Evaluation of Liquid Flow With PCM Particles in Microchannels," Journal of Heat Transfer, **127**(August), pp. 931-940.

[36] Sabbah R., Farid M. M., and Al-Hallaj S., 2008, "Micro-channel heat sink with slurry of water with micro-encapsulated phase change material : 3D-numerical study," Applied Thermal Engineering, **29**, pp. 445-454.

[37] Kondle S., Alvarado J. L., Marsh C., Kessler D., and Stynoski P., 2009, "Laminar Flow Forced Convection Heat Transfer Behavior of a Phase Change Material Fluid in Microchannels," Proceedings of the ASME 2009 International Mechanical Engineering Congress & Exposition, Lake Buena Vista, Florida, USA, pp. 1-10.

[38] Kuravi S., Kota K. M., Du J., and Chow L. C., 2009, "Numerical Investigation of Flow and Heat Transfer Performance of Nano-Encapsulated Phase Change Material Slurry in Microchannels," Journal of Heat Transfer, **131**(June), pp. 1-9.

[39] Kuravi S., Du J., and Chow L. C., 2010, "Encapsulated Phase Change Material Slurry Flow in Manifold Microchannels," Journal of Thermophysics and Heat Transfer, **24**(2), pp. 364-373.

[40] Alquaity A. B. S., Al-Dini S. A., Wang E. N., Shuja S. Z., Yilbas B. S., and Suabedissen K. J., 2010, "Heat Transfer Enhancement In Microchannel Flow:Presence of Microparticles In a Fluid," Proceedings of ASME 2010 3rd Joint US-European Fluids Engineering Summer Meeting and 8th International Conference on Nanochannels, Microchannels, and Minichannels, Montreal, Canada.

[41] Morsi S. A., and Alexander A. J., 1972, "An investigation of particle trajectories in two-phase flow systems," Journal of Fluid Mechanics, **55**(02), pp. 193-208.

[42] Vand V., 1945, "Theory of viscosity of concentrated suspensions," Nature, **155**(3934), pp. 364-365.

[43] Maxwell J. C., 1954, A Treatise on Electricity and Magnetism, Vol. 1, Dover Publications, New York.

[44] Nan C. W., Birringer R., Clarke D. R., and Gleiter H., 1997, "Effective thermal conductivity of particulate composites with interfacial thermal resistance," Journal of Applied Physics, **81**, p. 6692.

[45] Buongiorno J., Venerus D. C., Prabhat N., McKrell T., Townsend J., Christianson R., Tolmachev Y. V., Keblinski P., Hu L., and Alvarado J. L., others, 2009, "A benchmark study on the thermal conductivity of nanofluids," Journal of Applied Physics, **106**(9), p. 94312.

[46] Patankar S. V., 1980, Numerical heat transfer and fluid flow, Hemisphere Publishing Corporation.

[47] Li J., and Kleinstreuer C., 2010, "Entropy Generation Analysis for Nanofluid Flow in Microchannels," Journal of Heat Transfer, **132**, p. 122401.

Vita

Name: Awad Bin Saud Alquaity

Nationality: Indian

Present address: P.O. Box: 5386, c/o Dr.Saud Bin Ali Alquaity, M.S.Badruddin Polyclinic, Batha, Riyadh 11422, Kingdom of Saudi Arabia.

Permanent address: H.No:10-2-354, Mahmood Bagh, Asifnagar, Hyderabad, 500028, A.P., India.

Telephone: 009665-4198-5096 (Present), 0091-40-23341107 (Permanent)

Education: Received Bachelor of Technology degree in Mechanical Engineering from National Institue of Technology, Warangal, India in 2009.

Joined Mechanical Engineering Department of King Fahd University of Petroleum and Minerals, Dhahran as Research Assistant in October 2009.

E-mail: awad.nitw@gmail.com, awadalquaity@yahoo.com